國立臺灣大學工學院環境工程學研究所

碩士論文

Graduate Institute of Environmental Engineering

College of Engineering

National Taiwan University

Master Thesis

以超重力技術碳酸化後煉鋼廢棄物作為水泥添加材料之表現評估

Performance Evaluation of Carbonated Steelmaking Slags for Supplementary Cementitious Materials via High-Gravity Carbonation Process

舒柏凱

Bo-Kai Shu

指導教授： 蔣本基 博士

Advisor: Pen-Chi Chiang, Ph. D

中華民國 108 年 7 月

July 2019

doi:10.6342/NTU201902030

國立臺灣大學碩士學位論文
口試委員會審定書

以超重力技術碳酸化後鹼性廢棄物作為水泥取代材料之表現評估

Performance Evaluation of Carbonated Steelmaking Slags for Supplementary Cementitious Materials via High-Gravity Carbonation Process

本論文係 舒柏凱 君(學號 R05541106)在國立臺灣大學環境工程學研究所完成之碩士學位論文，於民國 108 年 07 月 02 日承下列考試委員審查通過及口試及格，特此證明

論文審查委員：

顧洋 教授
國立台灣科技大學化學工程學系

陳奕宏 教授
台北科技大學化學工程與生物科技學系

林逸彬 教授
國立台灣大學環境工程學研究所

潘述元 教授
國立台灣大學生物環境系統工程學系

蔣本基 教授
國立台灣大學環境工程學研究所

指導教授：

所　　長：

摘要

雖然鋼鐵業作為國家經濟發展之重要產業，但其生產過程中不僅產生有害廢棄物還會排放大量之二氧化碳。本研究旨在利用超重力碳酸化技術將不同煉鋼廢棄物進行碳酸化，同時吸收二氧化碳並探討各材料對碳捕捉的能力，而後再將碳酸化後煉鋼廢棄物作為礦粉摻料添加於水泥材料中，探究其對水泥材料的工作性、強度及耐久性的影響。在本研究中預先將磨細的轉爐石、精煉鋼渣、電弧爐碴與水混合形成泥漿，泵送進超重力旋轉床（RPB）中與二氧化碳反應 60 分鐘，透過改變轉速（700-1300rpm）、液固比（10-50 mL / g）和粒徑（32-160μm）求出不同反應條件下之碳酸化轉換率，並找出碳酸化程序的最佳工況點。據本研究顯示，1100rpm、20 mL / g、32μm 之電弧爐還原碴具有高達 19.29±0.05 克-二氧化碳/100 克-爐碴的捕碳容量。同時也透過 TGA、SEM、XRD 分析可看出碳酸化過程成功將原料中游離氧化鈣、氫氧化鈣及矽氧化鈣轉換為碳酸鈣附著於反應後材料表面。反應後將材料以 5-15%添加於水泥漿體和砂漿中，發現水泥雖然流動性稍微下降，但黏性提高可以防止拌和混凝土發生析離，而凝結部分透過碳酸化可打斷電弧爐氧化碴的緩凝機理並使其順利凝結。碳酸鈣過程消除了游離氧化鈣和鹼金屬離子可以防止水泥晚期吸水後發生膨脹，提高水泥的晚期強度和耐久性。另外碳酸化過程形成的碳酸鈣可以和水泥中的鋁酸三鈣進行反應，形成產物填補孔隙，提高水泥早期強度和抗硫性。最後透過強度動力學模式分析添加材料對水泥強度發展的影響。故本研究之碳酸化過程不僅能做到處理二氧化碳，煉鋼廢棄物，同時將其資源化後還能提高水泥性能，極具發展前景。

關鍵字：煉鋼爐碴；碳捕捉再利用；混合水泥；超重力技術；鹼骨材反應

doi:10.6342/NTU201902030

doi:10.6342/NTU201902030

Abstract

Steelmaking industry plays an important role in economical development. However, steelmaking slags and carbon dioxide are generated simultaneously during production which are harmful for the environment. This research focused on carbonation of four kinds of steelmaking slags via High-Gravity Carbonation Process and also investigated the workability, strength and durability of cement with partial replacement of slags. In this study, slags after pretreatment were added in tap water and blended into slurry. Next, the slurry would be pumped into the rotating packed bed reactor, react with carbon dioxide for 60 minutes with different operating parameters. The results indicate that the EAFRS under 1100 rpm, 20 mL/g and 32 μm had the best carbonation conversion yield, which could fixed 19.29±0.05 g-CO2/100 g-slag. The difference of slags between carbonation can be analyzed by thermo-gravavimetric analysis (TGA), scanning electron microscopy (SEM) and X-ray diffraction (XRD). During the carbonation process, free lime, calcium hydroxide and calcium silicates would be leached out, react with CO_2 and yield calcium carbonate attached on the slags' surface. After that, carbonated slags were used as supplementary materials, blended in cement with 5 to 15% replacement. With slags added, although the fluidity of cement declined, the viscosity of the mortar got increased, which might prevent the cement segregated from aggregates. The carbonation process could wash out the organic compounds in the EAFOS, break off the retarding mechanism and make the cement specimens set normally. Besides, the carbonation process could also eliminate free lime, calcium hydroxide and alkali ions, which prevented the specimens expanding from

doi:10.6342/NTU201902030

hydration process and alkali-aggregate reaction. Furthermore, calcium carbonated generated form the carbonation process could react with tricalcium aluminate in clinker, which produced C-A-$\bar{C}$-H gel and filled up the porosity between hydration products. Thus, the compressive strength at early age, later age and the durability of mortars could be improved. Consequently, this study can not only deal with carbon dioxide and alkaline wastes from steelmaking, but also produced products which can promote the properties of cement.

Key words: steelmaking slags; carbon capture and utilization; blended cement; High-Gravity Carbonation Process; Alkali-aggregate reaction

doi:10.6342/NTU201902030

Table of Contents

doi:10.6342/NTU201902030

doi:10.6342/NTU201902030

doi:10.6342/NTU201902030

Table of Figures

doi:10.6342/NTU201902030

doi:10.6342/NTU201902030

doi:10.6342/NTU201902030

List of Tables

doi:10.6342/NTU201902030

doi:10.6342/NTU201902030

Comments for Oral Defense

林逸彬 教授:

Question and Suggestions	Answers
為何要用 RPB? RPB 較快之原因為何?	感謝老師詢問，關於使用 RPB 的原因和其優點已於第 1 章和 2-1-4 中描述。
碳酸化轉換率該如何計算?	感謝老師提問，詳細內容已列於 3-4-1 中。
模式中的 P 和 k_0 如何求得?	感謝老師提問，模式部分已於 4-3 詳述。

陳奕宏 教授:

Question and Suggestions	Answers
建議做性質和成分做迴歸分析。	感謝老師建議，未來會加入 ANOVA 分析化學成分對水泥性質的影響。
未來方向除 LCA，應更在意經濟效益分析。	感謝老師建議，會列入未來考量並在 5-2 加以修正。
可結合廢氣之實際二氧化碳濃度評估。	感謝老師建議，實驗室正在進行模擬實場煙道氣 15%二氧化碳去除實驗。

doi:10.6342/NTU201902030

顧洋 教授:

Question and Suggestions	Answers
參考資料應該補齊，格式統一。	感謝老師建議，格式方面已經予以修正。
XRF 測定之缺點(定性，非定量)是否造成測定不準。	感謝老師提問，根據參考資料 XRF 測得結果與 ICP 相近，後續會再進行相關實驗核實。
文中碳酸化轉化率 conversion yield 與 conversion 算法有何不同？文中應用該採用何者？	感謝老師提問，conversion yield 為氧化鈣轉變為碳酸鈣的產出率，而 conversion 則單純為二氧化碳轉變為碳酸鈣的比率，本研究使用的試驗方法皆屬於前者。
強度預測模式僅是回歸公式，有無物理意義？為何不使用 kt，而是 k ln(t)?	感謝老師提問，目前 4-3 的模式僅為回歸公式，後續會結合 ANOVA 分析進行化學成分對強度的探討。

doi:10.6342/NTU201902030

Chapter 1 Introduction

Steelmaking industry plays an important role of industry development. According to the report provided by World Steel Association, the amount of crude steel production and steel consumption per capita in Taiwan ranked 12 and 2 respectively in the world. However, steelmaking is a high pollutant industry, which not only emits a great amount of carbon dioxide but also produce a lot of alkaline waste. As the situation of global warming grows intensively, fighting against greenhouse gases (GHGs) should not be delayed. Carbon dioxide is the most important anthropogenic GHGs, which is responsible for about two third of the enhanced greenhouse effect. According to the information provided by intergovernmental panel in climate change (IPCC), the global CO_2 emission reached to 49 Gt in 2010. In the meanwhile, international energy agency (IEA) also proposed that the techniques of carbon capture, utilization and storage (CCUS) can lead to the reduction of CO_2 up to 15%. Therefore, people have gradually laid more emphases on the techniques of CCUS.

CCUS can be divided into carbon capture and storage (CCS) and utilization (CCU). While people conduct CCS, many restrictions must be taken into consideration. For example, people need to choose the suitable geological storage, such as anticline. The storage might also cause earthquakes. What's more, the process of the storage can't provide any economic benefit. On the other hand, CCU can be used as chemical feedstock, fuel, enhanced oil recovery, mineral carbonation, which can provide extra commercial value and have a promising future. Among the above techniques of CCU,

doi:10.6342/NTU201902030

mineral carbonation is equipped with thermodynamically stability. Besides, carbonation is an exothermic reaction, which doesn't need extra energy consumption. It also lowers environmental impacts. Thus, mineral carbonation is regarded as the most acceptable technique in CCUS.

In consideration of green chemistry and economical effect, alkaline waste from the steel industry mentioned above can be used as carbon-catching materials because it contains a large amount of calcium oxide. In the meanwhile, the process of carbonation can also neutralize the alkalinity of the waste. However, during carbonation, the low diffusion rate of calcium ion may be the rate determined step in the reaction. In order to elevate the efficiency and rate of carbonation, the effect of mass transfer has to be improved. In this study, rotating packed bed is employed because it can break liquid drops into even smaller particles to enhance mass transfer rate. Carbonated alkaline waste can be used as a kind of pozzolanic material, which can be added into cement to intensify its properties. In this way, the outcome can reach to the aim of cleaner production and circular economy. In conclusion, the objectives in this study includes:

1. To evaluate the performance for carbonation conversion by different steelmaking slags.
2. To investigate the properties of cement with partial replacement by different steelmaking slags.
3. To establish the strength prediction model of mortar replaced by different steelmaking slags.

doi:10.6342/NTU201902030

Chapter 2 Literature Review

2-1 Carbonation Process

2-1-1 Accelerated Carbonation

To mitigate the global warming, many kinds of technology have been developed for each phase of carbon capture utilization and storage. CO_2 may be captured from post-combustion, pre-combustion or oxy-fuel combustion technology. After capturing, the mineralization method is regarded as a promising and feasible alternative to CO_2 sequestration. Mineral carbonation is a chemical process in which CO_2 reacts with a metal oxide such as magnesium or calcium to form carbonates. Magnesium and calcium are normally found in nature in the form of silicate minerals such as serpentine, olivine，wollastonite and etc., which are largely deposited in Finland, Australia, Portugal and the USA. All of these mineral carbonation reactions, which is called weathering, are shown in table 2-1 (Zha et al.,2015). They can occur spontaneously in nature due to the products of these reactions which have lower Gibbs free energy than reactant as in figure 2-1. However, the reaction rate of nature carbonation is too slow due to the relative low CO_2 concentration in the atmosphere, which is about 400 ppm (Bertos et al., 2004). Thus, the accelerated carbonation was proposed by Seifritz in 1990 by using minerals as feedstock to react with a high purity of CO_2 and was proven thermodynamically practical to enhance natural weathering process (Lackner et al., 2005). *Costa et al*. (2007) also indicated that the accelerated carbonation process has the potential to reduce time requirement for carbonation up to a few hours to days.

doi:10.6342/NTU201902030

Table 2-1 Carbonation Reaction of Minerals (Zha et al., 2015)

Minerals	**Reaction equation**	**ΔH (kJ/mol)**
Anorthite	$CaAl_2Si_2O_8 + CO_2 \rightarrow CaCO_3 + Al_2O_3 + 2SiO_2$	-81
Calcium Hydroxide	$Ca(OH)_2 + CO_2 \rightarrow CaCO_3 + H_2O$	-68
Chrysotile (Serpentine)	$Mg_3Si_2O_5(OH)_4 + 3CO_2 \rightarrow 3MgCO_3 + 2SiO_2 + 2H_2O$	-35
Diopside	$CaMgSi_2O_6 + 2CO_2 \rightarrow CaCO_3 + MgCO_3 + 2SiO_2$	-71
Enstatite	$Mg_2Si_2O_6 + 2CO_2 \rightarrow 2MgCO_3 + 2SiO_2$	-81
Forsterite (Mg-Olivine)	$MgSiO_4 + 2CO_2 \rightarrow 2MgCO_3 + SiO_2$	-88
Grossular Garnet	$Ca_3Al_2(SiO_4)_3 + 3CO_2 \rightarrow 3CaCO_3 + Al_2O_3 + 3SiO_2$	-67
Lime	$CaO + CO_2 \rightarrow CaCO_3$	-167
Magnesium Hydroxide	$Mg(OH)_2 + CO_2 \rightarrow MgCO_3 + H_2O$	-37
Periclase	$MgO + CO_2 \rightarrow MgCO_3$	-115
Pyrope Garnet	$Mg_3Al_2(SiO_4)_3 + 3CO_2 \rightarrow 3MgCO_3 + Al_2O_3 + 3SiO_2$	-92
Talc	$Mg_3Si_4O_{10}(OH)_4 + 3CO_2 \rightarrow 3MgCO_3 + 4SiO_2 + H_2O$	-44
Tremolite	$Ca_2Mg_5Si_8O_{22}(OH)_2 + 7CO_2 \rightarrow 2CaCO_3 + 5MgCO_3 + 8SiO_2 + H_2O$	-37
Wollastonite	$CaSiO_3 + CO_2 \rightarrow CaCO_3 + SiO_2$	-87

doi:10.6342/NTU201902030

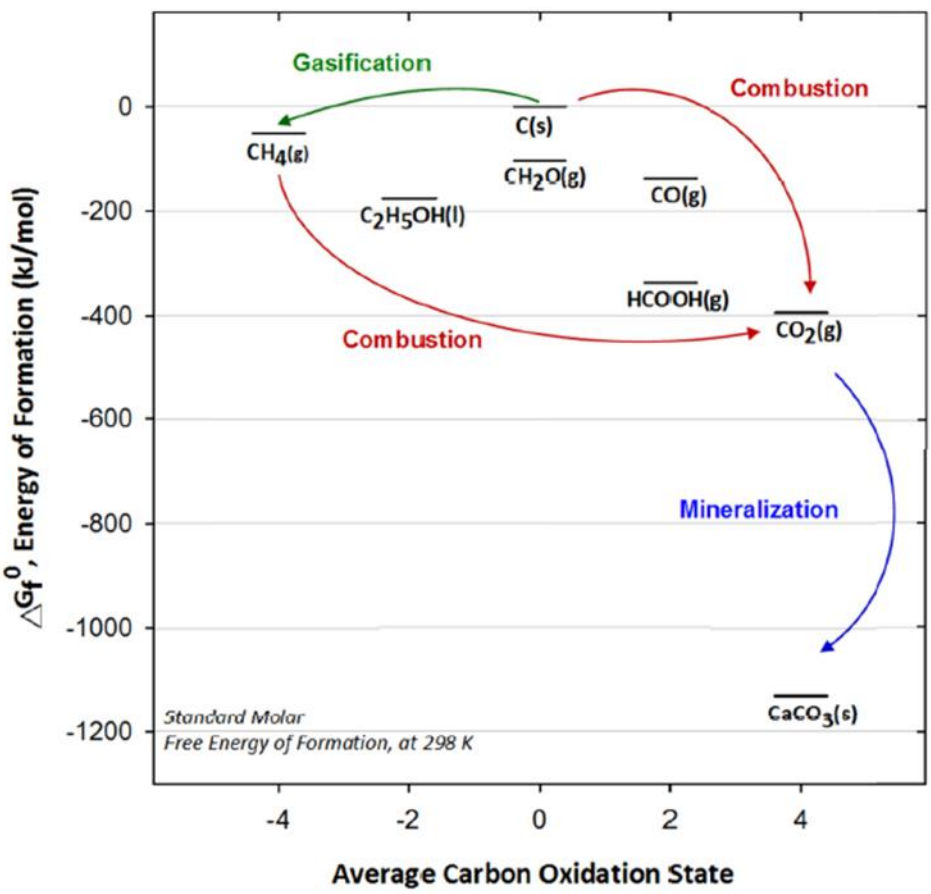

Figure 2-1 Standard Molar Gibbs Free Energy of Formation for Several Carbon-related Substance at 298K (Pan et al. 2015)

Accelerated carbonation processes can be divided into two categories: the direct carbonation process and the indirect carbonation process, which are shown in Table 2-2. The direct carbonation process is the carbonation taking place in a single step, which can be accomplished via gas-solid reactions or mineralization in aqueous solutions. The indirect carbonation process takes place in a multi-step process. It includes hydrochloric (HCl) acid extraction, the molten salt process, other acid extraction, bioleaching, ammonia extraction and caustic extraction followed by carbonation reactions (Bobicki et al. 2012).

doi:10.6342/NTU201902030

Table 2-2 Summary of Accelerated Carbonation Processes Routes. (Bobicki et al., 2012)

Mineral carbon sequestration methods		**Characteristics**
Direct carbonation	Gas-solid	• CO_2 reacted with mineral in a gas-solid reaction • Simplest method of mineral carbonation • Not feasible for silicate minerals
	Aqueous	• CO_2 reacted with mineral in aqueous suspension • Pre-treatment required • Most promising technique
Indirect carbonation	HCl Extraction	• Metal ion extracted from mineral using HCl • Metal ion precipitated as hydroxide for carbonation • HCl recovered • Very energy intensive
	Molten Salt	• Molten magnesium chloride salt used to extract metal ion from silicate minerals • Molten salt highly corrosive • Make-up chemical cost is prohibitive
	Acid Extraction	• Acids used to extract metal ion from minerals • Extracted metal carbonated • Various acids used • High carbonate conversions achieved • Multiple process steps allow contaminants to be separated, resulting in a pure carbonation product • Chemically intensive • Energy intensive if acid recovered
	Bioleaching	• Chemolithotrophic bacteria combined with acid generating substances and silicate minerals to extract metal ions for aqueous carbonation • Passive and inexpensive
	Ammonia Extraction	• Ammonia salts used to extract metal ion from silicate rock for carbonation • Selective leaching of alkaline earth metals • Reagent recovery possible • Reasonable carbonate conversions achieved
	Caustic Extraction	• Caustic solid used to extract metal ion from silicate rock for carbonation • Not a promising technique

doi:10.6342/NTU201902030

2-1-1-1 Direct Carbonation

The processes of carbonation of the solid minerals or alkaline wastes, which take place in a single route step, are called the direct carbonation processes. In these processes, reaction conditions such as temperatures and pressure have significant influence on the reaction rate. The processes can be divided into two types for discussion, which are carbonation in gaseous (gas-solid) and aqueous phase.

The gas-solid process is the simplest method of mineral carbonation and it can usually produce high temperature steam and electricity during the converting process. However, the performance of reaction, such as reaction rate and carbonation conversion yield of minerals, is still too poor to be utilized due to the thermodynamic limitations (Sipilä et al. 2008).

In the aqueous process of direct carbonation, CO_2 reacts with water to form carbonic acid and bicarbonate which can react with metal ion from mineral to form carbonate precipitation (Bobicki et al. 2012). It seems to be the most promising CO_2 mineralization alternative to date due to the reaction rate and the carbonation degree are more acceptable. However, the cost of pre-treatment steps during the aqueous accelerating carbonation process is higher than that in the gas-solid carbonation process (Sipilä et al. 2008).

doi:10.6342/NTU201902030

2-1-1-2 Indirect Carbonation

Indirect mineral carbonation refers to the mineral carbonation processes, which take place in more than one stage. Typically, indirect carbonation involves the extraction of reactive components (Mg^{2+}, Ca^{2+}) from the minerals, using acids or other solvents, followed by the reaction of the extracted components with CO_2 in either the gaseous or aqueous phase. For example, the processes of using acetic acid to extract calcium ion from wollastonite. After extraction, the residue minerals are removed and carbon dioxide dissolves in the calcium-containing solution to form calcium carbonate precipitation. The reaction is shown in Eq. 2-1 and 2-2.

$$CaSiO_3 + 2CH_3COOH \rightarrow Ca^{2+} + 2CH_3COOH^- + H_2O + SiO_2 \quad (2\text{-}1)$$

$$Ca^{2+} + 2CH_3COOH^- + H_2O + CO_2 \rightarrow 2CH_3COOH + CaCO_3 \downarrow \quad (2\text{-}2)$$

The main advantage of indirect carbonation processes compared to the direct one is pure calcium carbonate, which can be produced due to the removal of other impurities during the leaching process. Pure calcium carbonate can be marketed at a higher price, which contributes to more capital investment for the carbonation process (Eloneva et al. 2008).

doi:10.6342/NTU201902030

2-1-2 Alkaline Wastes Utilization for Accelerated Carbonation

Both natural minerals and alkaline wastes can be used in carbonation process, however, alkaline wastes from the industry have not only higher carbon capture capacity but also lower energy consumption during mining. As presented, an enormous amount of industry alkaline waste is produced by the steelmaking industry, the thermal power plants, the cement industry, the paper-manufacturing industry and the petrochemical industry. Alkaline wastes often seen above are summarized in Table 2-3:

Table 2-3 Alkaline Waste in Industry (Pan et al. 2012)

Alkaline Solid Waste Group	Example
Slag	• Steelmaking slags (BOFS, EAFS, BFS) • Coal slag
Air pollution control residue	• Municipal solid waste incinerator (MSWI) APC residue • Cyclone dust
Fly ash	• MSWI fly ash • Coal fly ash • Oil shale ash
Bottom ash	• MSWI bottom ash
Cement wastes	• Cement kiln dust • Cement bypass dust • Construction and demolition waste • Cement / Concrete waste • Blended hydraulic slag cement
Mining waste	• Asbestos tailings • Nickel tailings • Bauxite tailing
Sludge (incinerator) ash	• Sewage sludge incinerator ash • Steel wastewater sludge • Paper sludge incinerator ash
Paper pulping and mill waste	• Paper mill waste (calcium mud) • Green sludge dreg • Lime mud • Lime slaker grits

doi:10.6342/NTU201902030

The alkaline wastes are abundant, cheap, and usually cogenerated with CO_2 (Table 2-4) in many industries, so they are suitable in carbonation. Figure 2-2 summarized the relationship between CO_2 capture capacity in terms of CaO and MgO contents and hardness in terms of Fe_2O_3 and Al_2O_3 contents for different types of solid wastes. In general, the contents of CaO and MgO in the steelmaking slags are relatively higher than those in the fly ash or bottom ash. Thus, steelmaking slags such as blast-furnace slags (BFS), basic-oxygen-furnace slag (BOFS), and electric-arc-furnace slags (EAFS) have the advantage of carbon capture.

Table 2-4 Global Alkaline Wastes Production and their CO_2 Emission (Azdarpour et al., 2015)

Alkaline Wastes	**Global Production (Mt/yr)**	**CO_2 Emission (Mt/yr)**
Steelmaking Slags	315-420	171
Waste Cement	1100	62
Coal Fly Ash	600	12000
Red Gypsum	1.25	3.6

doi:10.6342/NTU201902030

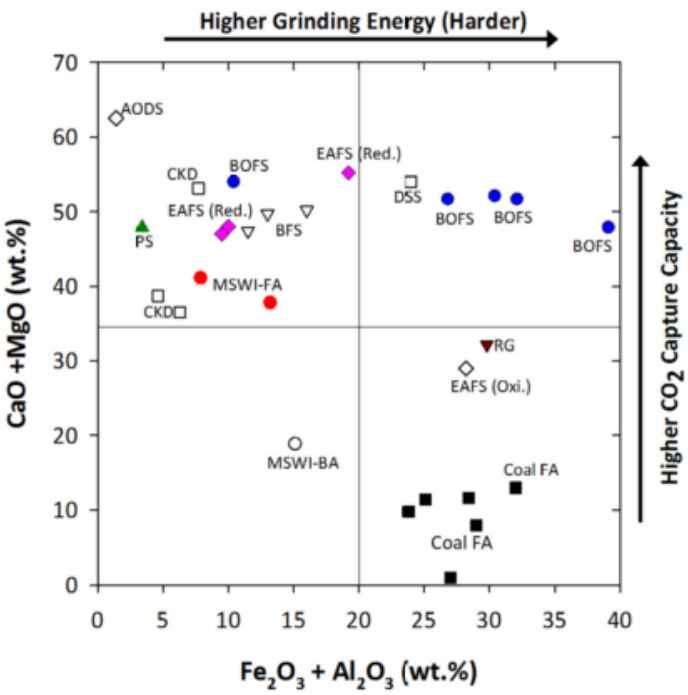

Figure 2-2 Relationship of CO_2 Capture Capacity and Hardness for Different Types of Alkaline Wastes (Pan et al. 2015)

doi:10.6342/NTU201902030

2-1-3 Mechanism of Carbonation Process

Carbonation reaction is an exothermic reaction, which can be divided into three steps. Firstly, calcium ion is leached from minerals or the alkaline wastes and dissolved in the solution. Secondly, CO_2 is dissolved in the solution simultaneously to form carbonic acid (H_2CO_3), which will be ionized into bicarbonate and carbonate in alkaline condition. Finally, calcium ion reacts with bicarbonate and carbonate to form precipitation of calcium carbonate. The processes of mineral carbonation is shown in Table 2-5. (Huijgen et al., 2005; Huntzinger et al., 2009; Haug et al., 2011)

Table 2-5 Processes of Carbonation Reaction

Step	Reaction
Leaching of Calcium ion	$CaO + H_2O \rightarrow Ca^{2+} + 2OH^-$ (alkaline wastes) $Ca_2SiO_4 + 4H_2O \rightarrow 2Ca^{2+} + H_4SiO_4 + 4OH^-$ (minerals)
CO_2 Dissolution and Ionization	$CO_2 + H_2O \rightarrow H_2CO_3$ $H_2CO_3 \leftrightarrow H^+ + HCO_3^- \leftrightarrow 2H^+ + CO_3^{2-}$
$CaCO_3$ Precipitation	$Ca^{2+} + H_2CO_3 \rightarrow CaCO_3 \downarrow + 2H^+$ $Ca^{2+} + HCO_3^- \rightarrow CaCO_3 \downarrow + H^+$ $Ca^{2+} + CO_3^{2-} \rightarrow CaCO_3 \downarrow$

doi:10.6342/NTU201902030

Additionally, the reaction rate is also influenced by factors as follow:

a) Transportation-controlled mechanisms of Ca^{2+} and CO_3^{2-} diffusion.

b) Boundary layer effect of diffusion across silica-rich layer and $CaCO_3$ coating layer.

c) Precipitate coating.

d) Pore blockage.

e) Dissolution of Ca^{2+} from minerals and alkaline waste.

Where a) and b) are usually affected by reactor categories and reaction condition, c) and d) are mainly influent by the material characters, and e) is affected by the liquid agent categories and the material characters.

doi:10.6342/NTU201902030

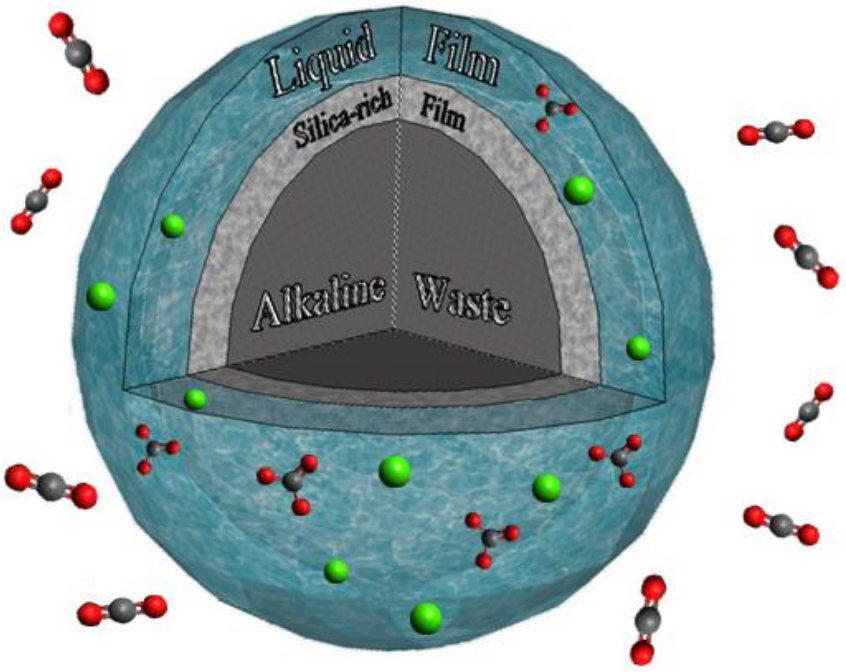

(a)

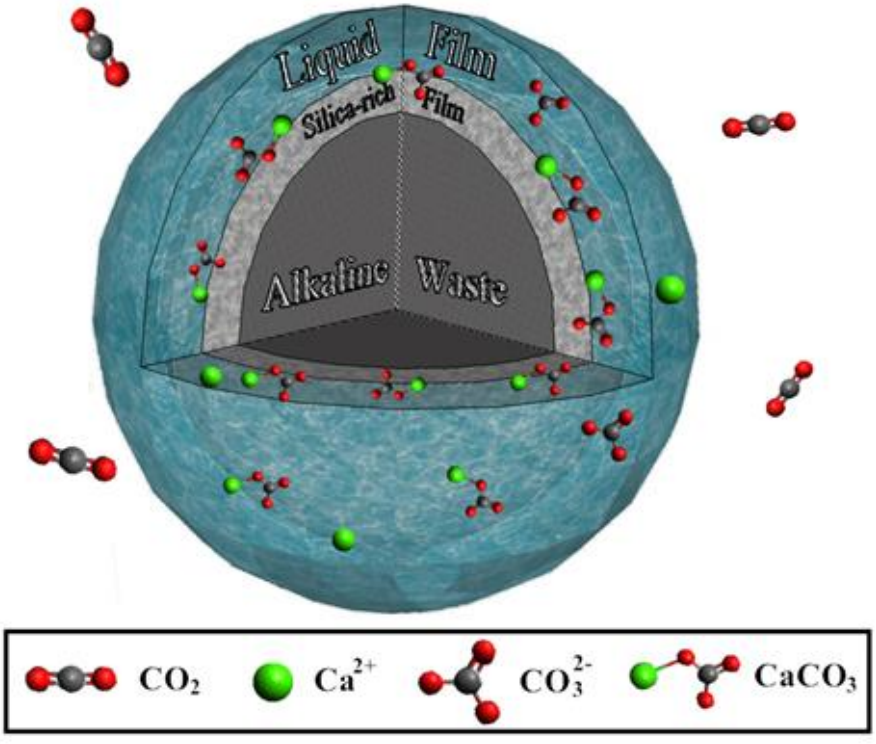

(b)

Figure 2-3 Carbonation Reaction Mechanism of Alkaline Wastes. (a) Leaching of Calcium ion and CO_2 Dissolution (b) $CaCO_3$ Precipitation.

doi:10.6342/NTU201902030

2-1-4 Rotating Packed Bed (RPB)

2-1-4-1 Features and Characteristics

In 1979, the rotating packed bed (RPB) was designed by Ramshaw and Mallinson for intensifying the mass transfer between the gas and the liquid in the distillation and absorption process. In the PRB reactor, the thinner liquid film and the smaller liquid drops can be provided by a high centrifugal force, which contributes to 10 to 100 times of mass transfer coefficient (Lin et al., 2011). Compared with the traditional packed bed (PB), the advantages of RPB reactor are concluded as follows:

a. RPB has better performance in micro-mixing and mass transfer.
b. RPB has higher flooding capacity that can be operated at the higher gas and liquid flow rates.
c. Smaller size of reactor is needed due to its high reaction rate. Thus, the capital and operation costs can be reduced. (Ramshaw, 1983)
d. RPB has higher self-cleaning ability to prevent blocking in packing material.

The RPB reactors can be divided into 3 categories according to flowing direction of gas and liquid as in figure 2-4. In the countercurrent type, the liquid is sprayed from the center of the RPB and move outward through the packing materials. In the meanwhile, the gas flows inward from the outer edge of RPB and react with the liquid drops. In the co-current type, the liquid and the gas move outward from the center of the reactor spontaneously. In the cross-flow type, the gas moves from the bottom to the top of the reactor and intersect with the liquid flow orthogonally.

doi:10.6342/NTU201902030

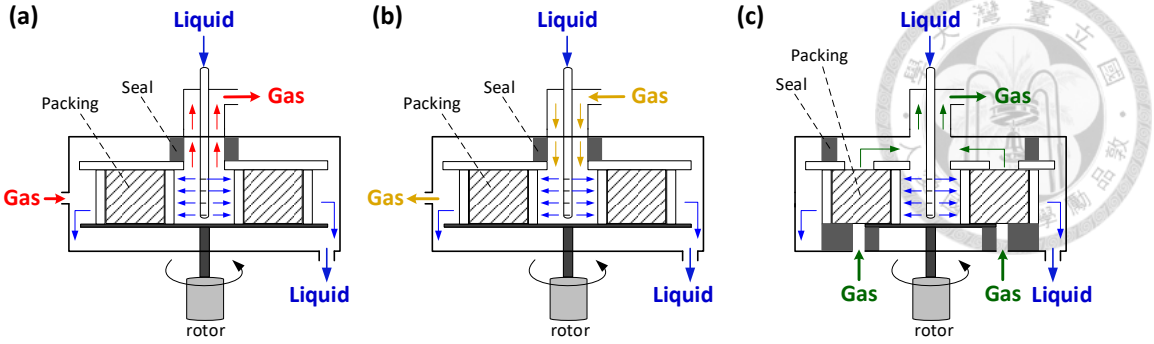

Figure 2-4 Various Types of RPB Reactors: (a) Countercurrent flow, (b) Co-current flow, (c) Cross-flow.

2-1-4-2 Mass transfer Coefficient

Mass transfer coefficient of liquid-gas reaction is based on *two-film theory*. In this theory, the area near the liquid-gas interface can be divided into parts as bulk liquid, liquid film, gas film, and bulk gas. Molecules in the bulk phase are assumed to move by convection and mass transfer in the film is assumed to be diffusion motivated by concentration gradient. The overall mass transfer coefficient of gas in this theory can be expressed as:

$$\frac{1}{K_{OG}} = \frac{1}{K_G} + \frac{H}{K_L} \tag{2-3}$$

where K_{OG} is the overall mass transfer coefficient, H is the Henry's law constant, K_G is the mass-transfer coefficient in the gas film, K_L is the mass-transfer coefficient in the liquid film. Owing to the solubility of CO_2, mass transfer in this reaction is controlled by the gas-film. Thus, K_{OG} can be regarded as K_G, and K_G may be estimated by eq. 2-4 (Liu et al., 2013):

$$\frac{K_G}{\mathcal{D}_G a_t} = 2Re_G^{0.7} Sc_G^{1/3} (a_t D_p)^{-2} \tag{2-4}$$

doi:10.6342/NTU201902030

where $\mathcal{D}_G$ presents the diffusion coefficient of the gas-film; D_p is the droplet diameter; a_t is the total surface area of packing materials. Then the gas-liquid surface area can be calculated by eq. 2-5 (Onda et al., 1968):

$$\frac{a}{a_t} = 1 - \exp[-1.45(\frac{\sigma_c}{\sigma})^{0.75} Re_L^{0.1} We_L^{0.2} Fr_L^{-0.05}] \quad (2\text{-}5)$$

Dimensionless numbers in (2-4) and (2-5) is listed as follow:

Reynolds number: $Re_L = \frac{L}{a\mu_L}$

Schmidt number: $Sc_L = \frac{\rho_L}{\mu_L g}$

Grashof number: $Gr_L = g{d_p}^3(\frac{\rho_L}{\mu_L})^2$

Froude number: $Fr_L = \frac{{\mu_g}^2}{\varepsilon^2 g\delta}$

Weber number: $We_L = \frac{{\mu_g}^2 \delta \rho_L}{\varepsilon^2 \sigma_L}$

where a is the wet surface area of packing material; μ_L is the viscosity of the liquid agent. Then the RPB sizes and operation parameters can be determined by $K_G a$ in eq. 2-6:

$$K_G a = \frac{Q_G}{\pi Z({r_o}^2 - {r_i}^2)} NTU = \frac{Q_G}{\pi Z({r_o}^2 - {r_i}^2)} \ln(\frac{Y_i}{Y_o}) \quad (2\text{-}6)$$

and HTU in rotating packed bed can be obtained as eq. 2-7 (Cheng and Tan, 2011):

$$HTU = \frac{r_o - r_i}{ln(\frac{Y_i}{Y_o})} \quad (2\text{-}7)$$

where r_o and r_i is the outer and inner diameter of the packing material; Z is the height of the packing material, and Y_i and Y_o is the concentration of gas at inflow and outflow. According to the experimental results of Pan et al., the performance during the *High-Gravity Carbonation Process*, such as carbonation conversion yield and the reaction rate is proven to be better than other traditional methods.

doi:10.6342/NTU201902030

2-2 Alkaline Waste from Steelmaking

Steelmaking industry plays an important role of economic development. However, different kinds of wastes are produced simultaneously which are difficult to deal with. Figure 2-5 elaborates the procedure of steelmaking, including consistent operation of steelmaking and electric arc furnace steelmaking. The detailed principles and procedures will be shown in this section.

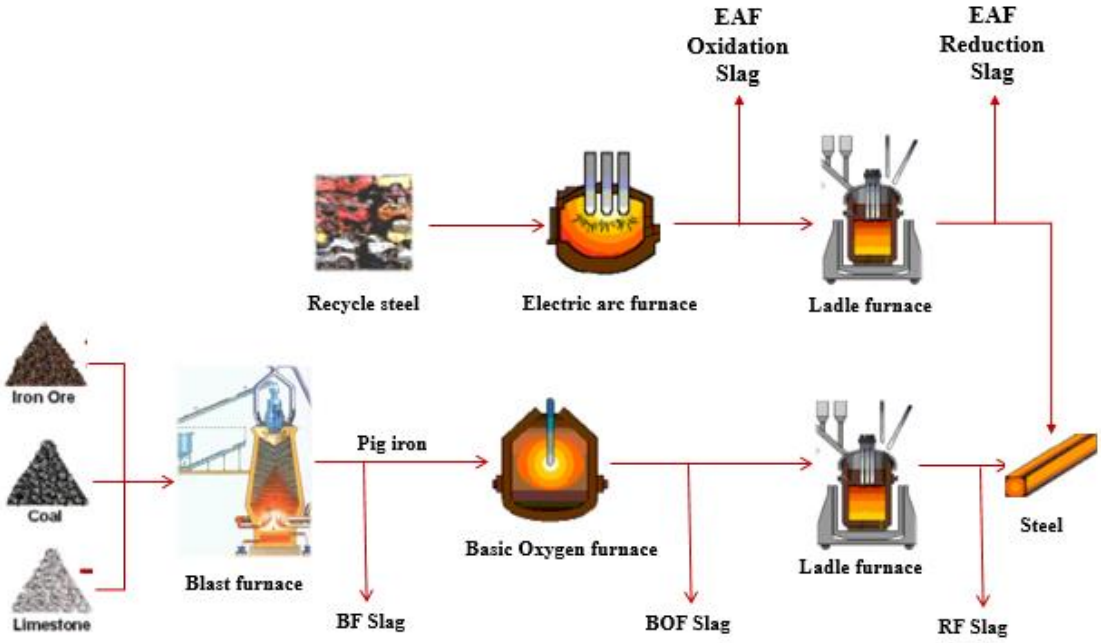

Figure 2-5 Steelmaking Procedure

doi:10.6342/NTU201902030

2-2-1 Blast Furnace

A blast furnace (BF) is a type of metallurgical furnace used for smelting to produce industrial metals, generally pig iron. In a blast furnace, fuel (coke), ores, and flux (limestone) are continuously supplied through the top of the furnace and stack alternately. In the meanwhile, air with oxygen enrichment reacts with coke to produce carbon monoxide and heat as in eq. 2-8.

$$C + O_2 \rightarrow CO + heat \tag{2-8}$$

After that, the hot blast air is blown into the lower section of the furnace and reacts with the material falls downward as in eq. 2-9 to 2-11.

$$Fe_2O_3 + 3CO \rightarrow 2Fe_3O_4 + CO_2 \tag{2-9}$$

$$Fe_3O_4 + CO \rightarrow 3FeO + CO_2 \tag{2-10}$$

$$FeO + CO \rightarrow Fe + CO_2 \tag{2-11}$$

As the material travels downward, the counter-current gases both preheat the feed charge and decompose the limestone to calcium oxide and carbon dioxide. The calcium oxide can react with various acidic impurities in the iron (notably silica) to form a calcium silicate slag.

$$CaCO_3 \overset{\Delta}{\rightarrow} CaO + CO_2 \tag{2-12}$$

$$SiO_2 + CaO \rightarrow CaSiO_3 \tag{2-13}$$

After the reaction, the molten iron and blast furnace slag are tapped from the bottom separately. Molten iron produced by the blast furnace is called the pig iron, which contains carbon more than 2 percent. Unfortunately, carbon in the pig iron makes

doi:10.6342/NTU201902030

it hard and brittle, which is hard to forge and process. Thus, another process is needed to purify the impurities, such as carbon, sulfur, and phosphorus in the pig iron.

Slag from BF can be divided into two categories according to the differences of the cooling procedure. The slag cooling naturally after being taken out from the BF is named as the *air-cooling blast furnace*, and it can be used as concrete aggregate after being crushed and graded due to its hardness and strength. The properties of the slags vary with their composition and the rate of cooling. Acid slag generally produces a denser aggregate, and basic slag tends to produce a vesicular or honeycombed structure with a lower apparent specific gravity. On the whole, the bulk density of air-cooling slag typically ranges from 1120 to 1360 kg/m^3, which is between the normal-weight natural aggregate and structural lightweight aggregate.

Another category of BF slag is called the *water-quenching blast furnace slag*, which is rapidly cooled by the high-pressured water after being obtained from the BF. Glassy surface and amorphous structure are developed in this type of slag due to the rapid cooling procedure. Since the defects and element replacement in the crystal may cause activity, grounded water-quenching blast furnace slag is weakly cementitious and pozzolanic, which can be used as a kind of mineral admixture in concrete to improve the strength development.

doi:10.6342/NTU201902030

2-2-2 Basic Oxygen Furnace

Basic oxygen furnace is the place where turns the molten pig iron into steel by an oxygen converter process. As mentioned above, the pig iron produced from the blast furnace is rich in carbon due to cokes added as reducing agents and fuels. Among the constitution of pig iron, carbon mainly exists as iron carbide (Fe_3C) which makes the pig iron brittle and hard. In order to solve this problem, process is used to improve the tenacity of iron and makes it easier to forge. In the oxygen converter process, oxygen is blown into the molten pig iron to reduce the carbon content and changes it into low-carbon steel.

In addition, chemical base materials such as burnt lime and dolomite are added as fluxes to lower the melting point and absorb the impurities in the molten iron to form slag. The BOF slag is rich in calcium silicates, which are similar to the clinker of Portland Cement. The slag after rapid cooling may generate cementing ability that can be regarded as a kind of pozzolanic material in the concrete. In addition, BOF slag can be used as aggregate of Portland concrete or asphalt concrete due to its abrasion rate and soundness. However, free-CaO and free-MgO in the slag may cause expand after reacting with water that modification or stabilization should be adopted before using.

The content of sulfur and phosphorous in the BOF molten steel may be to high because they are hard to be removed in a oxygen-rich condition. Therefore, another refining process is needed to improve its purity. During the process, molten steel is first placed in a ladle furnace. Desulfurizer such as calcium alloy (CaSi) or $CaO\text{-}Al_2O_3\text{-}CF_2$

doi:10.6342/NTU201902030

are added after that to combine with sulfur. After cooling, CaO-FeO is added to bind with phosphorous.

2-2-3 Electric Arc Furnace

Instead of using ores as raw materials in consistent operation of steelmaking, the electric arc furnace (EAF) process smelts the ferrous scrap by means of an electric arc to produce steel. Thus, the EAF process has a lower fuel consumption and CO_2 emission. Moreover, comparing with the BF cannot vary their production by much, the EAF is more flexible in steelmaking due to it can be rapidly started and stopped to vary production according to demand. However, impurities in ferrous scrap such as sulfur, phosphorous or even organic materials may affect the quality of steel, so other processed is needed to purify them.

The EAF process can be divided into three periods: melting, oxidation and reduction. At the beginning, ferrous scrap and flux such as lime or dolomite are added into the EAF. After the roof and the graphite electrodes moving down, electrical energy is supplied to melting operations. During the melting period, lime and ores are added appropriately to remove prosperous and fluorite is added to enhance the fluidity.

Once all of the scrap is melted, oxidant is added for further dephosphorization and decarburization. In the early stage of the oxidation period, iron ore and lime would react with phosphate as eq. 2-14 and 2-15:

$$5FeO + 2Fe_3P \rightarrow P_2O_5 + 11Fe \quad (2\text{-}14)$$

$$P_2O_5 + 3CaO \rightarrow 3\mathrm{CaO} \cdot P_2O_5 \quad (2\text{-}15)$$

doi:10.6342/NTU201902030

Later, the EAF is heated to 1550℃ and the oxygen and the iron ore are added into the furnace to oxidize the residual carbon. The reaction is shown in eq. 2-16 and 2-17:

$$C + O \rightarrow CO \quad (2\text{-}16)$$

$$FeO + C \rightarrow Fe + CO \quad (2\text{-}17)$$

The impurities after reaction may float on the top of the melting phase and combine to form the *oxidation slag*. Due to its hardness, high density and abrasion resistance, the slag through the removing, cooling and sorting processes can be used as asphalt concrete aggregate.

After all of the oxidation slags are removed, the melting steel is transferred to a ladle furnace for reduction and refining. The most important task in this period is deoxidation and desulfurization by adding manganese, lime, fluorite, silicates and toner. As the reduction reaction proceeds, a thin layer of *reduction slag* is formed gradually. Different with the oxidation slag, the reduction slag has a higher calcium and lower iron contents. Owing to the free-CaO and free-MgO may cause expansion during absorption of moisture, the reduction slag has to be stabilized before utilization.

doi:10.6342/NTU201902030

2-3 Cement Chemistry

Hydraulic cement is a gel-material for binding aggregates. After water added, the cement will harden gradually hydration reaction. Compare to other kinds of cement, Portland Cement (PC) has higher durability and lower manufacturing cost. The most popular category of Portland cement is type I which is widely used in driveway, railway, military constructions. There are four other derivative types that applicable to different scenarios. Table 2-6 lists the properties of utilizations of typical Portland cements.

Table 2-6 Summary of the Characteristics and Utilizations of Portland Cements

Class	Property	Implementation
Type I	Non-specific requirement	Regular construction
Type II	Moderate sulfate resistance and hydration heat	Drainage, Foundations
Type III	High early strength	Cold-weather constructions
Type IV	Low hydration heat	Massive construction
Type V	High sulfate resistance	Foundations in high-sulfate soils

doi:10.6342/NTU201902030

2-3-1 Composition of Portland Cement Clinker

The principal feedstock of Portland cement are limestone and clay, which provide calcium and silica-alumina respectively. During the process of heating raw materials to 1450 ℃, clinker materials will be crystallized according to the following sequences:

1. Moisture in the raw materials will be removed at 100℃
2. Crystallization water will be removed and the raw materials are decomposed to SiO_2 and Al_2O_3 at 400 to 600℃.
3. Calcium carbonate in limestone will be decomposed into calcium oxide and carbon dioxide at about 800℃. Later, CaO will combine SiO_2 to form dicalcium silicate (C_2S, $2CaO{\cdot}SiO_2$).
4. CaO starts to combine Al_2O_3 and Fe_2O_3 to form tricalcium aluminate (C_3A, $3CaO{\cdot}Al_2O_3$) and tetracalcium aluminoferrite (C_4AF, $CaO{\cdot}Al_2O_3{\cdot}Fe_2O_3$) at 900 to 1100℃.
5. Compounds start to melt into the liquid phase and the C_2S can combine the melting lime to create tricalcium silicate (C_3S, $3CaO{\cdot}SiO_2$) at 1200 to 1450℃
6. The products from the rotary kiln are rapidly cooled down to ensure the stability of β-C_2S, and the gypsum is added to control the setting time of the clinker. Finally, the clinker is ground into powder to store.

In these components of the clinker, C_3S make up most of the total mass, even up to 55% of all. It plays the most important role not only in strength development due to its high hydration rate but also in producing high strength hydration products. Thus, C_3S content is adjusted in type III and type IV PC to control the strength development

doi:10.6342/NTU201902030

rate and hydration heat. The structure of C_3S is the crystallization of isolated silicon oxygen tetrahedron and calcium ions. C_3S crystal structures at different temperatures are listed as below:

$$T_1 \overset{620\,℃}{\longleftrightarrow} T_2 \overset{920\,℃}{\longleftrightarrow} T_3 \overset{980\,℃}{\longleftrightarrow} M_1 \overset{990\,℃}{\longleftrightarrow} M_2 \overset{1060\,℃}{\longleftrightarrow} M_3 \overset{1070\,℃}{\longleftrightarrow} R$$

Where T corresponds to triclinic, M to monoclinic, R to rhombohedral. According to the unbalance of coordination, C_3S is relatively active, which can react with water molecules faster than C_2S.

C_2S in cement is divided into three categories according to temperatures and the cooling rates. α-C_2S is formed in high temperature and turns to β-C_2S and γ-C_2S during cooling.

$$\gamma \overset{500\,℃}{\longleftrightarrow} \beta \overset{650\,℃}{\longleftrightarrow} \alpha'_L \overset{1160\,℃}{\longleftrightarrow} \alpha'_H \overset{1425\,℃}{\longleftrightarrow} \alpha$$

Among them, β-C_2S is the major strength contributor to the final strength for cement and concrete due to its unbalance of coordination. However, C_2S will turn into γ phase, which is formed during natural cooling and is too stable to react with water. In addition, 10% of volume expansion will occur during the phase change from β to γ. Thus, rapid cooling of the clinker to keep C_2S in the β phase is important.

C_3A, usually existing in vitreous texture, also plays an important role in the early strength development due to its hydration reaction, which can arise immediately. However, rapid hydration may not only cause flash setting to reduce the workability but also produce a great amount of heat liberation. What's more, hydration product of C_3A can't provide enough strength, which may cause defect in the cement and concrete structure. To prevent the disadvantage of C_3A reaction, gypsum is added to react with

doi:10.6342/NTU201902030

C_3A and form ettringite (AFt, $C_3A{\cdot}3CaSO_4{\cdot}32H_2O$) and monosulfoaluminate (AFm, $C_3A{\cdot}CaSO_4{\cdot}12H_2O$).

The formation of C_4AF is similar to C_3A, which can be regarded as a solid solution of C_2A-C_2F. Because the hydration reaction of C_4AF can be decelerated significantly, its heat liberation is lower than C_3A, which can prevent exothermic expansion of mass concrete. Additionally, hydration products from C_4AF and gypsum have better sulfate resistant compared with those from C_3A. Although C_4AF isn't considered to be a strength contributor to cement and concrete, Bytt et al. pointed out that ions such as V^{5+}, Ti^{4+}, Mn^{4+} exchanged Fe^{3+} in the crystal may improve the hydraulic activity to enhance the strength development of C_4AF.

Except for major compositions mentioned above, there are still other minor compositions in the clinker, which may influence the durability of cement. During the calcination process of the clinker, partial of lime doesn't combine other raw materials. Besides, a small amount of C_3S may decompose into C_2S and CaO during the cooling process. These two types of CaO which exist in the clinker are also called free-CaO, which will cause fatal expansion after hydration. Similarly, free-MgO in the clinker can also react with water, which also produces the same effect to damage the microstructure of the cement.

Another important minor composition in the clinker is alkali, which includes sodium and potassium. During the hydration, Alkali ions can react with silicates and aluminates in the aggregates to form Na_2SiO_3 gel, which may expand after water absorption.

doi:10.6342/NTU201902030

2-3-2 Properties of Fresh Concrete

The properties of fresh concrete can be discussed in workability and the setting time. The workability influences the adhesion between concrete and templates to avoid structural defects caused by cavities. However, the workability tests of cement and concrete are usually empirical and it is hard to compare results from one test to another. Fortunately, rheology provides a fundamental measurement for flowing. By comparing the linear regression results between different samples and Portland Cement, chemical admixtures are considered to be added for fluidity adjustment.

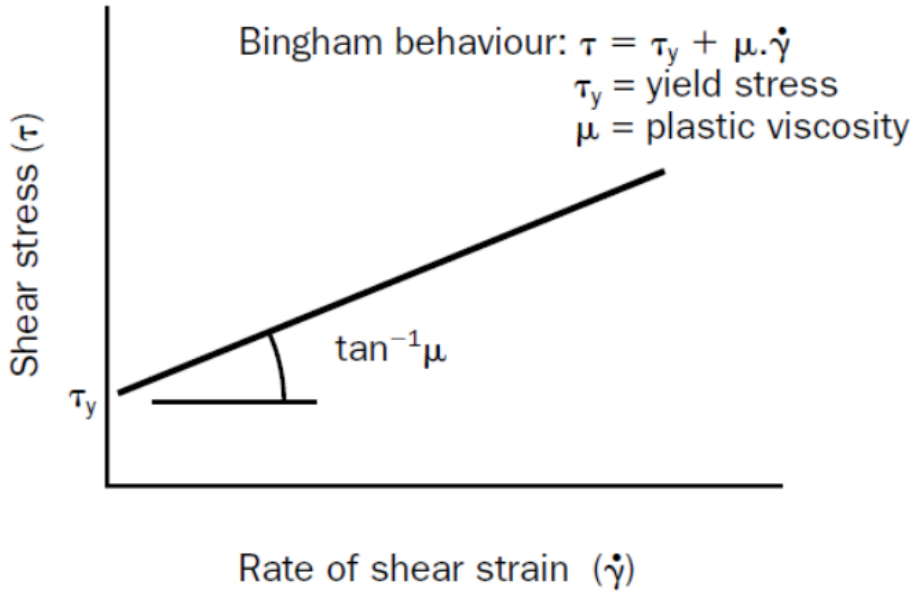

Figure 2-6 Correlation Between Shear Strain Rate and Shear Stress

Apart from workability, setting time also plays an important role in the properties of the fresh concrete. An appropriate setting time not only ensures that concrete can maintain in plasticity during transporting and pouring but also demonstrates that the strength can be built in a period of time. Calcium silicates, which make up more than

doi:10.6342/NTU201902030

80% of mass, play an important role in cement hardening. The hydration reaction of C_3S and C_2S is shown in eq. 2-18 and 2-19:

$$2C_3S + 6H \rightarrow C_3S_2H_3 + 3CH \quad (2\text{-}18)$$

$$2C_2S + 4H \rightarrow C_3S_2H_3 + CH \quad (2\text{-}19)$$

However, C_2S compared with C_3S is less active to hydrate. Therefore, its contribution to setting can be neglected. The hydration model of C_3S proposed by *Young and Skany* is divided into five processes as table 2-7:

Table 2-7 Hydration Processes of C_3S

Stage	Rate Determining Step	Rate	Properties Related to Concrete
I	Dissociation	Fast	
II	Nucleation	Slow	Initial Setting Time
III	Hydration reaction	Fast	Final Setting Time
IV	Hydration and Diffusion	Moderate	
V	Diffusion	Slow	Compressive Strength

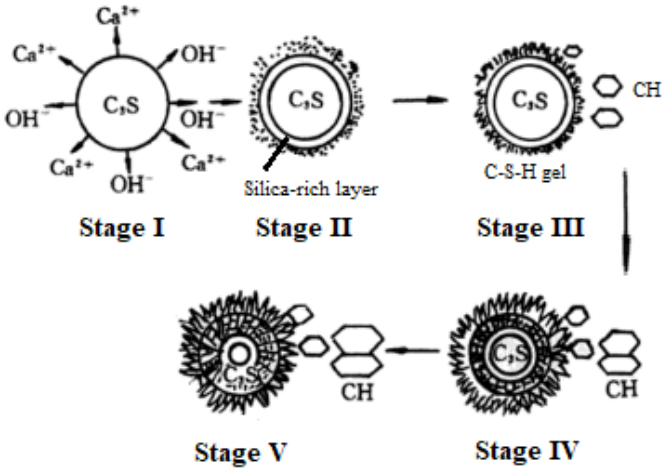

Figure 2-7 Schematic Diagram for Different Hydration Stage of C_3S

doi:10.6342/NTU201902030

- Stage I: Once the water is added to react with calcium silicates, Ca^{2+} and OH^- start to dissociate accompanying heat release. As the concentration of leached ions in the liquid phase raise, the dissociating rate decelerates continuously. After reacting for about 15 minutes, the reaction is almost stopped and starts to enter stage II.
- Stage II: A silica-rich layer is formed at the outer parts of C_3S granules due to the continuously dissociating of Ca^{2+} and OH^-. In the meanwhile, the dissociation rate of ions is restricted by the impermeability of the silica-rich layer. At the latter part of this stage, ions in the liquid phase have already reached supersaturated and $Ca(OH)_2$ starts to nuclear. In engineering, transporting and pouring should be done in stage II due to its plasticity. The time length of stage II also influents the initial setting time of cement.
- Stage III: After reaching to a certain extent of supersaturate, Ca^{2+} and OH^- in the liquid phase start to form $Ca(OH)_2$ crystal. In the meanwhile, Ca^{2+} also react with the silica-rich layer to from C-S-H gel. There is another exothermic peak in stage III due to the rapid reaction rate of C-S-H gel and $Ca(OH)_2$ formation.
- Stage IV: After rapid reacting for 4 to 8 hours, the C-S-H gel formation from the reaction is coated on the surface of C_3S granule to obstruct the water diffusion. Thus, fresh C_3S in the inner part of the granule is hard to react with water, so the C-S-H gel formation reaction starts to decelerate.
- Stage V: After 12 to 24 hours, the hydration reaction tends to be stable and the total reaction is controlled by water diffusion.

doi:10.6342/NTU201902030

Except C_3S, C_3A can also influence the setting time with its high tendency to interact with water. The direct hydration of C_3A is shown as eq. 2-20, accompanying with a great amount of heat released.

$$2C_3A + 27H \rightarrow C_4AH_{19} + C_2AH_8 \quad (2\text{-}20)$$

Hydration of C_3A will make the cement and concrete harden rapidly, which is hard to operate in engineering. Furthermore, C_4AH_{19} and C_2AH_8 will turn into C_3AH_6, which may cause strength attenuation. Thus, gypsum is added in the cement to form ettringite and monosulfoaluminate as eq. 2-21 and 2-22 in order to extend the setting time and enhance the durability.

$$C_3A + 3C\bar{S}H_2 + 26H \rightarrow C_6A\bar{S}_3H_{32} \quad (2\text{-}21)$$

$$2C_3A + C_6A\bar{S}_3H_{32} \rightarrow 3C_4A\bar{S}H_{12} \quad (2\text{-}22)$$

Attention must be paid to the differences of setting caused by adding various amounts of gypsums. For example, scarcity of gypsum may cause flash setting, which hardens and releases a great amount of hydration heat in a short time. The setting processes between different scenarios of C_3A activity and SO_4^{2-} concentration is expressed in table 2-8.

doi:10.6342/NTU201902030

Table 2-8 Setting Processes Between Different Scenarios

Activity of C_3A	SO_4^{2-} in solution	Hydration Time			
		<10 min	10-45 min	1-2 h	2-4 h
Low	Less	Plastic 	Plastic 	Plasticity decrease 	Setting 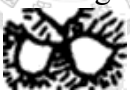
High	Much	Plastic 	Plasticity decrease 	Setting 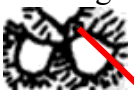	
High	Less	Plastic 	Fast Setting 	Ettringite formation	
High	Less or none	Flash Setting 	Monosulfoalumiate formation		
Low	Much	False Setting 	Crystallization of dehydrated gypsum		

doi:10.6342/NTU201902030

2-3-3 Properties of Harden Concrete

The properties of harden concrete are discussed in strength development and durability. Strength development especially compressive strength is the most important item for evaluating the concrete. Among all kinds of operation factors, composition of the reactant influents most significantly to the strength. When water is added, a set of chemical reactions named hydration occur between water and cement clinkers. Gradually, the products of hydration began to fill in the void among the aggregates on the course of hydration, giving a solid block with high uniformity. As mention above, C_3S hydrates more rapidly than C_2S due to its unbalance of coordination, which results in the fact that C_3S contributes strengths in both early and late ages while C_2S is only responsible for long-age strength development.

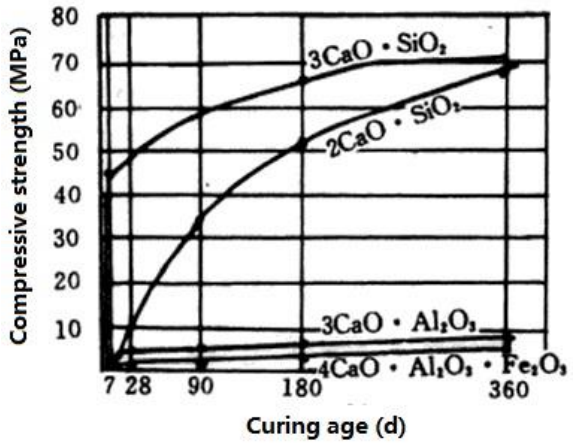

Figure 2-8 Strength Development of Different Minerals in Clinker

Except the composition of reactant, other properties also have significant influence on strength. For instance, W/C ratio and porosity also have an adverse influence on strength. The empirical relationships raised by *Powers* between W/C, hydration degree and the strength of cement paste is expressed as eq. 2-23:

doi:10.6342/NTU201902030

$$\sigma = \sigma_0[0.68\alpha/(0.32\alpha + W/C)]^3 \quad (2\text{-}23)$$

where σ is the compressive strength of the cement paste, σ_0 is the theoretical strength of cement paste without porosity, which is about 237 MPa, α is the degree of hydration, W/C is the weight ratio of water to cement.

Another equation of porosity to the compressive strength of cement paste is proposed by Rossler and Odler:

$$\sigma = \sigma_0(1 - EP) \quad (2\text{-}24)$$

where E expresses the constant correlated to the porosity, P is the porosity of the paste.

Besides strength, durability also receives a great concern in modern cement industry. Factors which affect the durability of the concrete are listed in table 2-9. As this research is focused on the influence of adding carbonated alkaline wastes as mineral admixtures in the cement, only the free-CaO and free-MgO expansion, the sulfate expansion and the alkali-aggregate reaction are discussed in this section.

Table 2-9 Influenced Factors of Concrete Durability

Abrasion	Mechanical wear	
	Scour abrasion	
Physical erosion	Freeze-thaw cycle	
	Dry-wet cycle	
	Water penetration	
	Salt crystallization	
Chemical erosion	Chemical medium	Hydrolysis
		Displacement
		Sulfate erosion
	Composition of concrete	Alkali-aggregate reaction
		Free-CaO and free-MgO expansion
Reinforcement erosion	Neutralization of concrete by CO_2 in atmosphere	
	Chloride ion in concrete	

doi:10.6342/NTU201902030

As mention above, free-CaO is produced not only by the lime which doesn't combine other raw materials in the rotary kiln but also by the decomposition of C_3S during cooling. Additionally, most of the magnesium in the clinker is existed as the periclase crystal, which is also called the free-MgO. Free-CaO and MgO in the cement or other mineral admixtures will react with water and form calcium hydroxide and magnesium hydroxide, which cause 97.7% and 148% of expansion respectively after few days to months. To ensure the stability of concrete after hydrating, the amount of free-CaO is restricted under 1.5%. The proportion of free-CaO and MgO may exceed the regulation when choosing alkaline wastes as mineral admixtures. Thus, stabilization of these alkaline waste such as carbonation to improve the properties is essential.

Alkali-aggregate reaction (AAR) also affects the durability significantly. In the reaction as shown in eq. 2-25, the active silicate, such as opal, chert and chalcedony are attacked and decomposed by hydroxyl. The decomposed silicates would combine with sodium and potassium to produces alkali-silica gel, which would expanse significantly and stress the structure when excessive water exists. Therefore, the amount of alkali (Na_2O+0.66 K_2O) is restricted under 0.6% in the ASTM regulation.

$$2NaOH + nSiO_2 \rightarrow Na_2O \cdot nSiO_2 \cdot H_2O \quad (2\text{-}25)$$

As for sulfate attack, the aggressive sulfate from the surroundings would interact with calcium hydroxide and produce gypsum, which would further reacts with hydrated calcium aluminate and monosulfoaluminate to form ettringite as eq. 2-26 to 2-28.

$$Ca(OH)_2 + Na_2SO_4 + 2H_2O \rightarrow CaSO_4 \cdot 2H_2O + 2NaOH \quad (2\text{-}26)$$

$$3CaO \cdot Al_2O_3 \cdot CaSO_4 \cdot 12H_2O + 2CaSO_4 + 20H_2O$$

doi:10.6342/NTU201902030

$$\rightarrow 3CaO \cdot Al_2O_3 \cdot 3CaSO_4 \cdot 32H_2O \quad (2\text{-}27)$$

$$4CaO \cdot Al_2O_3 \cdot 19H_2O + 3CaSO_4 + 14H_2O$$

$$\rightarrow 3CaO \cdot Al_2O_3 \cdot 3CaSO_4 \cdot 32H_2O + Ca(OH)_2 \quad (2\text{-}28)$$

The concrete after reacting with sulfate will expand due to the ettringite has a larger crystal size, causing fatal damage of the structure. Moreover, if the surroundings has a higher magnesium concentration, magnesium and sulfates will decompose the calcium silicate and calcium hydroxide in the concrete as in eq. 2-29 and 2-30, creating defects in the structure.

$$Ca(OH)_2 + MgSO_4 + 2H_2O \rightarrow CaSO_4 \cdot 2H_2O + Mg(OH)_2 \quad (2\text{-}29)$$

$$3CaO \cdot 2SiO_2 \cdot nH_2O + 3MgSO_4 + mH_2O$$

$$\rightarrow 3(CaSO_4 \cdot 2H_2O) + 3Mg(OH)_2 + 2SiO_2 \cdot (m + n - 3)H_2O \quad (2\text{-}30)$$

doi:10.6342/NTU201902030

Chapter 3 Materials and Methods

3-1 Research Flow Chart

In this study, a systematic approach to determine the influence how the different steelmaking slags under the different operating conditions, including the rotating speed, liquid-to-solid ratio, particle size interact with the carbonation conversion rate is performed. This way, the best operating condition in engineering aspect is determined and the steelmaking slags before and after the carbonation are analyzed. Then the steelmaking slags are incorporated into the cement clinker at 5-15%. The tests include workability, strength, and durability. Finally, strength prediction models of mortar can be built by means of analyzing chemical composition and strength.

Figure 3-1 depicts the flow chart of this study, including carbonation process, cement replacement and strength prediction.

doi:10.6342/NTU201902030

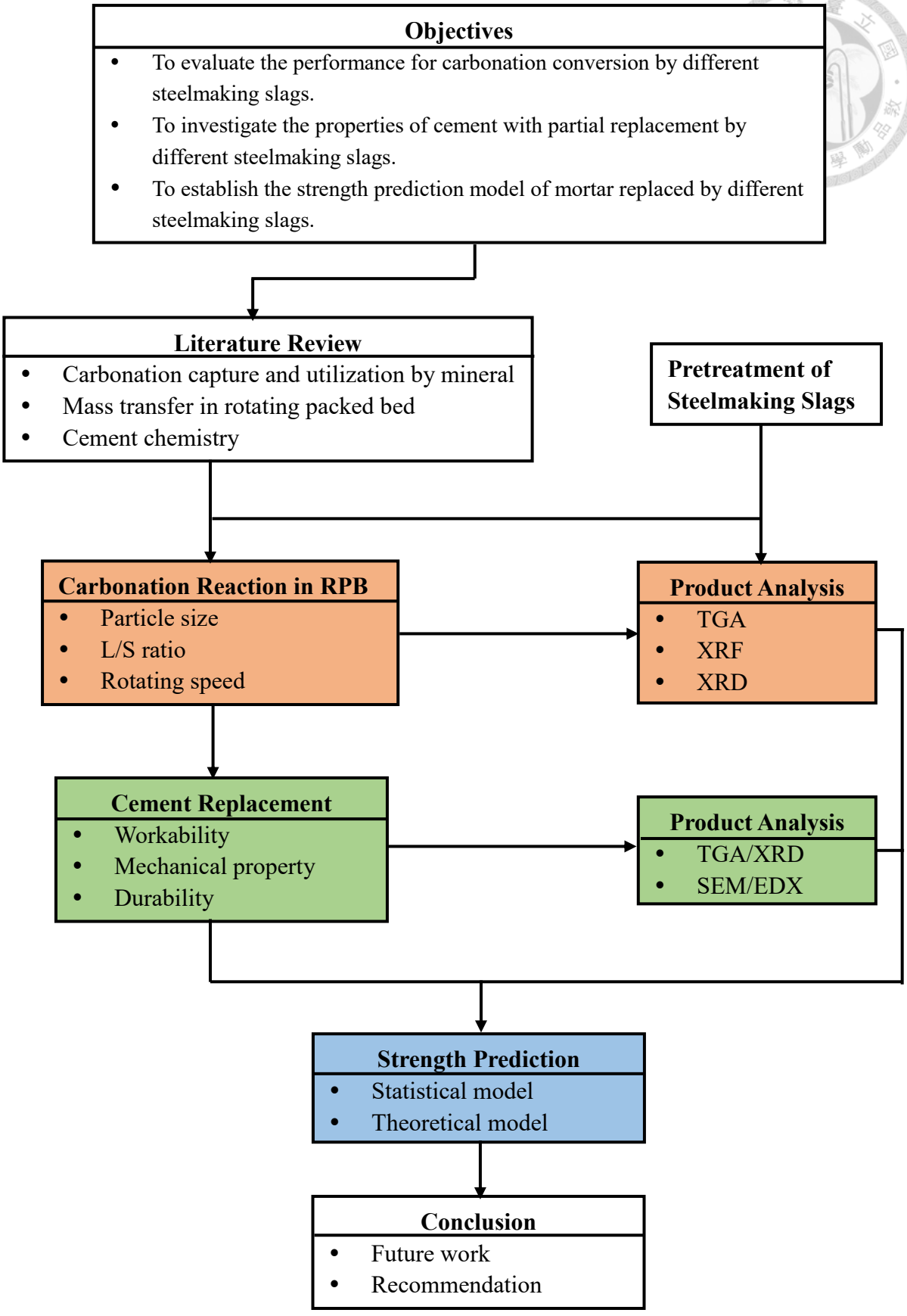

Figure 3-1 Research Flow Chart in This Study

doi:10.6342/NTU201902030

3-2 Materials

3-2-1 Source of Feedstock

There are many units which can produce alkaline wastes in the process of steel making, such as slags produced by blast furnace, basic oxygen furnace, electric arc furnace and steel refining facility. However, only ground granulated air-cooled blast furnace slag and water-quenched blast furnace slags are allowed to be used as aggregates and pozzolanic materials in concrete according to Taiwan's regulations. Other slags are confronted with the restriction of legislation due to their high alkalinity and toxicity, which may cause creaking of concrete and environmental pollution. In this research, basic oxygen furnace slag, refining slag, electric arc furnace slag were chosen to be used as feedstock for carbonation. Through the carbonation process, the disadvantage properties of slags can be improved and the way to utilization in concrete may be clarified.

Materials used in this study were obtained from the sources below:

1. Basic oxygen furnace slag (BOFS) and refining slag (RFS) were obtained from China Steel Corporation (CSC) in Kaohsiung, Taiwan.

2. Electric arc furnace reduction slags (EAFRS) and oxidation slags (EAFOS) were obtained from Tung Ho Steel Enterprise Corporation in Miaoli County, Taiwan.

doi:10.6342/NTU201902030

3. CO_2 with high purity (99.5%) was purchased from Ching-Feng Gas Corporation, Taipei, Taiwan.

4. Mass flow controller of CO_2 was purchased from Kaoduen Technology, Taiwan.

5. De-ionized water (DIW): Laboratory P.C. Chiang, Lab RB09, Graduate Institute of Environmental Engineering, National Taiwan University, conductivity = 18.24MΩ/cm.

3-2-2 Rotating Packed Bed (RPB)

The carbonation process was performed at the lab by a customized rotating packed bed to enhance the mass transfer efficiency. To promote the micro mixing of gas-stream and slurry and extend retention time, a maze-liked stainless steel packing has to be employed. The inner diameter, outer diameter and height of RPB in this study are 0.06, 0.205 and 0.04 meters respectively, and thus its volume is $1.2*10^{-3}m^3$. Additionally, the rotating speed ranges from 0 to 1820, corresponding to 118.9 times of gravity.

The size and characteristics of the reactors are shown in Table 3-1

doi:10.6342/NTU201902030

Table 3-1 Parameters of Rotating Packed Bed Used in This Study

Items	Units	Value
Rotational speed	rpm	0 ~ 1820
Gravity value	G	0 ~ 118.9
Inner radius (D_1)	m	0.06
Outer radius (D_2)	m	0.205
Mean radius(D_{mean})	m	0.132
Axial height (Z_B)	m	0.04
Volume (V_B)	m^3	$1.2*10^{-3}$

Pretreatment of Steelmaking slags

The Slags in this study provided from China Steel and Tung Ho Corp. were first crushed by a crusher into smaller pieces. Secondly, mill the slags into particle sizes below 250 μm with a ball mill. Finally, separate the slags into 5 ranges of particle size with sieves. From coarse to fine are: 150-250, 106-150, 75-106, 53-75, 0-53 μm. The pretreatment procedure is listed in Figure 3-2.

Figure 3-2 Material Preparation of Steelmaking Slags

doi:10.6342/NTU201902030

3-3 Equipment

3-3-1 Thermal Gravimetric Analysis (TGA)

Thermal gravimetric analysis (TGA, STA 6000, PerkinElmer) is a method of thermal analysis where the mass of a sample is measured over time during the temperature changes. This measurement provides information about physical and chemical phenomena. The former concludes phase transitions, absorption and desorption. The latter contains chemisorption, thermal decomposition, and solid-gas reactions. Each component in the solid sample will be decomposed in different temperature scales, which are regarded as the unique fingerprint for the component. Thus, the various substances can be determined by recognizing different decomposition temperature ranges.

Figure 3-3 TGA (STA 6000) used in this study

In this study, steelmaking slags after carbonation would be analyzed by calculating the weight loss from the thermal decomposition. Four zones of weight loss could be found in the curve of temperature to differential thermal gravity (DTG) in Figure,

doi:10.6342/NTU201902030

correspond to: (1) 50℃ to 105℃; (2) 105℃ to 380℃; (3) 380℃ to 500℃; (4) 500℃ to 900℃.

- Zone (1) is relative to moisture from the calcium sulphoalumiates and hexagonal tetracalcium aluminatehydrat (Marsh and Day, 1988).

- Zone (2) is associated with the decomposition of organic components (Jo, Park et al., 2014).

- Zone (3) is relative to pyrogenic decomposition of calcium hydroxide (Jo, Park et al., 2014).

- Zone (4) is associated with the decomposition of calcium carbonation (Chen et al.,2011).

To be more precise, weight loss from 650℃ to 850 ℃ are used in calculation.

3-3-2 Scanning Electron Microscope (SEM)

A scanning electron microscope (SEM) is a type of electron microscope that produces images of a sample by scanning the surface with a focused beam of electrons. The electrons interact with atoms in the sample, producing various signals that contain information about the sample's surface topography and composition. The morphology investigations of steelmaking slags and mortars were performed with a scanning electron microscope (SEM) (JIB-5410, JEOL) in this study. The surface topography, composition, and electrical conductivity could be observed by SEM. The detail

doi:10.6342/NTU201902030

distributions of the elements in samples were also detected by energy dispersive x-ray spectroscopy (EDX), which can identify $CaCO_3$ on the surface of slag and cement. Therefore, the performance of $CaCO_3$ precipitation can be evaluated by comparing the SEM images of fresh and carbonated slags and mortars.

Figure 3-4 Scanning Electron Microscope (SEM)

Figure 3-5 Energy Dispersive X-ray Spectroscopy (EDX)

doi:10.6342/NTU201902030

3-3-3 X-Ray Fluorescence (XRF)

X-ray fluorescence (XRF) is the emission of characteristic "secondary" (or fluorescent) X-rays from a material that has been excited by bombarding with high-energy X-rays or gamma rays. The phenomenon is widely used for elemental analysis and chemical analysis, particularly in the investigation of metals, glass, ceramics and building materials. The electrons in the inner layer can be excited by extra energy from the X-ray. After that, the outer layer electrons may transit to the inner layer to fill up vacancy and release a secondary X-rays (fluorescent) in the meanwhile. Different elements can be determined by the wavelength of fluorescent due to their specific energy bandgap. The obtained wavelength is calculated by Moseley's law:

$$\lambda = K(Z - s)\text{-}2 \tag{3-1}$$

Additionally, abundance of each element can be obtained from energy of fluorescent by quantum theory of light:

$$E = h\nu = hc/\lambda \tag{3-2}$$

doi:10.6342/NTU201902030

3-3-4 X-ray Diffractometer (XRD)

X-ray diffractometer (XRD) is a method that analyzes the diffraction pattern to obtain the material composition, the structure or morphology of the atoms or molecules inside the material. Crystals can be used as gratings for X-rays. The coherent scattering produced by these large numbers of atoms (atoms, ions, or molecules) will interfere with the light and thus increase or decrease the intensity of scattered X-rays.

In energy dispersive analysis, the X-rays diffracted by the material sample are directed into a detector, which produces a "continuous" distribution of pulses, and the voltages of which are proportional to the incoming photon energies. This signal is processed by a multichannel analyzer (MCA), which produces an accumulating digital spectrum processed to obtain analytical data. In wavelength dispersive analysis, the X-rays diffracted by the material sample are directed into a diffraction grating monochromator. The adopted diffraction grating is usually a single crystal. By varying the angle of incidence and take-off on the crystal, a single X-ray wavelength can be selected. The wavelength obtained is given by Bragg's law:

$$n \cdot \lambda = 2d \cdot sin(\theta) \tag{3-3}$$

doi:10.6342/NTU201902030

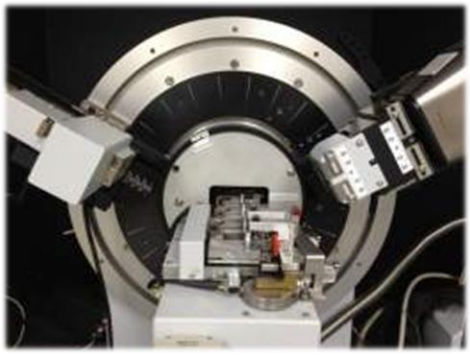

Figure 3-6 X-ray Diffraction (XRD)

3-4 Methods

3-4-1 Carbonation Conversion Process

In the beginning of this study, all of the steelmaking slags had to be analyzed by *X-ray fluorescence* (XRF) and *X-ray diffractometer* (XRD) to understand their chemical composition. After that, the experiment was designed and performed as the schematic set-up diagram in Figure 3-7.

All of the design of experimental factors in this study is shown in Figure 3-8. The pure CO2 steam flowed with a rate of 0.5 L/min and the slurry was pumped by peristaltic pump at the rate of 1L/min. All of the experiments were operated for 60 minutes. The operating parameters, including liquid to solid ratio (10 to 50 mL/g), rotating speed (700 to 1300 rpm), and particle size (32 to 160 μm), were evaluated on the performance of the carbonation reaction.

doi:10.6342/NTU201902030

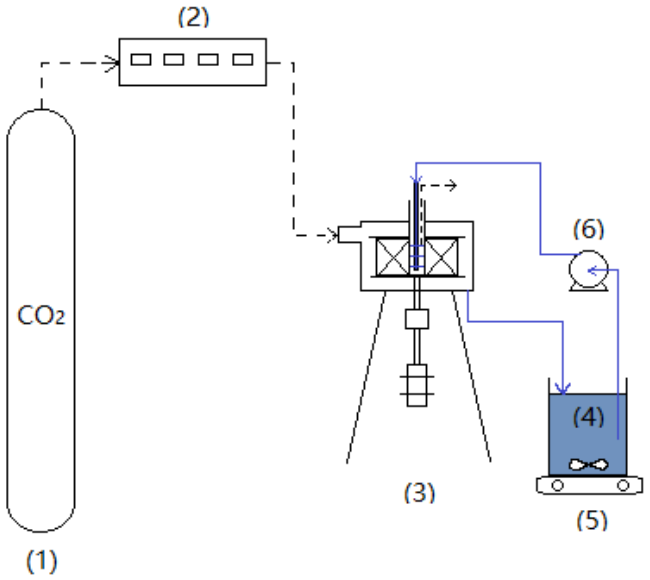

Figure 3-7 Schematic diagram of experimental set-up for carbonation in a RPB:

(1) CO_2 Cylinder; (2) Gas flow controller; (3) High-gravity RPB; (4) Slurry; (5) Stirring and Heating Machine; (6) Peristaltic Pump.

Firstly, high purity (99.5%) carbon dioxide gas flowed into the RPB reactor and the gas flow rate was adjusted by the gas flow controller. Secondly, the steelmaking slags and tap water was completely mixed with different L/S ratio in a beaker to create slurry. Thirdly, the slurry was pumped into the RPB reactor by a peristaltic pump. After entering the RPB reactor, the slurry was sprayed on the inner layer of the packing and moved outward by the centrifugal force. In the meanwhile, CO_2 flowed as a countercurrent dissolved and reacted in the slurry liquid drops. The reacted slurry was discharged from the bottom of the RPB back into the beaker to keep recycling, and the exhausted gas was expelled from the top of RPB. After a one-hour-process of

doi:10.6342/NTU201902030

carbonation, the slurry was filtered by a 0.45 μm filter paper and the filtered solid sample was dried in the oven (105℃, 24 hours) for the *thermal gravimetric analysis* (TGA) measurement to evaluate the carbonation conversion at different reaction time.

doi:10.6342/NTU201902030

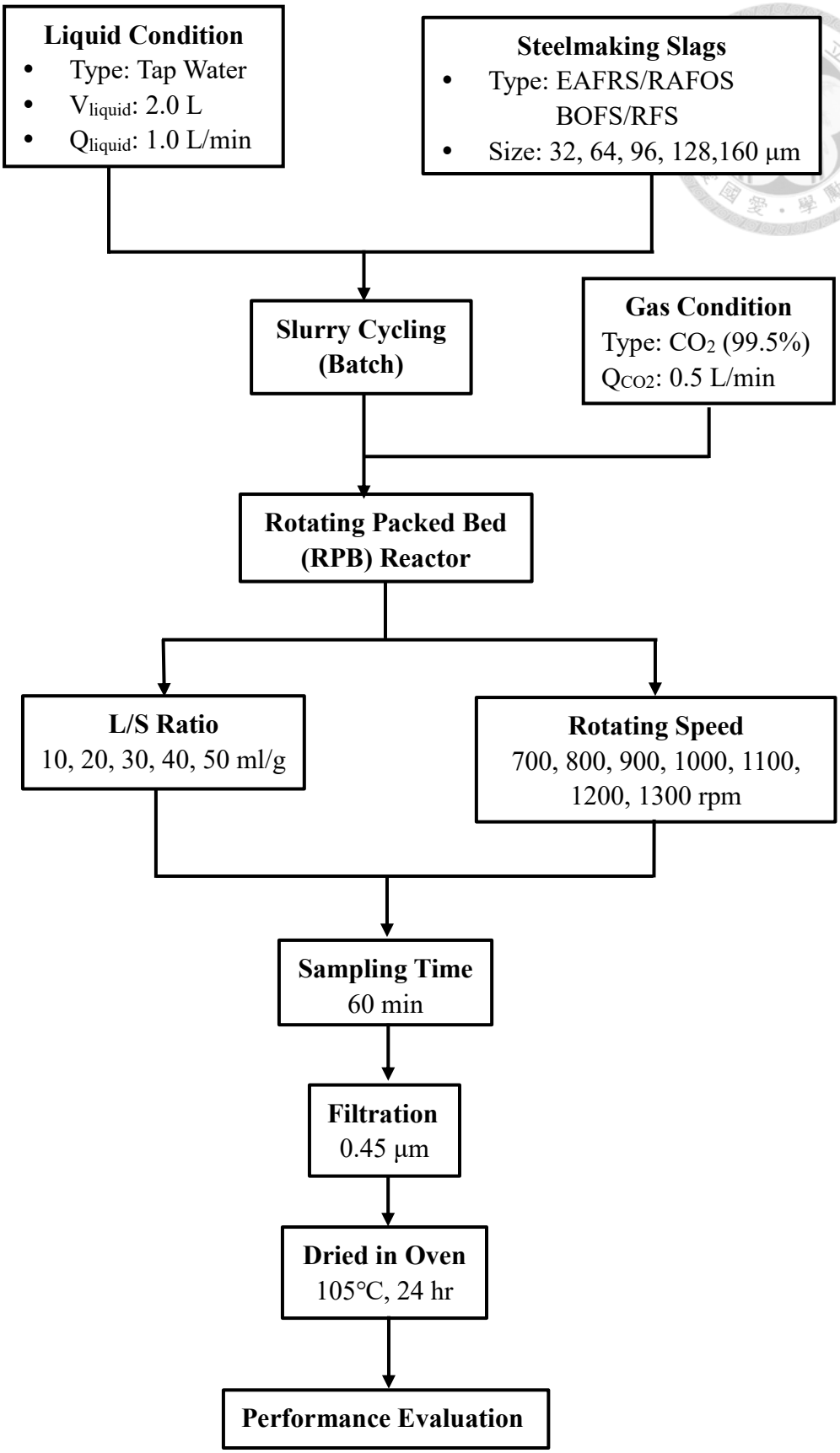

Figure 3-8 Designs of Experimental Factors in Carbonation Process

doi:10.6342/NTU201902030

During the analyzing procedure of TGA, the samples were heated directly from 50 to 900 °C at the heating rate of 10°C /min under pure nitrogen gas at 19.8 mL/min. After the samples were heated, a TG curve and DTG curve diagram could be obtained to provide the information on temperature at the maximum peak and other important peak parameter. By subtracting the weight loss from 650℃ to 850℃, where calcium carbonate was decomposed into carbon dioxide and calcium oxide, the amount of CO_2 captured in the carbonation process could be obtained by eq. (3-4):

$$CO_2(wt.\%) = \frac{\Delta m_{CaCO_3}}{m_{105℃}} \times 100 \quad (3\text{-}4)$$

Where CO_2 (wt.%) means the amount of CO_2 actually captured in the dry mass of each sample, Δm_{CaCO3} is the weight loss fraction due to the decomposition of $CaCO_3$, and $m_{105℃}$ is the weight without moisture. Thus, the CO_2 captured by slags could be expressed as the mass of CO_2 captured per mass of slags, which is shown in Eq. (3-5).:

$$\mathrm{CO_2\ uptake}\ (\%) = \frac{\mathrm{CO_2(wt\%)}}{100-\mathrm{CO_2(wt\%)}} \quad (3\text{-}5)$$

Additionally, the theoretical mass fraction of CO_2 capture achievable based on the composition of the fresh slags and stoichiometry was expressed as *$ThCO_2$*, which is shown in Eq. (3-6) with the assumption that all of the CaO could be transformed to $CaCO_3$.

$$\mathrm{ThCO_2(mol/kg)} = \frac{\mathrm{CaO_{total}(kg/kg)}}{\mathrm{MW_{CaO}(kg/mol)}} \quad (3\text{-}6)$$

doi:10.6342/NTU201902030

Where the MW_{CaO} is the molecular weights of CaO (kg/mol), CaO_{total} is the weight fraction of CaO of fresh slags analyzed by XRF. Consequently, the carbonation conversion yield could be estimated by Eq. (3-7):

$$\zeta_{Ca}(\%) = \frac{\frac{CO_2(wt\%)}{100-CO_2(wt\%)} \times \frac{1}{MW_{CO_2}(kg/mol)}}{THCO_2(mol/kg)} \quad (3\text{-}7)$$

The carbonation conversion yield (ζ_{Ca} (%)), was defined as the actually captured amounts of CO_2 in dry mass of carbonated feedstock with the calculated theoretical extent of carbonation based on the reactive-oxide content of feedstock.

3-4-2 Properties of Cement Replacement

In this study, the steelmaking slags ware utilized as cementitious material with a substitution ratio of 5 to 15%. However, utilization of fresh slags as cementitious material may cause fatal structural damage due to the existence of free-CaO and alkali metal oxides which will expand as the formation of calcium carbonate ($CaCO_3$) and alkaline-silica gel ($Na_2SiO_3 \cdot 2H_2O$). Thus, carbonation process was expected to be able to eliminate free-CaO and neutralized alkalinity to improve mechanical properties. In the experiment, the workability of cement pastes and mortars were first determined by the standard consistency, setting time, and flow test. Later, the best ratio of water to binding materials obtained from the workability test would be used for the strength test and the durability test. Figure 3-9 shows the flow chart of cement replacement experiment in this research.

doi:10.6342/NTU201902030

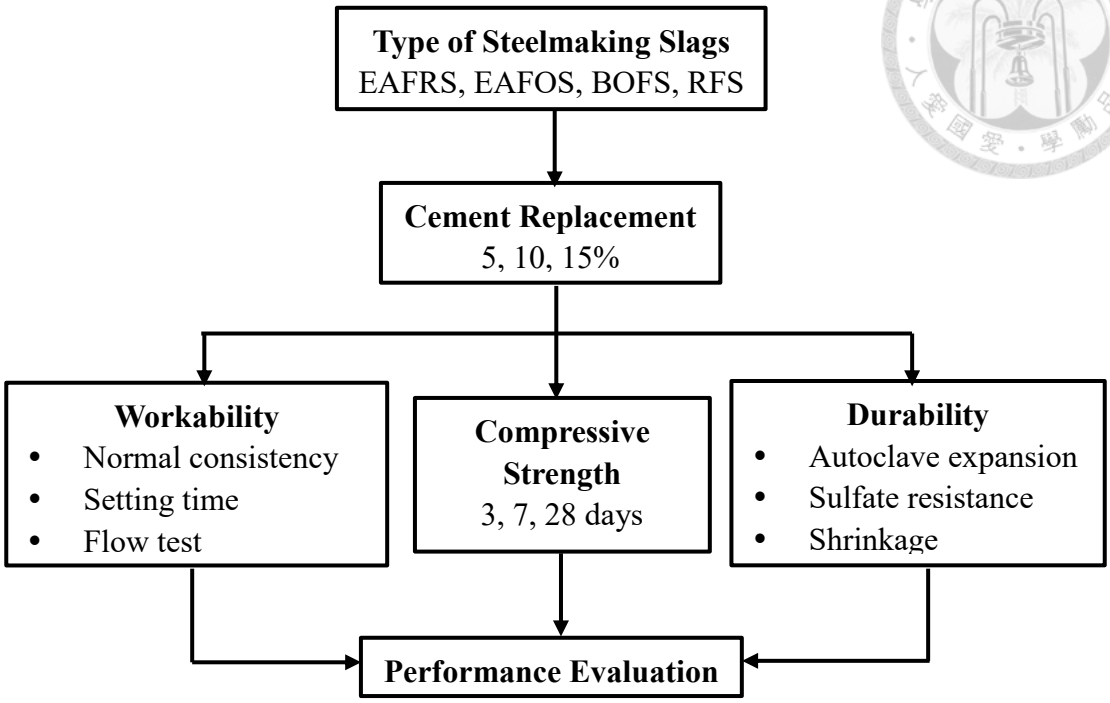

Figure 3-9 Flow Chart of Cement Replacement Experiment in this Research

3-4-2-1 Normal Consistency

According to Chinese National Standards (CNS) 3590, normal consistency is intended to be used to determine the amount of water required to prepare hydraulic cement pastes with normal consistency. The experiment was carried out in a *Vicat apparatus* which is depicted in Figure 3-10. The testing procedure is listed below:

a. Mix 650 g of cement with a specific amount of water by the standard of CNS 3655 to produce a cement paste.

b. Form the cement paste into an approximate ball and toss it six times through a free path of about 150 mm from one hand to another.

doi:10.6342/NTU201902030

c. Fill the conical specimen mold with cement paste sample and remove the excess.

d. Place the specimen mold on a glass plate on its larger end.

e. Lower the plunger to the cement surface. Tighten the set-screw. Then set the movable indicator to the upper zero mark of the scale.

f. Release the set-screw to let the plunger sink into the paste naturally.

g. Note the reading after 30 seconds.

h. Repeat the procedure until the reading sets within 10 ± 1 mm.

i. Calculate the ratio of water needed to cement added in weight.

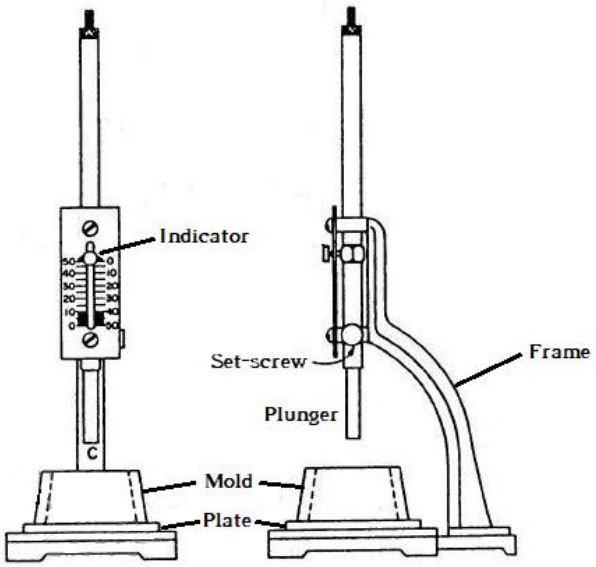

Figure 3-10 Vicat Apparatus for Normal Consistency Test

doi:10.6342/NTU201902030

3-4-2-2 Setting Time

Setting time is essential to cement because it determines the available time for construction before the cement solidified. The experiment was also carried out in a *Vicat apparatus* but introduced the *Vicat needle* instead of the plunger. The procedure of setting time test in this study was followed with the standard of CNS 786, which was listed as followed:

a. Prepare a cement paste and fill the specimen mold with it in the same way as the normal consistency (CNS 3590).

b. Rest the specimen in constant humidity environment for 30 min.

c. Perform the penetration test by lowering the needle of the rod until it rests on the surface of the cement paste.

d. Tighten the set-screw and set the indicator at the upper end of the scale.

e. Release the set-screw quickly to allow the Vicat Needle penetrate into the paste for 30 seconds.

f. Note the reading of penetration for every 15 minutes. Remember to make each penetration test at least 6 mm away from any previous penetration and at least 9 mm away from the inner side of the mold.

doi:10.6342/NTU201902030

g. Record the results of all penetration tests and determine the time when a penetration of 25 mm is obtained by interpolation.

h. The time between the first contact of cement and water and the penetration of 25 mm is termed as initial setting time.

i. Determine the Vicat final time of setting end point to be the first penetration measurement that does not mark the specimen surface with a complete circular impression.

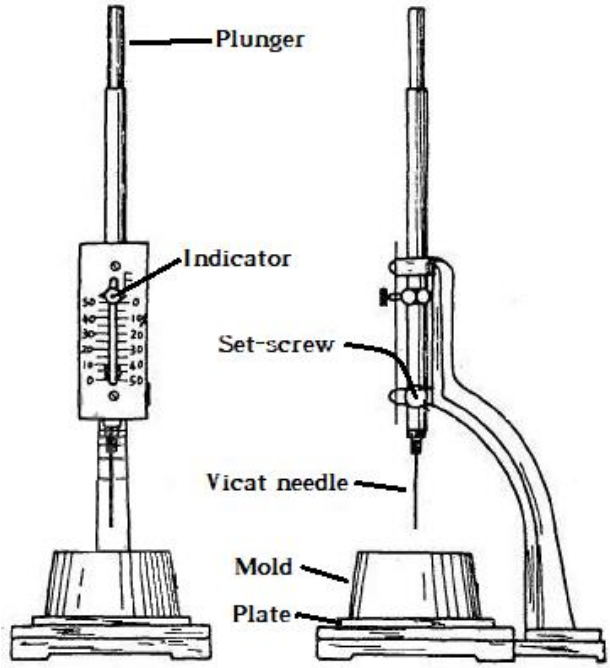

Figure 3-11 Vicat Apparatus for Setting Test.

doi:10.6342/NTU201902030

3-4-2-3 Flow Test

Flow test is designed to determine the flow of hydraulic cement mortars, and of mortars containing cementitious materials other than hydraulic cements. The test was performed on the flow table as Figure 3-12, following the guide of CNS 1010 and CNS 15992.

a. The standard mortar shall be mixed by 1 time of binder, including Portland cement and steelmaking slags, 2.75 times of graded standard sand, and 0.485 times of water by weight. The quantities of materials to be mixed at one time in the batch of mortar for making six test specimens included 500g of cement with steelmaking slags, 1375g of sand, and 242 ml of water.

b. The mixture of mortars were added into the stirring machine and operated by following the standard of CNS 3655.

c. Place a layer of mortar about 25 mm in thickness in the mold and tamp 20 times with the tamper and repeat it again to fill up the mold.

d. Lift the mold away from the mortar 1 min after completing the mixing operation. Immediately drop the flow table for 25 times in 15 seconds.

e. Measure the mean diameter of the mortar along the four lines scribed on the flow table.

f. Calculate the increase rate of diameter and express it as percentage.

doi:10.6342/NTU201902030

g. Repeat the procedure until fitting the result within 110 ± 5 %

i. Calculate the ratio of water needed to cement added in weight.

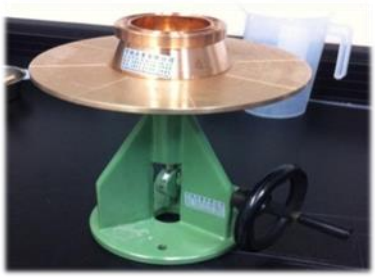

Figure 3-12 Flow Table for Flow Test in this study

3-4-2-4 Compressive Strength

Compressive strength indicates the maximum pressure that the mortar is capable of bearing. The test was carried out via compression machine and the procedure was in conformance to CNS 1010.

a. Apply a thin coating of release agent to the interior faces of the mold (cubic of 50 mm) and non-absorptive base plates and assemble the mold.

b. Prepare the mortar as the same way in the flow test (CNS 15992).

c. Fill the mold with mortar of 25 mm in thickness. Tamp the mortar in each cube compartment 32 times in about 10 s in 4 rounds, each round to be at right angles to the other and consisting of eight adjoining strokes over the surface of the specimen.

doi:10.6342/NTU201902030

d. Repeat procedure c. again to fill up the mold.

e. Immediately after molding, keep all test specimens in the molds in the moist closet or moist room for 20 to 24 hours with their upper surfaces exposed to the moist air.

f. Transform the specimens into saturated limewater immediately after removal from the moist closet. Prepare for compressive test by curing as age of 3, 7, 28 days.

g. Wipe out the water on the mortar specimen and smooth the uneven parts.

h. Adding compressive stress on the specimen until it collapsed. The process should be done in 20 to 80 seconds.

i. Record the data and calculate the average compressive strength of mortar specimen.

3-4-2-5 Autoclave expansion

The autoclave expansion test provides an index of potential delayed expansion caused by the hydration of CaO or MgO, or both, when present in hydraulic cement. The test was performed in autoclave following the guide of CNS 1258:

a. Prepare the cement paste in the same way to standard consistency.

b. Mold the test specimen in two approximately equal layers, each layer being compacted with the thumbs or forefingers by pressing the paste into the corners, around the gauge studs, and along the surface of the mold until a homogeneous specimen is obtained.

doi:10.6342/NTU201902030

c. Compact the top layer, cut off the paste flush with the top of the mold with a thin-edged trowel, and smooth the surface with a few strokes of the flat trowel.

d. At 24 h ±30 min after molding, remove the specimens from the moist atmosphere.

e. Immediately obtain a length comparator reading for each specimen, and place in the autoclave at room temperature in a rack. To maintain an atmosphere of saturated steam vapor, the autoclave shall contain enough water, at an initial temperature of 20 to 28℃.

f. Close the valve and raise the temperature of the autoclave at a rate that will bring the gauge pressure of the steam to 2 MPa in 45 to 75 minutes from the time the heat is turned on.

g. Maintain the 2 ± 0.07 MPa pressure for 3 hours.

h. At the end of the 3-hour period, shut off the heat supply and cool the autoclave at such a rate that the pressure will be less than 0.07 MPa at the end of 90 minutes.

i. At the end of the 90 minutes period, slowly release any remaining pressure by partially opening the vent valve until atmospheric pressure is attained.

j. Then open the autoclave and place the test specimen in water at a temperature above 90°C.

k. Maintain the water surrounding the specimens at 23°C for an additional 15 minutes.

doi:10.6342/NTU201902030

l. Remove one specimen at a time from the water blot the pins, but not the specimen, and obtain a length comparator reading

3-4-2-6 Sulfate Resistance

The sulfate resistance test was according to CNS 9746 requirement:

a. Make mortars 1 part cement, including Portland cement and EAFS, to 2.75 parts of sand by mass. Use a water-cement ratio by mass of 0.485. Mold the test bars in accordance with test method of autoclave expansion. Mold the cubes in accordance with test method of compressive strength.

b. Each litre of solution shall contain 50.0 g of Na2SO4 dissolved in 900 mL of water, and shall be diluted with additional distilled or deionized water to obtain 1.0 L of solution.

c. Cover the container with a lid and seal the lid so as to prevent evaporation and place the container into an oven at 35 ± 3°C for 23.5 hours ± 30 minutes. At 23.5 hours ± 30 minutes, remove molds from container and demold the specimens.

d. After demolding, store all bars and cubes, except the two to be tested, in a curing tank of saturated limewater at 23.0 ± 2.0 °C.

e. Measurements of Length Change and place all the bars in the sulfate solution.

doi:10.6342/NTU201902030

f. At 1, 2, 3, 4, 8, 13, and 15 weeks after the bars are placed in the sulfate solution, test them for length change using the length comparator.

3-4-2-7 Shrinkage

ASTM C596 demonstrated that the test method establishes a selected set of conditions of temperature, relative humidity and rate of evaporation of the environment to which a mortar specimen of stated composition shall be subjected for a specified period of time during which its change in length is determined and designated “drying shrinkage”.

a. Prepare the cement paste consisting of 750 g of cement, 1500 g of standard sand and sufficient water to produce flow of 100 ± 1 %.

b. Mix the cement and mold it.

c. Cure, store, and take comparator readings of the test specimens.

doi:10.6342/NTU201902030

3-4-3 Strength Prediction Models

3-4-3-1 Statistic Model of Strength from Taylor's Equation

Generally, clinker composition affects the mechanical performance of cement mortar significantly. Thus, mathematical models for predicting strength development are frequently used in the cement-manufacturing industry to determine the optimal ingredient. (Barry and Glasser, 2000). To build up the model of compressive strength development of cement mortar in different curing ages, non-linear simulation can be used as eq. (3-8):

$$P = k \cdot ln(t) + P_0 \tag{3-8}$$

where P (MPa) is the compressive strength of mortars; t (day) is the curing age; P_0 (MPa) is the initial compressive strength of mortar, k (MPa/day) is the rate constant of strength development, which is a function of mineral compositions in the clinker expressed in Eq. (3-9):

$$k = a \times \text{Silicates}^{\,b} \times C_3A^{c} \times C_4AF^{d} \times C\bar{C}^{e} \tag{3-9}$$

where the coefficients from a to e are the coefficients for the non-linear regression analysis, which contributes to compressive strength by different mineral compositions. Silicates include tricalcium silicate ($3CaO \cdot SiO_2$) and dicalcium silicate ($2CaO \cdot SiO_2$). C_3A, C_4AF, $C\bar{C}$ are the notation of cement chemistry, present tricalcium aluminate ($3CaO \cdot Al_2O_3$), tetracalcium aluminoferrite ($4CaO \cdot Al_2O_3 \cdot Fe_2O_3$), and calcite ($CaCO_3$).

doi:10.6342/NTU201902030

However, the chemical compositions of cement and steelmaking slags are from the results of XRF analysis, which are expressed in the form of oxides. In order to transfer the results of XRF into the mineral constituents as mentioned before, the Taylor's equation (Taylor, 1989) in eq. (3-10) has to be used.

$$\begin{bmatrix} 0.7185 & 0.635 & 0.566 & 0.475 \\ 0.2515 & 0.315 & 0.037 & 0.036 \\ 0.01 & 0.021 & 0.313 & 0.219 \\ 0.008 & 0.009 & 0.051 & 0.214 \end{bmatrix} \cdot \begin{bmatrix} C_3S \\ C_2S \\ C_3A \\ C_4AF \end{bmatrix} = \begin{bmatrix} CaO \\ SiO_2 \\ Al_2O_3 \\ Fe_2O_3 \end{bmatrix} \quad (3\text{-}10)$$

where all of the contents in this equation are expressed as weight percent in this equation.

3-4-3-2 Kinetics Model of Hydration Products

Additionally, another strength prediction model can be established by using EDX-SEM, where the amount of production during cement hydration and pozzolanic reaction can be estimated. The testing results of compressive strength can be expressed as accumulation of each hydration product in eq. (3-11):

$$P = a \times CSH + b \times CH + c \times AFt + P_O \quad (3\text{-}11)$$

where the coefficients from a to c are the coefficients for the linear regression analysis, which contribute to compressive strength by different hydration products. *CSH, CH, AFt,* present the amount of C-S-H gel, calcium hydroxide ($Ca(OH)_2$), ettringite ($3CaO \cdot Al_2O_3 \cdot 3CaSO_4 \cdot 32H_2O$); P_O expresses the compressive strength attributed by other products from hydration and pozzolanic reaction.

doi:10.6342/NTU201902030

3-4-3-3 Strength Evolution Coefficient

Although the compressive strength of different curing ages can be obtained by the kinetics model of mineral compositions, modeling and comparing the results of different composition is still a time consuming work. Thus, the CEB-FIP Model can be used to understand the hardening speed of cement quickly. Strength evolution coefficient can be obtained easily by following the relationship of compressive strength between different curing age and 28-day in eq. (3-12):

$$f_{cm}(t) = e^{[S(1-(\frac{28}{t})^{0.5})]} \times f_{cm} \quad (3\text{-}12)$$

where $f_{cm}(t)$ is the mean compressive strength at the age of t days; f_{cm} is the mean 28-day compressive strength; S expresses the coefficient of different cement types. Usually, $S \approx 0.25$ for normal hardening cement, $S<0.25$ and $S>0.25$ express early strength cement and slow hardening cement respectively.

doi:10.6342/NTU201902030

doi:10.6342/NTU201902030

Chapter 4 Results and Discussions

4-1 Carbonation of Steelmaking slags through the RPB

Carbonation of steelmaking slags via High-Gravity Carbonation Process would be discussed in this section. It looks forward to take advantage of the steelmaking slags recycling and CO_2 reduction. In this study, examination of the change in physicochemical properties of slags and the best operating conditions include the rotating speed, liquid to solid ratio and particle size would be achieved.

4-1-1 Effect of Carbonation on Characteristics of Feedstock

The chemical composition of four types of slags with and without carbonation are shown in Table 4-1. According to the X-ray fluorescence analyses, the main elements in slags are calcium, silica, iron and aluminum. The proportion of calcium and magnesium in slags is related to the potential in capturing CO_2. Among all of the slags, electric arc furnace reducing slag (EAFRS) contains up to 54.36% of calcium, which is 1.5 to 2 times as much as that in other slags. Thus, it is expected to be the best materials for carbon capture in this study. As the calculating result, the amount of theoretical carbon captured by 1 ton of basic oxygen furnace slag (BOFS), refining slag (RFS), electric arc furnace reducing slag (EAFRS) and oxidizing slag (EAFOS) are 0.288, 0.277, 0.427, 0.172 tons respectively. Except calcium, the content of aluminum and iron also plays an important role in slags, which would affect their hardness and increase the

doi:10.6342/NTU201902030

energy consumption during crushing and milling. Among these four materials, only EAFRS could be crushed by pestle in lab easily.

In comparison with differences of the slags before and after the carbonation, the free-CaO content in these slag reduces greatly after carbonation. It shows that the High-Gravity Carbonation Process did transform calcium oxide into calcium carbonated effectively and get to the effect of being stabilized. Although the proportion of calcium oxide under 1.5% is acceptable according to ASTM regulations, if the free-CaO turns into calcium hydroxide in the hydration process, it will bring about 97% of expansion, generating micro creaks and causing fatal defect (Neville et al., 2002). To improve the strength development and durability, less content of free-CaO should be residue in the slags.

Besides, there are higher proportion of alkali metal such as sodium and potassium in the EAFOS. Despite the amount of the sodium and potassium residue in EAFOS slightly reduces during the carbonation process due to its high solubility, the proportion of alkali metal in carbonated EAFOS still reaches 5.23%, which is far exceed the requirement of ASTM regulation ($Na_2O+0.66K_2O < 0.6\%$).

doi:10.6342/NTU201902030

Table 4-1 Chemical Composition of Fresh and Carbonated Steelmaking slags from XRF Analysis (F=fresh, C=carbonated).

Compositions (%)	BOFS		RFS		EAFRS		EAFOS	
	F	C	F	C	F	C	F	C
SiO_2	10.22	9.58	23.48	23.91	26.32	25.16	41.29	42.00
Al_2O_3	4.12	4.42	17.06	17.69	3.86	3.24	8.53	9.27
Fe_2O_3	37.51	39.18	11.69	11.12	3.84	2.96	9.41	10.14
CaO	36.69	35.63	35.30	35.92	54.36	60.14	21.91	22.13
MgO	4.88	4.43	6.90	6.16	4.55	4.14	2.07	2.10
SO_3	0.21	0.23	1.02	0.70	1.79	0.73	1.72	0.95
K_2O	0.03	0.04	0.22	0.24	0.03	0.02	1.26	1.08
Na_2O	0.07	N.D.[1]	0.36	0.28	0.34	0.07	6.26	5.23
TiO_2	0.49	0.53	0.48	0.59	0.31	0.29	1.27	1.40
P_2O_5	2.49	2.86	0.37	0.41	0.07	0.04	2.76	3.24
MnO	2.45	2.64	1.51	1.51	0.67	0.53	0.25	0.27
f-CaO	0.66	0.25	1.13	0.83	1.09	0.33	0.99	0.12

[1] Not detected under 0.01%.

Table 4-2 is the crystal composition of steelmaking slags with and without carbonation. Comparing the analyzing result of XRD with Inorganic Crystal Structure Database (ICSD), the main compositions of slags are shown as below: FeO (no:01-075-1550) and $CaCO_3$ (no: 01-076-2712) in BOFS, $2CaO•Al_2O_3•SiO_2$ (no: 01-076-7523) and $CaO•Fe_2O_3$ (no: 00-032-0168) in RFS, $2CaO·SiO_2$ (no: 00-049-1672) in EAFRS, SiO_2 (no:01-087-2096) and $CaCO_3$ (no: 01-083-1762) in EAFOS. According to figure 4-1 to 4-4, the calcium carbonated diffraction peaks have higher intensity than those before carbonation. Implying that the amount of calcium carbonate in carbonated slags increase significantly during the High Gravity Carbonation Process. Furthermore, some of the mineral compositions in the fresh slags such as $CaO•Fe_2O_3$ would decomposed due to calcium ions leach out and interact with CO_2 in the solution. In the meanwhile,

doi:10.6342/NTU201902030

free-CaO in slags react with water forming calcium hydroxide, which can also combine with CO_2 to form $CaCO_3$.

Table 4-2 Major Crystal Structure of Steelmaking Slags from XRD Analysis

Items		Major structure
BOFS	Fresh	FeO, $CaCO_3$
	Carbonated	$CaCO_3$, FeO
RFS	Fresh	$2CaO•Al_2O_3•SiO_2$, $CaO•Fe_2O_3$
	Carbonated	$2CaO•Al_2O_3•SiO_2$, SiO_2
EAFRS	Fresh	$2CaO•SiO_2$, SiO_2
	Carbonated	$CaCO_3$
EAFOS	Fresh	SiO_2, $CaCO_3$
	Carbonated	SiO_2, $CaCO_3$

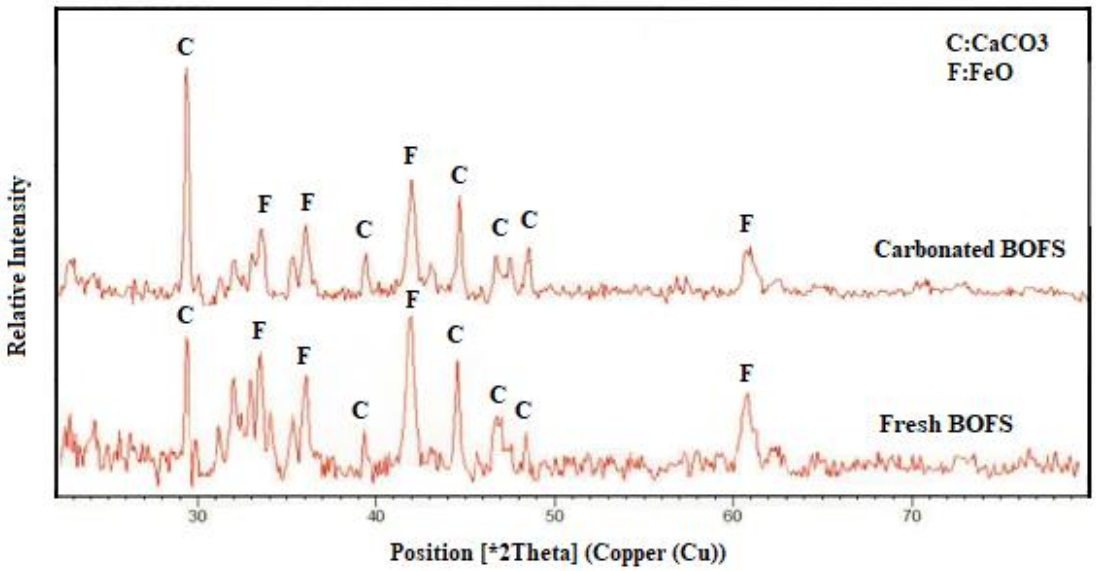

Figure 4-1 Diffraction Peak Comparison of BOFS

doi:10.6342/NTU201902030

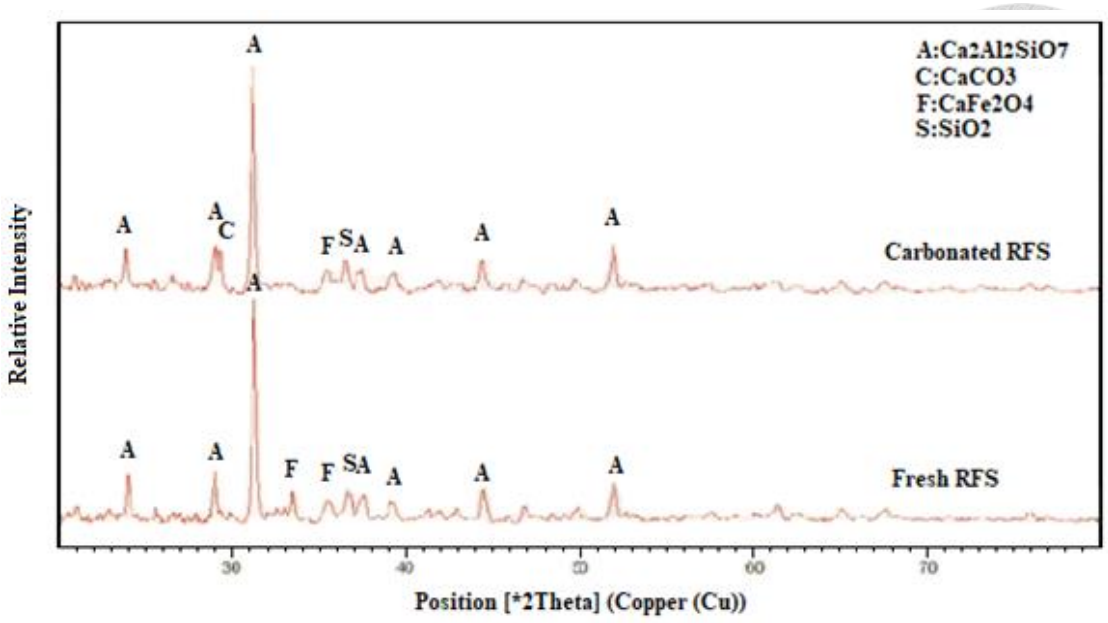

Figure 4-2 Diffraction Peak Comparison of RFS

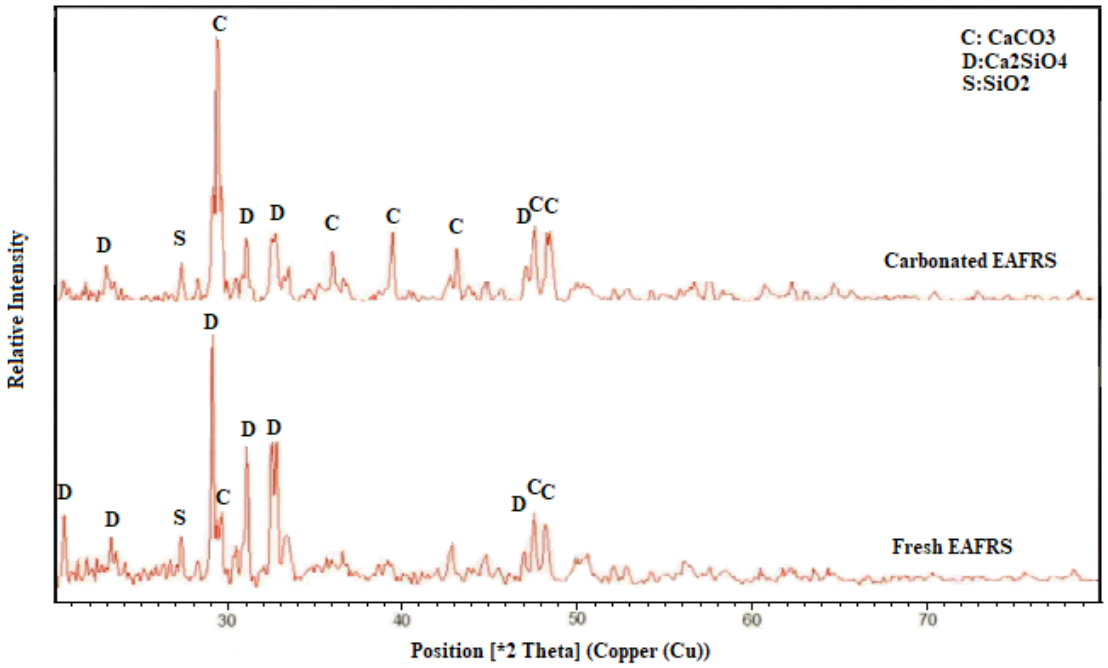

Figure 4-3 Diffraction Peak Comparison of EAFRS

doi:10.6342/NTU201902030

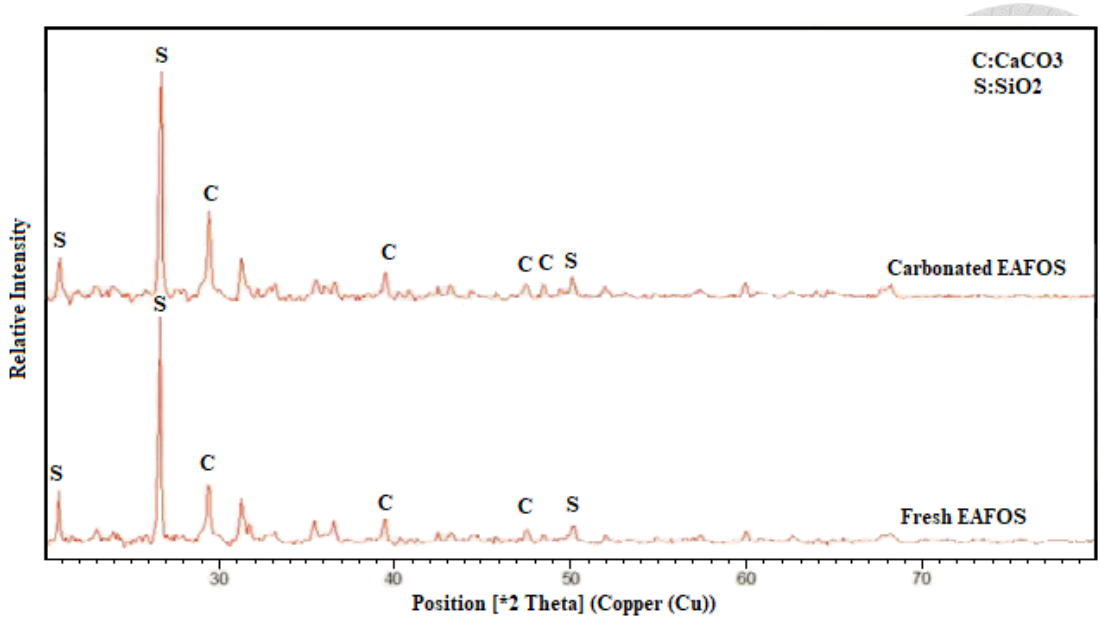

Figure 4-4 Diffraction Peak Comparison of EAFOS

Composition change during carbonation could also be presented by using the differential thermal gravity (DTG) curve, which is a technique to analyze the components with different derivative weight peak at a specific temperature. As shown in figure 4-5, the first peak of weight loss is illustrated at 50 to 110 ℃, corresponding to the removal of moisture. The second peak of weight loss is related to decomposition of amorphous C-S-H gel at 100 to 150 ℃. Some unobvious weight loss between 200-400 ℃ may related to dehydration of iron hydroxide and alumina hydroxide. The third peak of fresh BOFS at around 441℃ is associated to the calcium hydroxide dehydration. Then the last peak between 600 and 850 ℃ is related to the decomposition of calcium carbonated and magnesium oxide. Different from figure 4-5, there is just one significant peak being preserved in the DTG curve, which is the peak of $CaCO_3$ and $MgCO_3$ decomposition of figure 4-6. By comparing Figure 4-5 and 4-6, it implies that calcium in structures such as calcium hydroxide and amorphous C-S-H gel may be leached out, reacting with carbon dioxide to form calcium carbonated.

doi:10.6342/NTU201902030

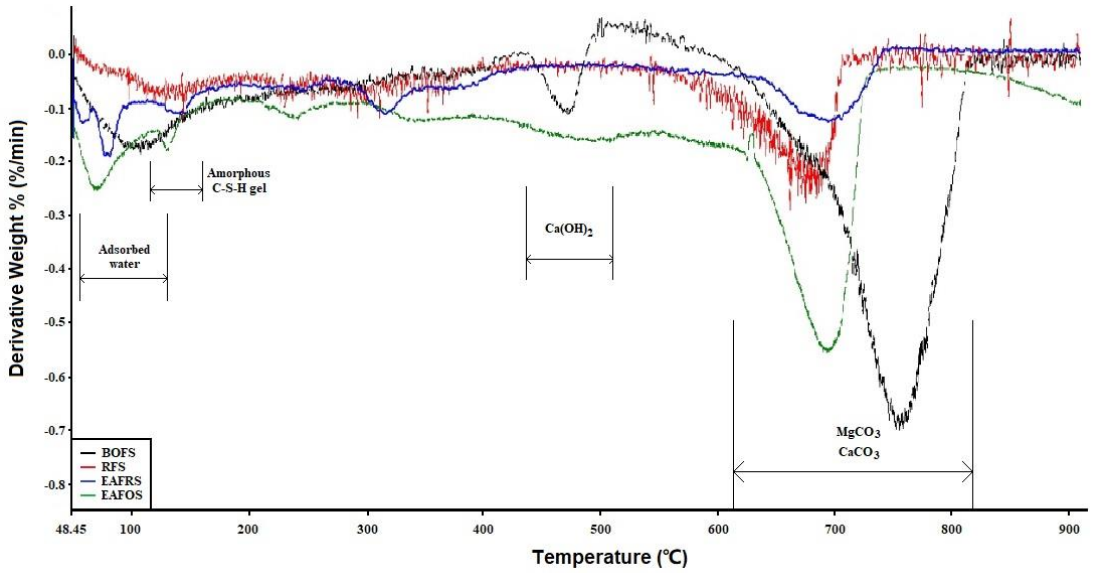

Figure 4-5 DTG Curves of Fresh Steelmaking Slags.

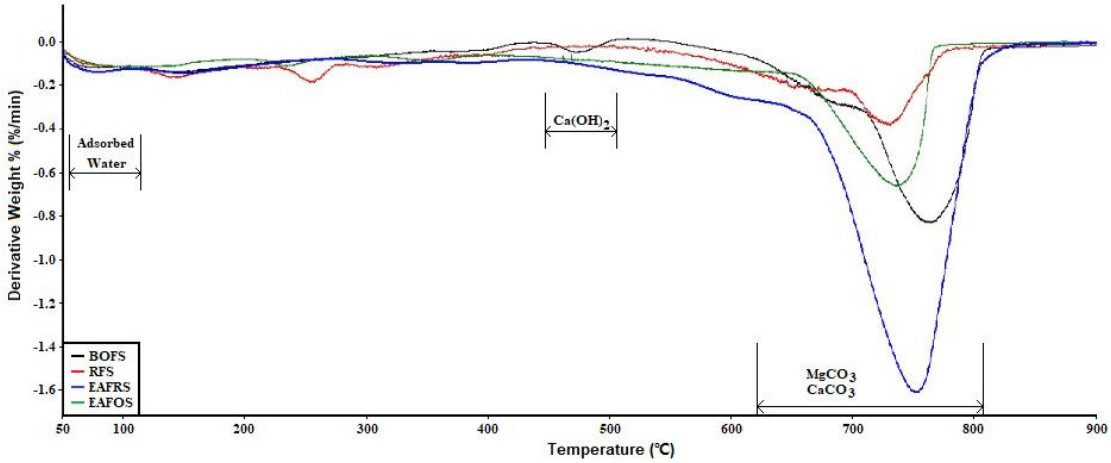

Figure 4-6 DTG Curves of Carbonated Steelmaking Slags

4-1-2 Effects of Operating Parameters for Carbonation

The first variance in the carbonation process is the liquid-solid ratio (L/S ratio). In this study, L/S is set between 10 to 50 ml/g. Higher liquid-solid ratio represents the proportion of slags in the whole system is relatively less, and lower liquid-solid ratio represents a relatively lower reaction kinetics of carbonation process. As shown in figure 4-7, under the rotating speed at 1100 rpm, liquid-solid ratio doesn't obviously

doi:10.6342/NTU201902030

affect the carbonation conversion yield. However, the conversion yield at higher L/S ratio (50ml/g) is slightly higher than that at lower L/S ratio. For example, EAFRS conversion yield at L/S=50 ml/g is 2.65% higher than that at L/S=10 ml/g. This phenomenon may be the combination effect of two opposite theories. At lower L/S ratio, higher calcium concentration condition can be produced, which is advantage to react with CO_2 and nucleate. However, higher calcium concentration makes the slag particles hard to leach out according to the Le Châtelier's principle. In this study, leaching seems more important than nucleation, resulting better conversion yield at higher L/S ratio.

Moreover, owing to carbonation conversion yield is calculated by subtracting the calcium content tested by TGA and XRF. Conversion yield between different slags may associate to the difference of calcium-related crystal forms. The higher amount of free-CaO and calcium hydroxide in slags, the easier calcium ions can be leached out from crystal and reacts with CO_2 in water. Unfortunately, some calcium mineral like dicalcium silicate which especially crystallized in the γ phase is hard to leached out owing to its stable regular-octahedron structure. This type of structure doesn't provide enough cavities for water molecules to penetrate in and break down the Ca-O bond.

Thoroughly considering the efficiency and the convenience of operation, including processes of the reactor cleaning and the slags filtration. The slags which offered to be used later in the cement substitution experiments are produced at the proportion of L/S=20 ml/g.

doi:10.6342/NTU201902030

Table 4-3 Effect of Carbonation Conversion Efficiency Under Different Rotating Speed.

Type of Slags	L/S Ratio (ml/g)	Rotating Speed (rpm)	Conversion Yield (%)	CO_2 Capture Capacity (g-CO_2/ 100 g-slag)
BOFS	10	1100	37.24±1.22	10.74±0.35
	20	1100	39.50±0.93	11.39±0.27
	30	1100	39.30±1.25	11.33±0.36
	40	1100	39.60±0.87	11.42±0.25
	50	1100	40.32±1.23	11.62±0.36
RFS	10	1100	19.85±1.12	5.51±0.31
	20	1100	21.19±0.43	5.88±0.12
	30	1100	21.23±1.83	5.89±0.51
	40	1100	22.65±1.43	6.28±0.40
	50	1100	21.89±1.31	6.07±0.64
EAFRS	10	1100	40.45±1.25	17.28±0.53
	20	1100	42.25±0.23	18.05±0.10
	30	1100	40.94±0.56	17.48±0.24
	40	1100	41.87±1.02	17.88±0.44
	50	1100	43.10±0.44	18.41±0.19
EAFOS	10	1100	22.40±1.31	3.86±0.23
	20	1100	23.78±0.12	4.09±0.02
	30	1100	22.50±0.44	3.87±0.08
	40	1100	23.37+1.38	4.02±0.24
	50	1100	23.39±0.54	4.03±0.09

doi:10.6342/NTU201902030

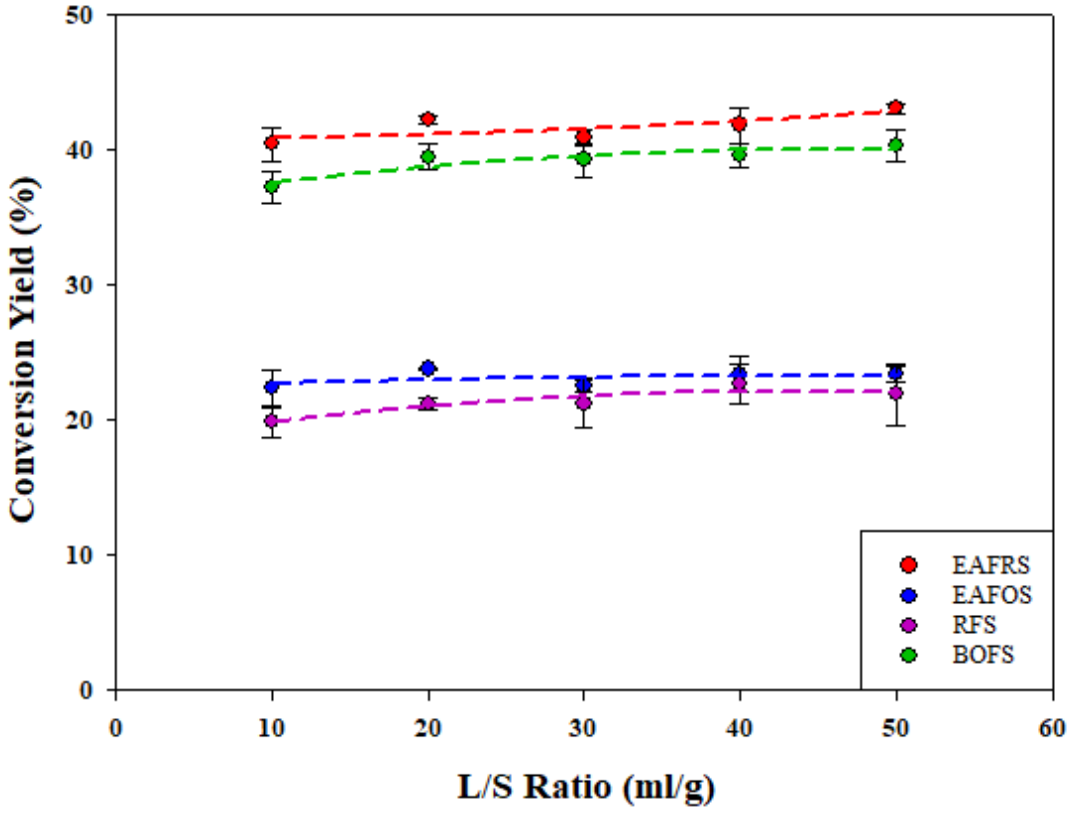

Figure 4-7 Effect Carbonation Conversion Yield under Different L/S Ratio (Rotating Speed = 1100rpm, Particle Size = 32μm).

Figure 4-8 shows the conversion yield change against to the rotating speed from 700-1300 rpm at L/S=20ml/g. Among the range from 700 to 1000 rpm, conversion yield increases apparently as the rotating speed accelerates. That's because higher rotating speed can break the slurry into smaller liquid drops on the stainless wire in rotating packed bed, which provides a larger surface area for CO_2 to dissolve from gas, forming carbonic acid and interacting with calcium ions in the slurry drops. Thus, the mass transfer efficiency can be elevated.

Unfortunately, the conversion yield slightly goes down as rotating speed accelerates beyond 1100 rpm. This phenomenon may also come from the mass transfer enhancement. Comparing with the leaching rate of slags, CO_2 dissolves in the aqueous

doi:10.6342/NTU201902030

phase too fast to react with calcium ions. Large amount of carbonic acid results in the decline of pH in the solution. Part of carbonic acid reacts with the precipitated calcium carbonated, creating calcium bicarbonate re-dissolves, which consequently affects the amount of calcium in the slags being filtered from carbonation.

Table 4-4 Effect of Carbonation Conversion Yield under Different Rotating Speed.

Type of Slags	L/S Ratio (ml/g)	Rotating Speed (rpm)	Conversion Yield (%)	CO_2 Capture Capacity (g-CO_2/ 100 g-slag)
BOFS	20	700	17.34±1.23	5.00±0.35
	20	800	26.34±0.95	7.59±0.27
	20	900	28.66±1.42	8.26±0.41
	20	1000	36.32±0.87	10.47±0.25
	20	1100	39.50±1.33	11.39±0.38
	20	1200	39.01±0.85	11.25±0.24
	20	1300	37.35±0.46	10.77±0.13
RFS	20	700	10.34±1.12	2.87±0.31
	20	800	12.43±0.43	3.45±0.12
	20	900	17.12±1.65	4.75±0.46
	20	1000	20.34±1.53	5.64±0.42
	20	1100	21.19±2.31	5.88±0.64
	20	1200	21.52±0.48	5.97±0.13
	20	1300	20.14±0.37	5.59±0.10
EAFRS	20	700	19.87±1.23	8.49±0.53
	20	800	24.92±0.54	10.64±0.23
	20	900	29.38±0.56	12.55±0.24
	20	1000	38.30±1.31	16.36±0.56
	20	1100	45.17±0.12	19.29±0.05
	20	1200	43.28±0.44	18.49±0.19
	20	1300	39.92±0.35	17.05±0.15
EAFOS	20	700	12.30±1.31	2.12±0.23
	20	800	16.06±1.17	2.76±0.20
	20	900	19.67±0.44	3.39±0.08
	20	1000	21.79±1.29	3.75±0.22
	20	1100	23.78±0.54	4.09±0.09
	20	1200	22.58±0.76	3.89±0.13
	20	1300	21.98±1.00	3.78±0.17

doi:10.6342/NTU201902030

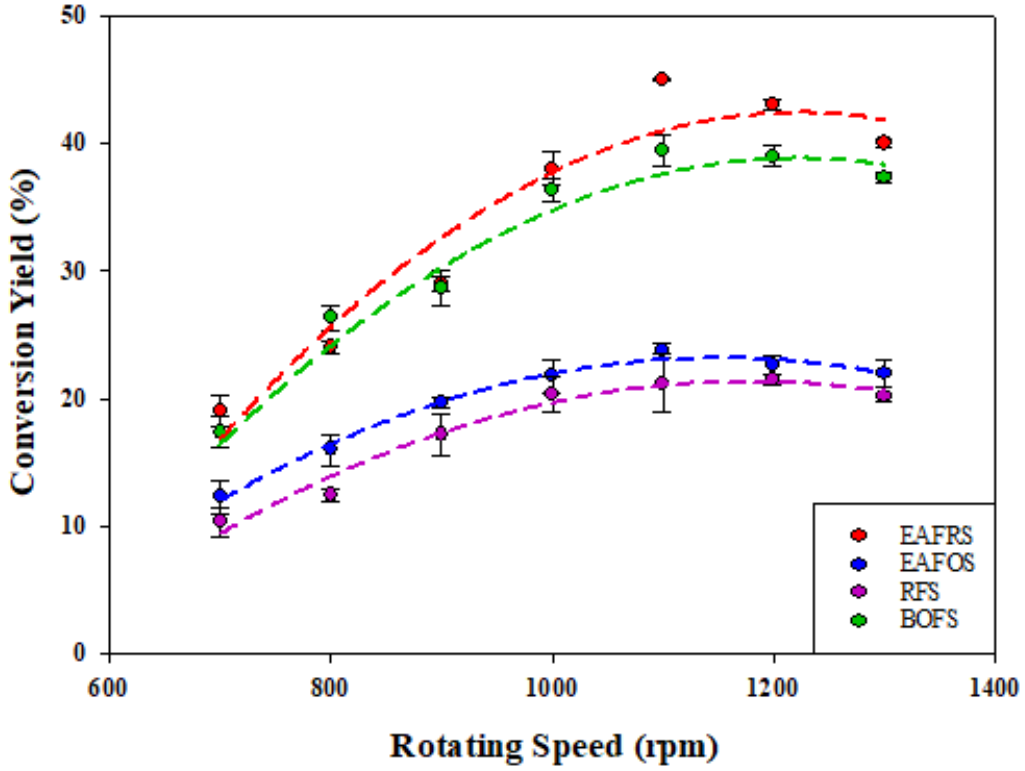

Figure 4-8 Effect of Carbonation Conversion Yield under Different Rotating Speed (L/S = 20 ml/g, particle size = 32μm).

Figure 4-9 shows that under the condition of 1100 rpm and 20 ml/g, different particle sizes of EAFRS affect carbonation conversion yield. Apparently, as the particle sizes become smaller, carbonation conversion yield becomes higher. What's more, according to table 4-5, the process of grinding and milling slags has little impact on chemicals. It means that the increasing of conversion yield completely results from higher surface area which smaller particles of EAFRS have. Therefore, calcium ions can leach out more easily and react with CO_2.

doi:10.6342/NTU201902030

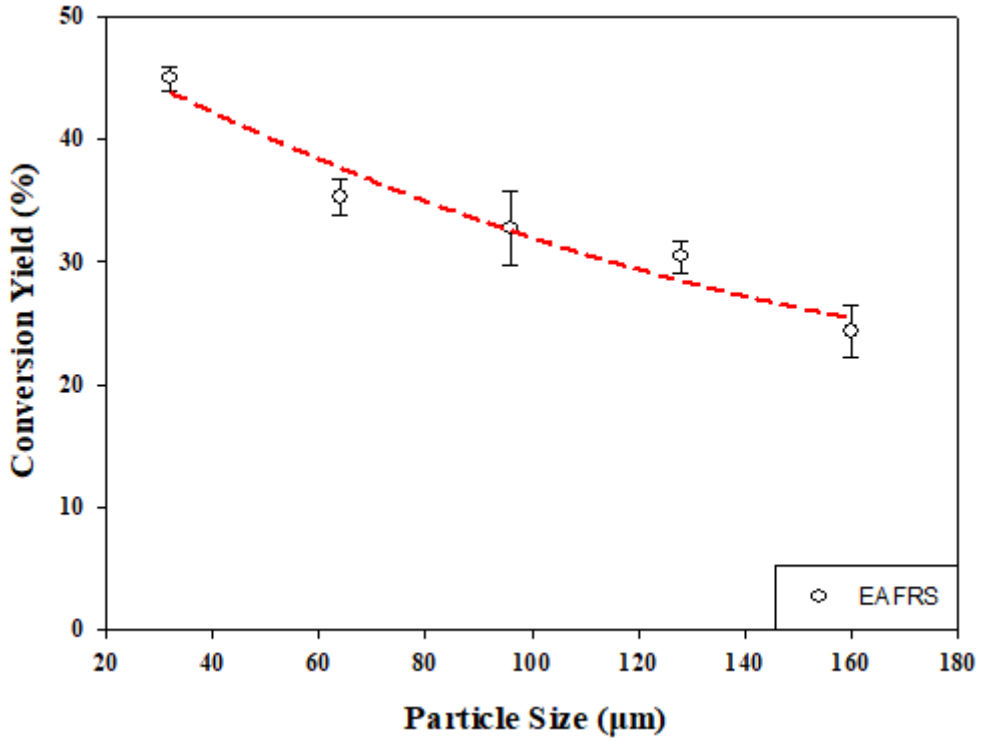

Figure 4-9 Effect of Particle Size on Carbonation Conversion Yield. (L/S=20 ml/g, rotating speed = 1100rpm)

Table 4-5 Chemical Composition of Fresh EAFRS with Different Particle Size

Particle size (μm)		32	64	96	128	160
Composition (%)	SiO_2	26.32	17.23	16.92	16.61	16.54
	Al_2O_3	2.64	2.64	2.92	3.29	3.78
	Fe_2O_3	1.89	1.94	2.00	2.57	3.37
	CaO	48.67	48.16	48.24	46.93	46.35
	MgO	5.65	5.60	5.60	5.80	6.33
	SO_3	1.31	1.34	1.48	1.62	1.64
	K_2O	0.01	0.01	0.01	0.01	0.02
	Na_2O	0.16	0.18	0.20	0.19	0.20
	f-CaO	1.22	1.21	1.40	1.55	1.47

doi:10.6342/NTU201902030

4-2 Cement Replacement by Steelmaking Slags

Slags contain calcium, silica and aluminum, which elements are similar to the Portland cement. Moreover, some lattice defects in slags which produce during the crystallization period can generate activity in slags. After grinding into microscale, these slags can be used as the supplementary cementitious materials (SCMs) in cement industry. Since cement manufacturing process will consume a great amount of original materials such as limestone, clay and coal and also emits a great tons of CO_2. Using SCMs in concrete to reduce the amount of cement usage can not only lessen environmental destruction but also cut down the CO_2 emission. In this research, slags within and without carbonation will replace partial of Ordinary Portland Cement at the substitution rate of 5, 10, 15% and tests are given to workability, strength, and durability to evaluate the feasibility.

4-2-1 Effect of Substitution on Workability of Cement

According to the standard consistency of pastes and standard fluidity of mortars in figure 4-10 and 4-11, the water demand for maintain the workability is getting more as the slags substitution rate getting higher. Compared with the Ordinary Portland Cement, the standard consistency of the pastes with 15% replacement of slags are 5.9-9.6% higher. This phenomenon is related to kinds of reasons include the surface area and hydrophobic. In 2007, Kourounis and people pointed out that cement mixed with the materials with more surface area will promote its effective wet surface area and total amount of adsorbed water. Because of calcium ions dissolving after the carbonation of

doi:10.6342/NTU201902030

slags can promote the nucleation, the mean particle size of carbonated slags becomes smaller than those before carbonation. Therefore, the hydroscopicity of carbonated slags slightly increases. Besides, the water requirement increase as the substitution rate goes up is also related to the hydrophilicity of slags. In this study, the hydrophilicity sequence of these slags are: OPC>BOFS>EAFOS>RFS>EAFOS. With some organic compounds residue, EAFOS is oilier and hydrophobic which makes it harder to scattered in water. This cause an abnormal result that the slag after carbonation needs even less water than those before carbonation while making mortar and paste.

Table 4-6 Standard Consistency of Paste with Different Replacing Ratio of Slags

Items	Replacing ratio	Standard consistency (W/B)		Standard fluidity (W/B)	
		Fresh	Carbonated	Fresh	Carbonated
OPC	-	26.9			
BOFS	5%	26.9±0.1	29.9±0.1	28.3±0.2	31.5±0.1
	10%	27.7±0.0	30.7±0.2	30.8±0.1	34.7±0.2
	15%	28.5±0.1	31.4±0.1	33.5±0.1	37.0±0.4
RFS	5%	27.7±0.0	30.0±0.0	29.1±0.2	31.7±0.1
	10%	28.5±0.2	30.8±0.1	31.6±0.2	34.2±0.2
	15%	29.2±0.1	31.6±0.2	34.3±0.1	36.8±0.3
EAFRS	5%	27.1±0.1	28.6±0.4	29.1±0.2	30.1±0.5
	10%	28.3±0.3	29.2±0.1	31.5±0.3	32.5±0.2
	15%	28.8±0.1	29.7±0.3	33.8±0.1	34.9±0.4
EAFOS	5%	28.3±0.0	28.0±0.0	29.8±0.0	29.5±0.3
	10%	29.2±0.1	28.3±0.1	32.5±0.1	31.5±0.2
	15%	29.5±0.2	28.8±0.1	34.8±0.2	33.8±0.1

doi:10.6342/NTU201902030

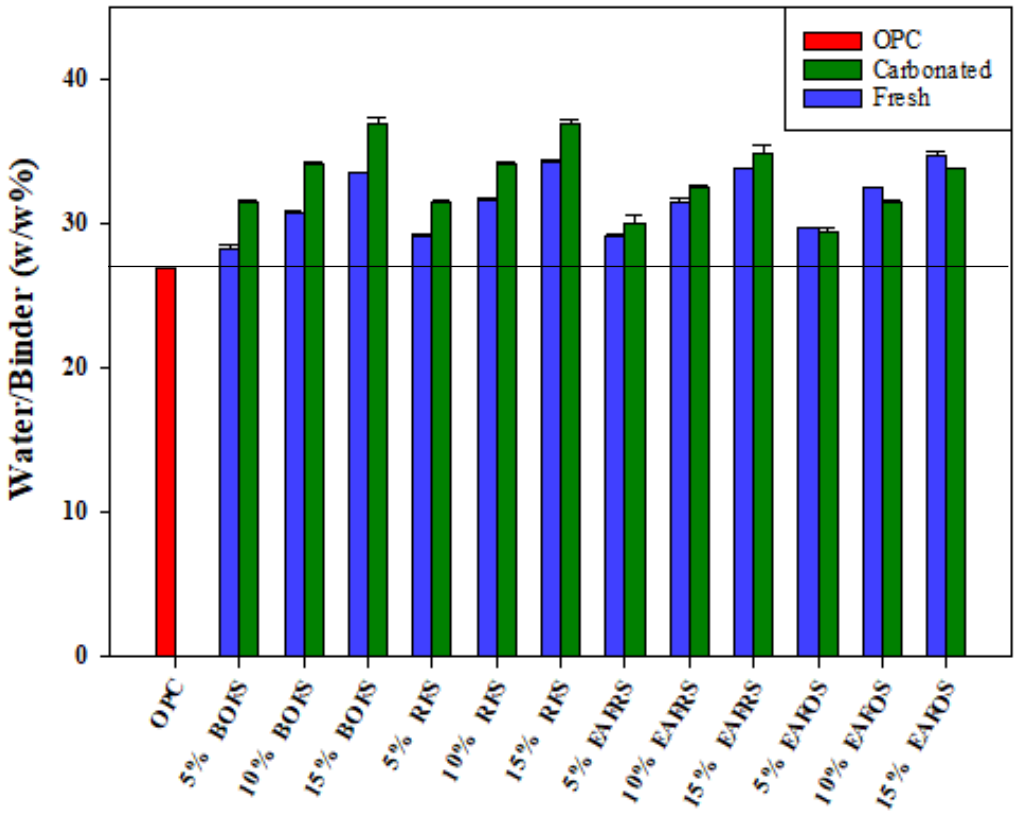

Figure 4-10 Standard Consistency of Paste with Different Replacing Ratio of Slags.

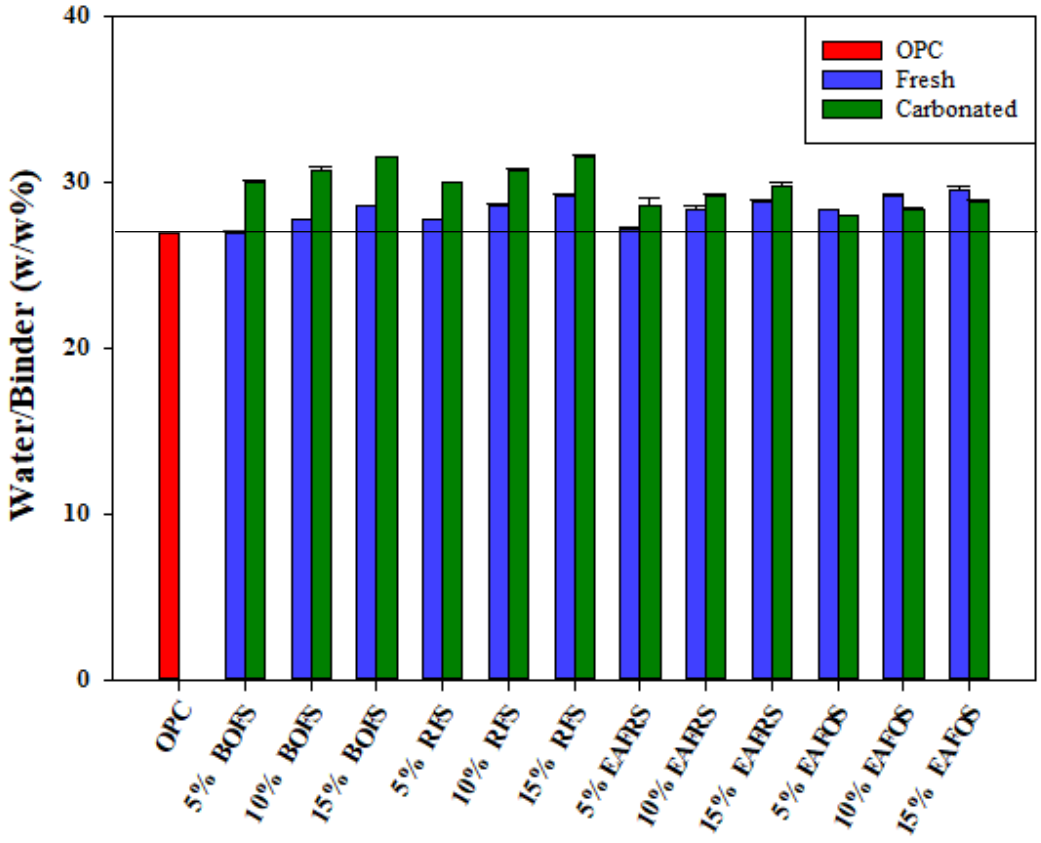

Figure 4-11 Standard Fluidity of Mortars with Different Replacing Ratio of Slags

doi:10.6342/NTU201902030

Figure 4-12 and 4-13 show the initial setting time and the final setting time of slags separately at the replacement ratio of 5%, 10%, and 15%. These figures can be divided into two types to discuss. The former concludes BOFS, RFS and EAFRS, which initial setting time and final setting time get 5-10% longer as increasing of the replacement ratio and carbonation doesn't affect the setting property of setting. This phenomenon isn't much related to the property of the material added. The delay of setting time results from the fact that standard consistency pastes with high replacement ratio need more amount of water, so the pastes take more time to lose their plasticity. Additionally, in 2013, Camiletti indicated that calcium carbonate can help nucleation in the aqueous phase during hydration and accelerate the process to shorten its setting time.

The latter is EAFOS, which is extremely different from the former type. Adding fresh EAFOS in paste will significantly lengthen the initial and final setting time. The final setting time of 15% fresh EAFOS replacement is up to 390 minutes, which is 62% higher than the OPC paste and even exceed the standard of CNS regulation. Besides, the final setting time of slags after carbonation is usually quite longer than slags before carbonation. However, the setting time of carbonated EAFOS pastes are obviously shorter than those partial replaced by fresh EAFOS and just 6-18% higher than the OPC paste. These phenomena can be explained that some organic compounds are residue in EAFOS, which act like adding retarders in cement paste. During the hydration process, the long chain shape organic substance will adsorb onto the particle surface of tricalcium silicate and tricalcium aluminate, blocking water from penetrating into the cement particles and slowing the hydration process down. Fortunately, organic

doi:10.6342/NTU201902030

compounds in EAFOS can be removed through the High-Gravity reactor during carbonation. Organic substance will dissolve in the water and be washed out. Furthermore, owing to calcium carbonate crystal can helps nucleation, the initial setting time and the final setting time go back to the normal scale right away. In conclusion, the reaction of materials processed with High-Gravity Carbonation Process has little influence on the workability of cement. What's more, the problem that EAFOS affects normal setting can be improved through the High-Gravity Carbonation Process

Table 4-7 Setting Time of Paste with Different Replacing Ratio of Slags

Items	Replacing ratio	Initial setting (min)		Final setting (min)	
		Fresh	Carbonated	Fresh	Carbonated
CNS regulation	-	>45		<375	
OPC	-	184±10		255±6	
BOFS	5%	172±16	170±7	225±3	240±2
	10%	176±3	174±12	225±4	225±7
	15%	175±5	177±8	240±10	255±12
RFS	5%	164±14	169±13	210±16	225±4
	10%	160±9	173±6	225±3	240±5
	15%	168±6	168±4	225±5	225±8
EAFRS	5%	211±3	211±5	240±14	270±13
	10%	189±4	215±**8**	255±9	285±11
	15%	213±6	214±13	270±6	285±7
EAFOS	5%	239±5	198±11	330±5	255±8
	10%	268±7	199±7	345±7	255±13
	15%	310±14	213±2	390±14	285±6

doi:10.6342/NTU201902030

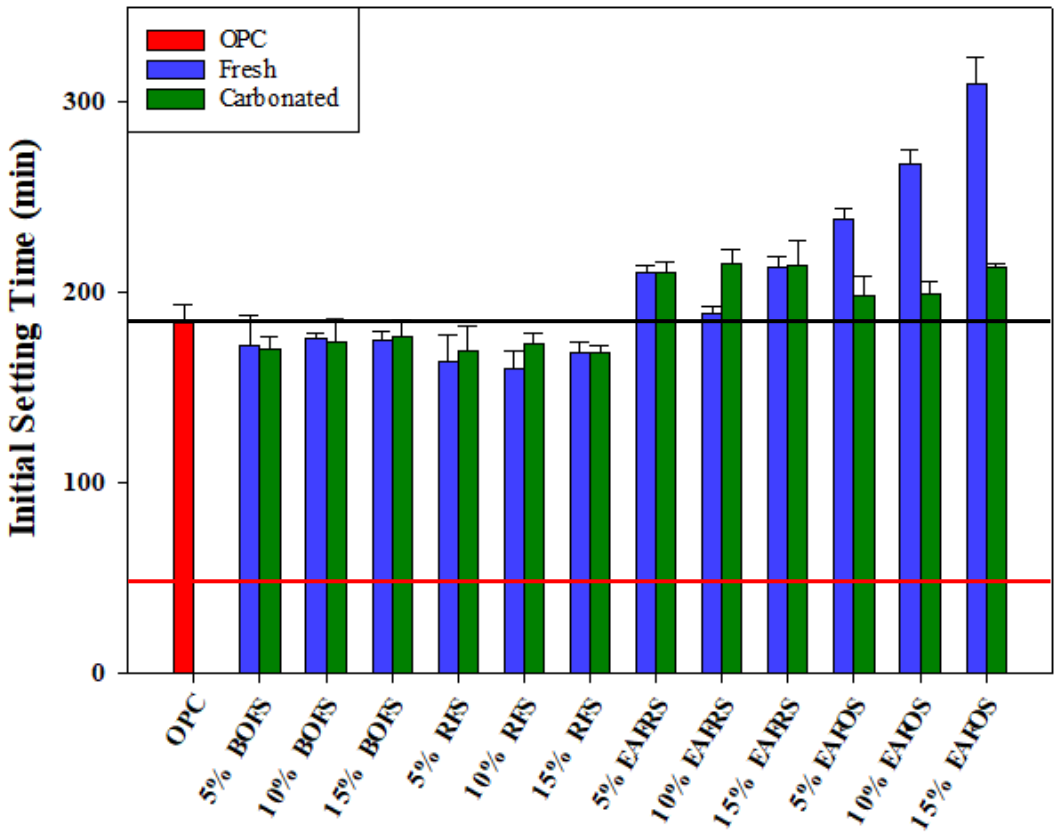

Figure 4-12 Initial Setting Time of Pastes with Different Replacing Ratio of Slags.

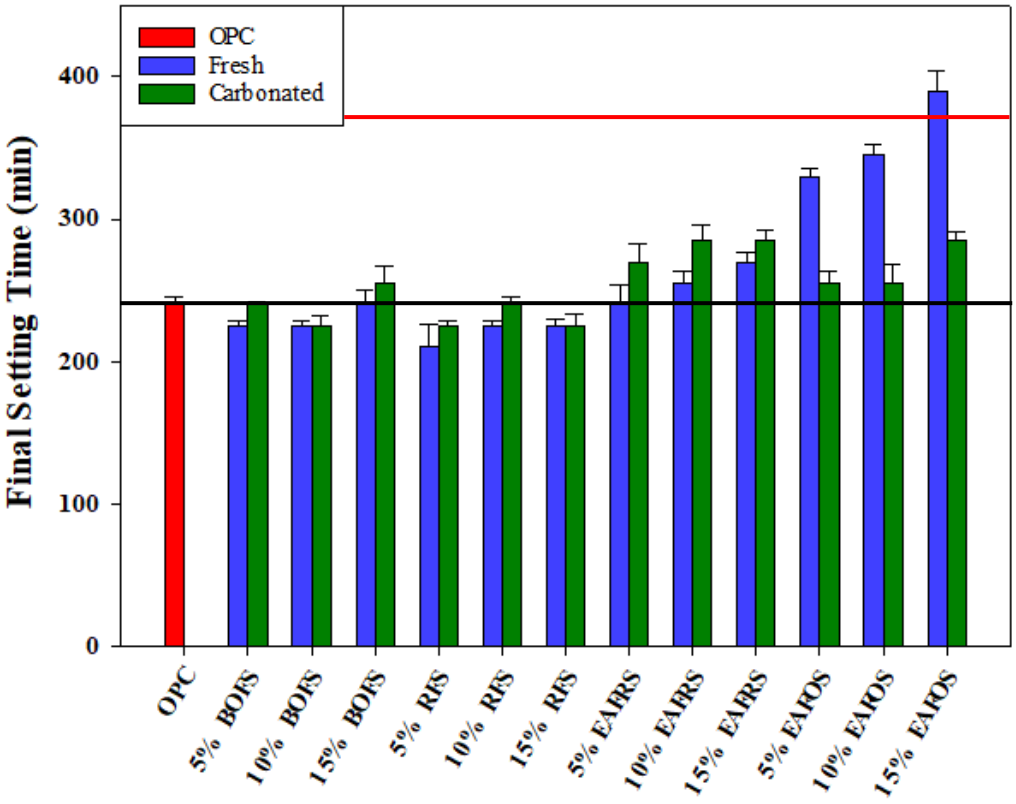

Figure 4-13 Final Setting Time of Pastes with Different Replacing Ratio of Slags

doi:10.6342/NTU201902030

4-2-2 Effect of Substitution on Strength of Cement

According to figure 4-14 to 4-16, the compressive strength of mortar specimens always getting worse as the substitution rate of slags growing higher and some specimens even can't fit the standard of CNS regulation. This is result from the lacking of binder. As cooling down at a slower rate, these slags have more time to crystalized in better arrangement, which have less defects in the crystal structure to dissolve during hydration. Thus, comparing to C_3S in OPC, these slags can't produce enough C-S-H gel to provide strength. Additionally, the specimens using carbonated slags as pozzolanic material usually perform better than those partial replace by fresh slags. This phenomenon can be explained by 2 reasons. The first is calcium carbonate can promote nucleation and accelerated the hydration reaction. The second is providing gel as shown in eq. 4-1 and 4-2. In this equation, calcium carbonate can react with calcium hydroxide and tricalcium aluminate to produce the ettringite type of C-A-$\bar{C}$-H structure, which can fill the crack and cavities in the specimens. However, there are still some detail in the compressive strength development trends of these four slags and they will be discussed as below.

$$2C_3A + 1.5C\bar{C} + 0.5CH + 22.5H \rightarrow C_3A \cdot C\bar{C} \cdot 11H + C_3A \cdot 0.5C\bar{C} \cdot 0.5CH \cdot 11.5H \quad (4\text{-}1)$$

$$C_3A + C\bar{C} + 11H \rightarrow C_3A \cdot C\bar{C} \cdot 11H \quad (4\text{-}2)$$

Compressive strength of specimens with fresh BOFS at different curing ages are 11.5-32.4% lower than the strength of OPC. However, the strength of specimens with carbonated BOFS even performed better than OPC at the early ages such as 3 and 7

doi:10.6342/NTU201902030

days. The cause of this result has been mentioned above. Furthermore, it is noteworthy that the carbonated BOFS mortar specimens doesn't maintain their advantage to the later age (28 days). This behavior is due to the properties of C-A-$\bar{C}$-H structure. Comparing with C-S-H gel, the C-A-$\bar{C}$-H structure isn't strong enough that it can just provide the filling function.

Unlike other slags, compressive strength of fresh RFS mortar specimens at the early age are stronger than OPC. This special phenomenon may associate with the crystal structure. According to table 4-2, minerals such as $2CaO•Al_2O_3•SiO_2$ may have higher reacting activity owing to Al^{3+} displaces Si^{4+} in the structure, causing inhomogeneous of charge distribution. Besides, the good performance of compressive strength in the early age may be attributed to its small particle size. Small particle blending in mortars may also provide a denser stacking, which enhance the strength in a physical view. Unfortunately, the advantage of strength just last until 7 days. As shown in figure 4-16, RFS mortar specimens do not perform remarkably. It's also due to the weaker strength of the hydration product.

Comparing with BOFS and RFS, EAFRS mortar specimens have weaker strength. Specimens with fresh EAFRS can barely meet the CNS regulation at the early stage such as 3 days and 7 days. At 28 days, the compressive strength of fresh EAFRS mortar specimens fail to reach the regulation because of lack of binder and the micro-cracks resulting from free-CaO expansion. Besides, the poor performance of compressive strength of EAFRS may also due to the larger particle size. Because EAFRS is less hard than other slags, the pretreatment of EAFRS in this study didn't use the crasher and

doi:10.6342/NTU201902030

miller. Using pestle to crush, the EAFRS has larger mean diameter and smaller specific surface. Thus, the compressive strength of fresh EAFRS mortar specimens at 3 days are slightly worse than the those before carbonation. However, the calcium carbonated in EAFRS after carbonation reacts with the calcium hydroxide which follows eq. 4-1 to 4-2 and produces C-A-$\bar{C}$-H hydration product, which can fill some micro-cracks. Therefore, the later compressive strength of carbonated EAFRS mortar specimens is higher than that before carbonation. Surprisingly, the 28-day compressive strength of carbonated EAFRS mortar even meets CNS regulation at 15% replacement ratio.

The most special one of these slags is EAFOS. EAFOS's strength development is similar to EAFRS's; however, there is another reason why the mortar specimens with slags EAFOS have a weak strength in later stage. According to table 4-1, EAFOS has excessive Na and K. According to CNS regulation, cement's total alkalinity （$Na_2O+0.66K_2O$） needs to be less than 0.6%. The total alkalinity in this EAFRS is 1081% over the regulation, which will cause serious Alkali-aggregate reaction, AAR). After being poured into molds, it will absorb water and produce fatal swelling as well as a large amount of micro-cracks, which does harm to the long-term strength just as shown in figure 4-17. On the other hand, carbonated EAFOS produces alkali-silica gel and absorbs water during the carbonation process, causing a large amount of swelling. After it is filled up in the molds, the second swelling won't occur. Thus, the long-term compressive strength is higher than mortar specimens with fresh EAFOS mixing inside.

To sum up, mortar specimens with partial replacement of carbonated slags via High-Gravity carbonation process have higher compressive strength in the later stage

doi:10.6342/NTU201902030

than those before carbonation. It's a good replacement material for CO_2 capture as well as cement. Although carbonated EAFOS's property is improved, only the specimens with 5% replacement ratio of slags can meet CNS strength regulation at 28 days.

Table 4-8 Compressive Strength of Cement Specimens at Different Curing Ages

Items		Replacement ratio	Compressive Strength (MPa)		
			3 Days	7 Days	28 Days
CNS Regulation	-	-	12.0	19.0	28.0
OPC	-	-	20.1	28.7	37.4
BOFS	Fresh	5%	19.5	24.0	39.5
		10%	17.8	22.2	34.1
		15%	14.1	19.4	33.1
	Carbonated	5%	25.4	33.0	39.4
		10%	22.9	29.7	35.9
		15%	23.5	28.7	33.9
RFS	Fresh	5%	25.7	31.6	33.7
		10%	23.2	26.4	33.1
		15%	17.8	26.3	32.3
	Carbonated	5%	29.3	33.2	39.6
		10%	24.2	32.1	37.9
		15%	21.6	28.2	33.1
EAFRS	Fresh	5%	20.1	20.5	26.6
		10%	19.0	19.9	28.1
		15%	13.1	18.0	24.3
	Carbonated	5%	19.0	27.1	37.3
		10%	18.5	27.7	33.9
		15%	15.2	23.3	30.2
EAFOS	Fresh	5%	21.4	22.7	27.6
		10%	19.4	20.4	22.8
		15%	12.7	17.2	20.4
	Carbonated	5%	20.3	25.2	31.1
		10%	17.4	23.5	25.3
		15%	12.3	19.2	21.5

doi:10.6342/NTU201902030

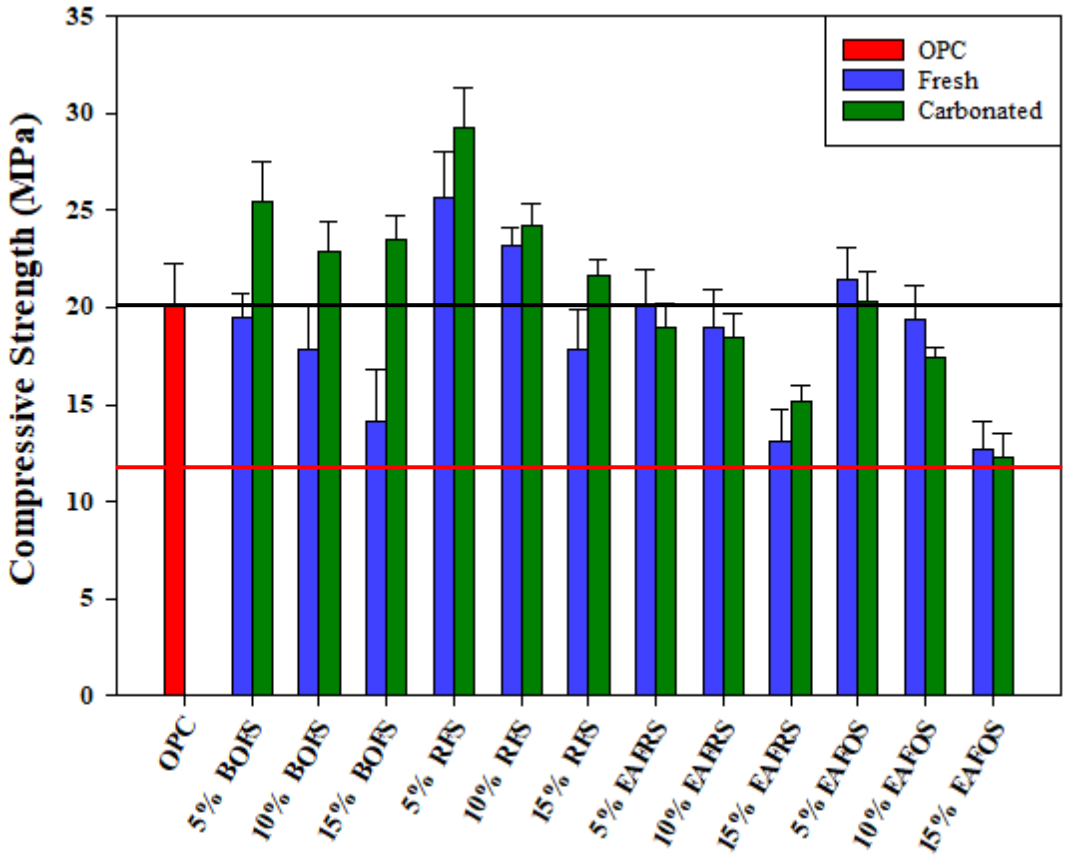

Figure 4-14 The 3rd day Compressive Strength of Mortars with Different Replacing Ratio of Slags.

doi:10.6342/NTU201902030

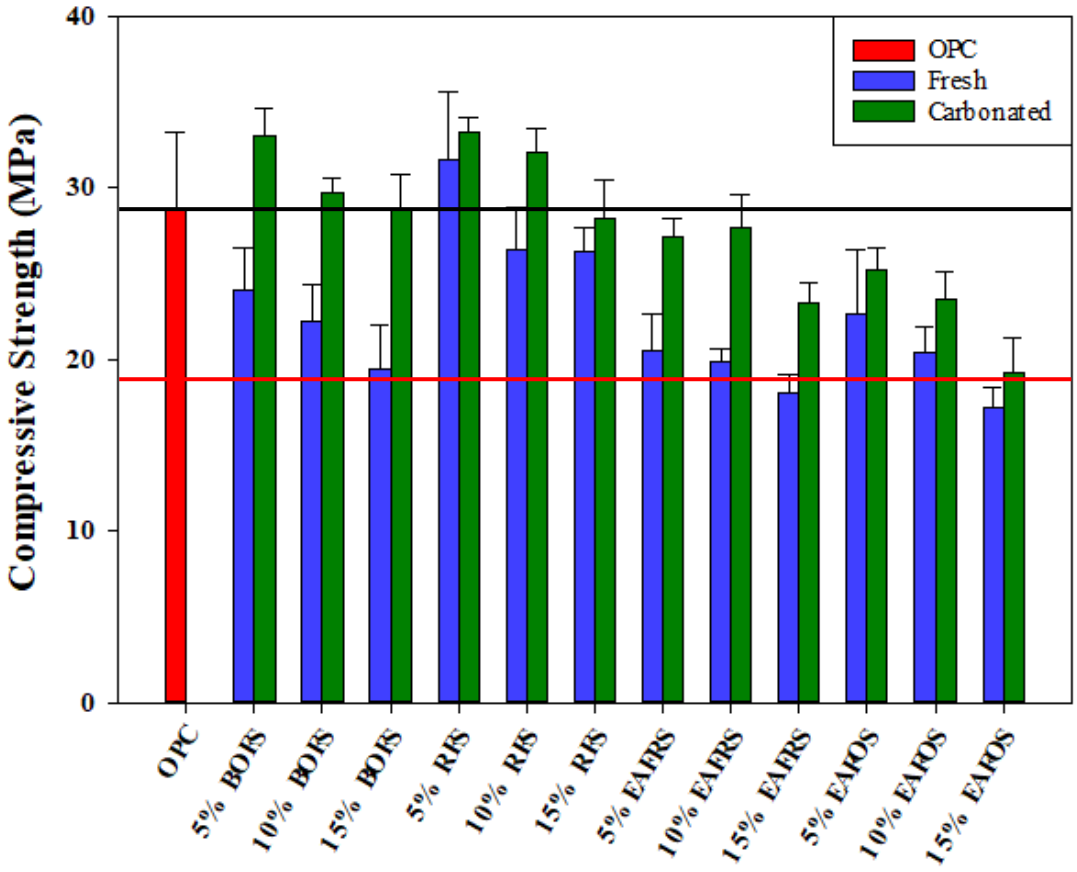

Figure 4-15 The 7th day Compressive Strength of Mortars with Different Replacing Ratio of Slags.

doi:10.6342/NTU201902030

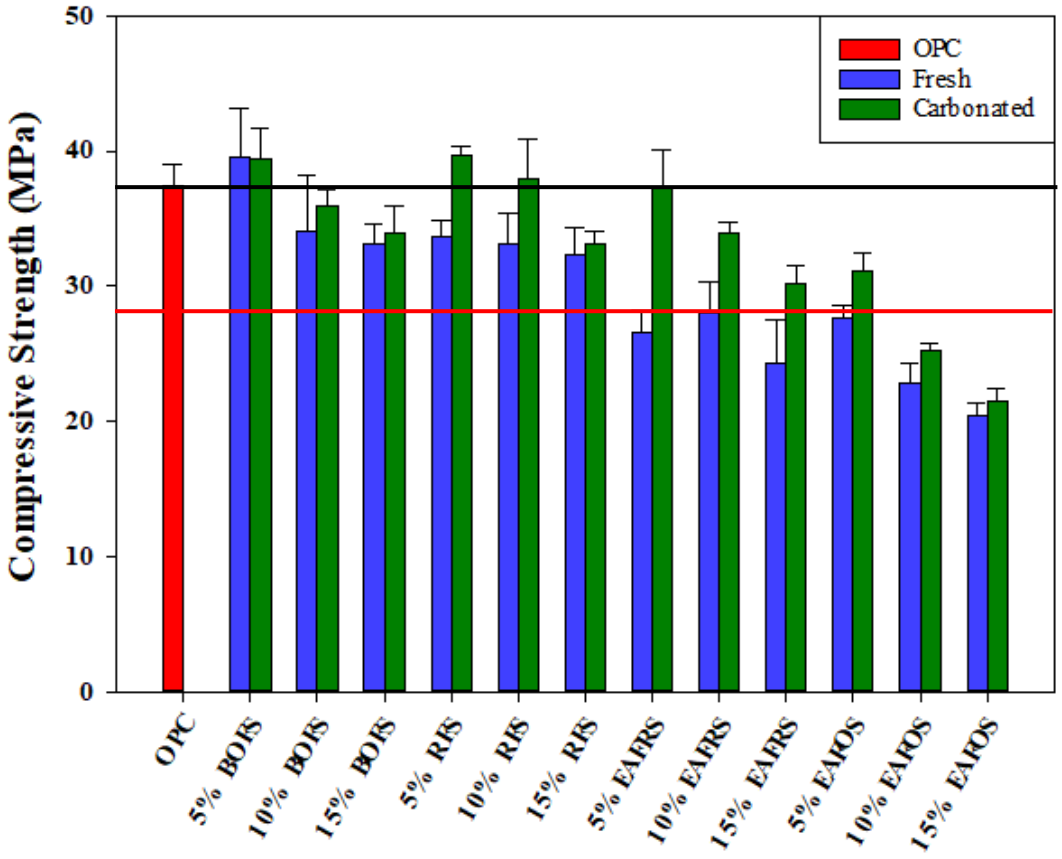

Figure 4-16 The 28th day Compressive Strength of Mortars with Different Replacing Ratio of Slags.

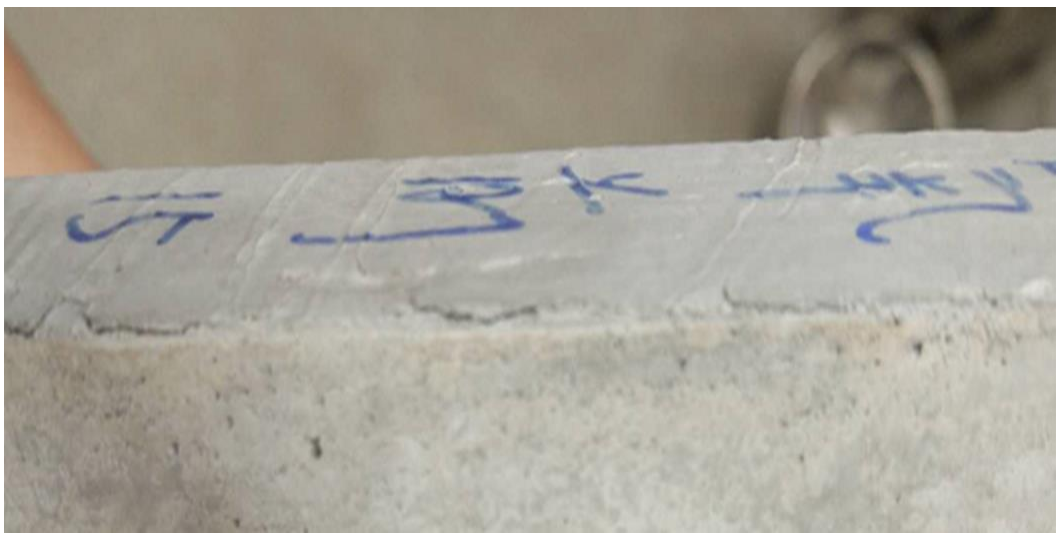

Figure 4-17 Fatal Expansion Causing by AAR in EAFOS Cement Bars.

doi:10.6342/NTU201902030

4-2-3 Effect of Substitution on Durability of Cement

Autoclave expansion mainly comes from the reaction of free-CaO and free-MgO with water. Through figure 4-18, because the free-CaO in slags turns into calcium carbonate during the carbonation process, the autoclave expansion rate of each kind of carbonated slag decreases greatly. Because volume change of cement will cause micro-cracks in the cement structure, which may affect its durability, autoclave expansion and the free-CaO contain should be standardize. Although the cement paste expansion ratio of bars blended with slags within and without carbonation both meet the CNS regulation, the durability of cement will performance better as the volume variate smaller. Additionally, the difference of expansion rate among different slags may also affect by the free-CaO. According to table 4-1, except EAFOS, the slags which has higher f-CaO content such as RFS or EAFRS will perform a larger expansion rate in this study.

The mechanism of expansion in EAFOS is different from others. With such low amount of f-CaO, fresh EAFOS comes into a higher expansion rate due to the alkali-aggregate reaction. During the heating period in autoclave, cement bars with fresh EAFOS will absorb moisture, using it to participate in the AAR reaction. AAR also cause smaller expansion rate in the carbonated EAFOS cement bars. Due to alkali-silica gel in EAFOS will absorb water and expand during carbonation, the carbonated slag will not re-expand to much in the autoclave expansion period.

doi:10.6342/NTU201902030

Table 4-9 Autoclave Expansion of Pastes with Different Replacing Ratio of Slags.

Items	Replacing ratio	Autoclave expansion rate (%)	
		Fresh	Carbonated
CNS regulation	-	0.8	
OPC	-	0.113±0.008	
BOFS	5%	0.141±0.007	0.121±0.009
	10%	0.181±0.013	0.152±0.008
	15%	0.203±0.013	0.173±0.010
RFS	5%	0.163±0.006	0.142±0.009
	10%	0.232±0.015	0.174±0.008
	15%	0.253±0.008	0.192±0.006
EAFRS	5%	0.182±0.010	0.161±0.015
	10%	0.227±0.009	0.182±0.008
	15%	0.275±0.017	0.244±0.010
EAFOS	5%	0.192±0.014	0.109±0.009
	10%	0.225±0.020	0.176±0.018
	15%	0.295±0.021	0.190±0.019

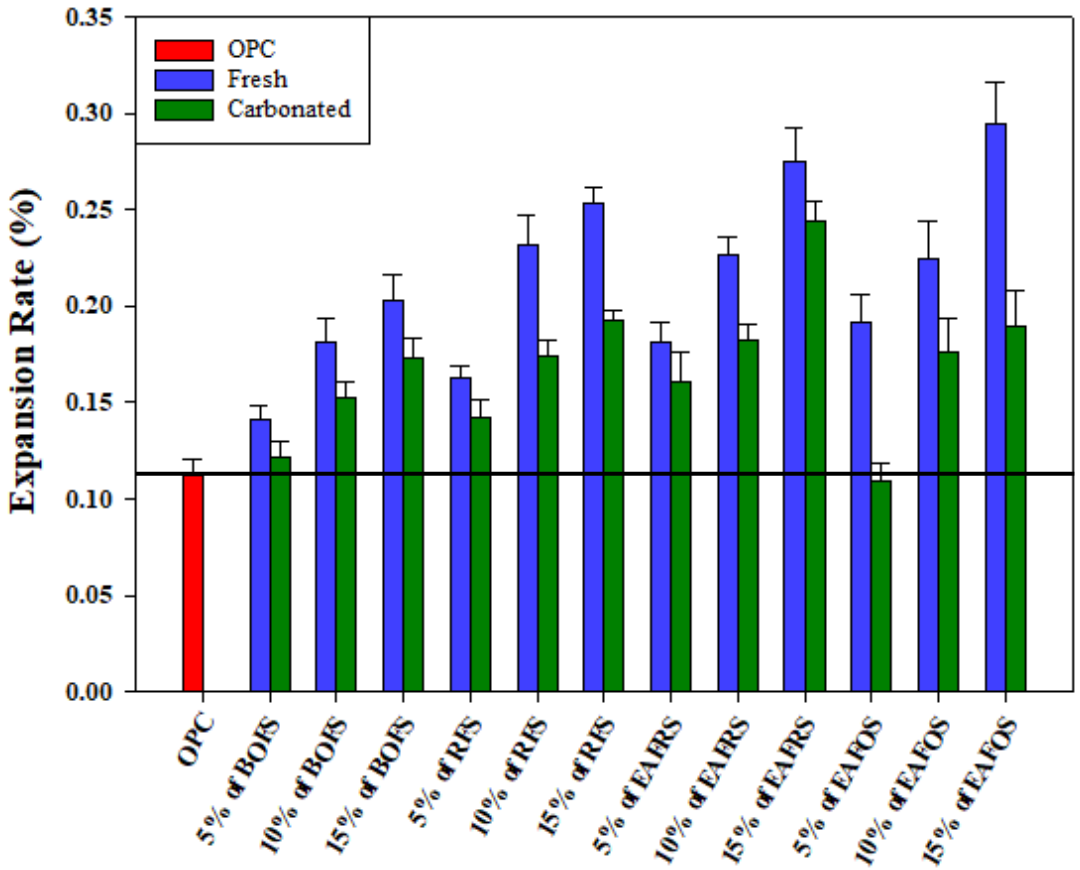

Figure 4-18 Autoclave Expansion of Pastes with Different Replacing Ratio of Slags.

doi:10.6342/NTU201902030

Another factor which would influent durability of cement is drying shrinkage. As the humidity goes down, free water in the porosity and water adsorb on the surface of C-S-H gel layer are removed and cause shrinkage. In this study, mortar bars with 10% replacement of slags are placed in a dryer environment to test the amount of shrink.

Through figure 4-19, it illustrates that the carbonated slags' mortar bars contain less amount of shrinkage. The calcium carbonated in the carbonated slags can reacts with tricalcium aluminate and form C-A-$\bar{C}$-H hydration product to fill in porosity, which results in the structure of mortar gets more densely. Thus, free water in porosity can't be easily removed and the amount of shrinkage decreases. However, the result of EAFOS containing mortar bars performed the opposite. The carbonated EAFOS mortar has larger dying shrinkage. It is speculated that during the carbonation, AAR produces alkali-silica gel and absorbs water previously. During the process of drying shrinkage, the absorption water in the gel is later removed and produces larger amount of drying shrinkage at the same time.

Table 4-10 Drying Shrinkage of Mortars with 10% Replacement of Slags.

Items		Shrinkage rate (%)			
		4 day	11 day	18 day	25 day
OPC	-	0.0367	0.0529	0.0575	0.0595
BOFS	Fresh	0.0342	0.0506	0.0574	0.0596
	Carbonated	0.0360	0.0522	0.0552	0.0593
RFS	Fresh	0.0378	0.0541	0.0599	0.0635
	Carbonated	0.0372	0.0540	0.0583	0.0599
EAFRS	Fresh	0.0375	0.0518	0.0580	0.0612
	Carbonated	0.0365	0.0517	0.0566	0.0584
EAFOS	Fresh	0.0346	0.0507	0.0563	0.0581
	Carbonated	0.0401	0.0582	0.0651	0.0683

doi:10.6342/NTU201902030

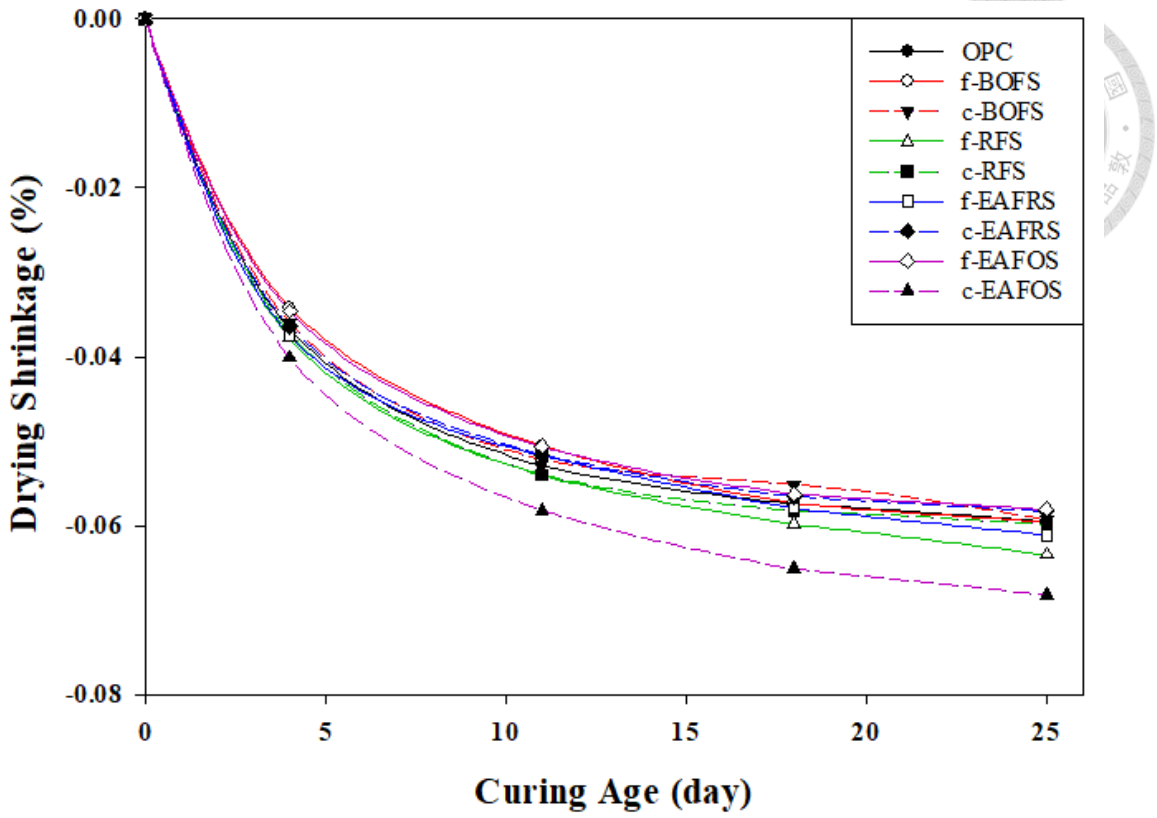

Figure 4-19 Drying Shrinkage of Mortars with 10% Replacement of Slags.

4-3 Strength Prediction Model of Clinker

When the steelmaking slags were added into the clinker, the constitution would be substantially different, causing the change in hydration behavior and the performance of the cement. According to the XRF results, the major composition in the clinker could be estimated by performing Taylor calculation. In the calculation, the used coefficient matrix was given as shown in equation 3-10. Although the mass fraction of oxide composition can be obtained easily from the XRF result, the value should be recalculated by subtracting the impurities. Considering to the crystallization and activity difference between these steelmaking slags and Portland Cement clinker, all of the supplementary materials in this study should be classified in the “others” category.

doi:10.6342/NTU201902030

The calculation results of eq. 3-10 is illustrated in table 4-11 and figure 4-20. As it shows, C_3S and C_2S, which are combined into "calcium silicate" to express in this study, provide 65.6 to 77.5% of the weight as the dominant phases in reactant. C_3A and C_4AF occupies about 5% and 10% of mass separately in the reactant. Although they seem insignificant compared with calcium silicates, the existence of them may still play an important role in cement properties such as affecting setting rate, early age strength development and increasing the potential of sulfate attack. The "others" category includes the impurities in cement clinker and kinds of steelmaking slags, which content increases from 6.4 to 20.5 % as the substitution rate grows higher.

Table 4-11 Variation in Weight Fraction of Major Compositions in Hydration Reactants.

	Calcium Silicate	C_3A	C_4AF	Others
OPC	77.48	5.59	10.5	6.43
5% Substitution	73.606	5.3105	9.975	11.1085
10% Substitution	69.732	5.031	9.45	15.787
15% Substitution	65.858	4.7515	8.925	20.4655

doi:10.6342/NTU201902030

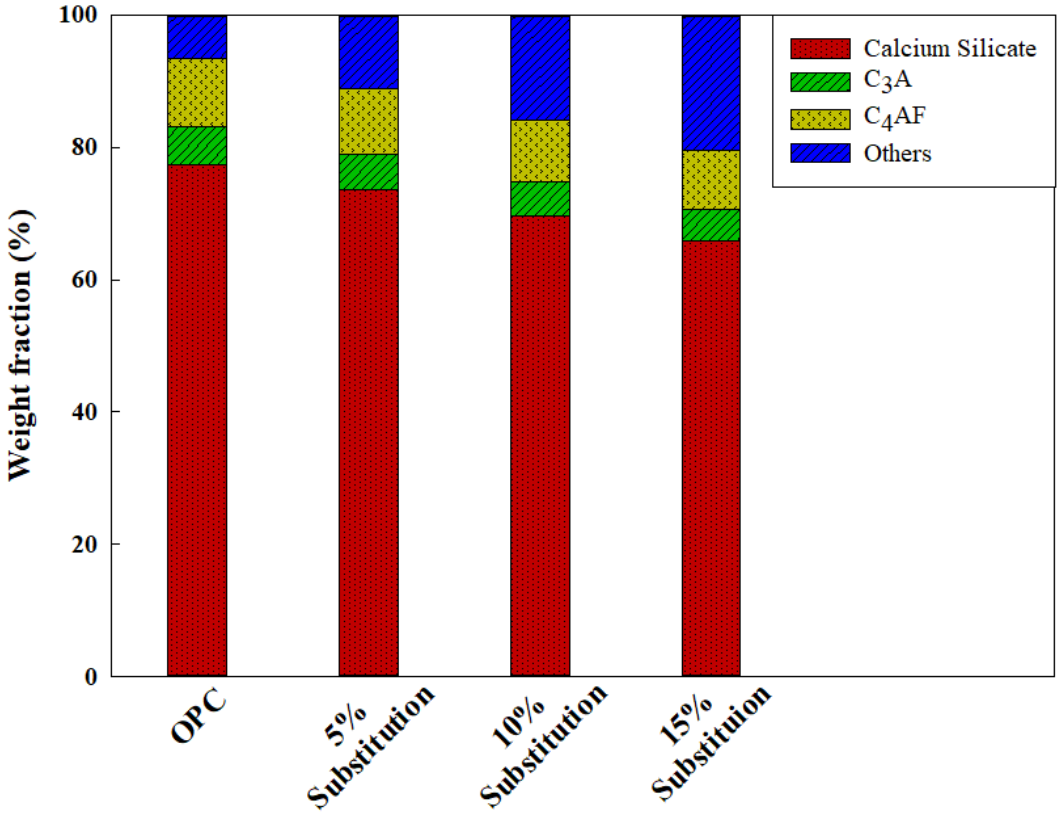

Figure 4-20 Variation in Weight Fraction of Major Compositions in Hydration Reactants.

To understand the strength development trend, a non-linear regression kinetic model has to be established. Table 4-12 lists the corresponding kinetic constants of blended cement, which is related to strength development under different operating conditions.

P_0 is the compressive strength of mortars at the initial age. This parameter might affect by the tightness of filling in the structure because it doesn't have a lot of hydration product being produced at this stage. Moreover, the reaction rate of nucleation which may affect the generation rate of hydration product in the early age may also affects the P_0 value. k is the rate constant of strength development, which is a function of mineral compositions in the reactants. The k value is not only related to the bonding strength

doi:10.6342/NTU201902030

between hydration products but also corresponds to the pozzolanic reaction products, which will re-fill in the porosity of C-S-H gel and make the structure denser.

As the table shown, P_0 goes down from 3.2% to 53.2% as the substitution rate getting up. This phenomenon is based on that higher substitution rate implies lower C_3S in the blended reactants, which is lack of binder and can't provide enough strength support. The mortars with carbonated slags used to have a higher initial strength than those with fresh slags, which prove that calcium carbonate can elevate the nucleation of hydration. What's more, carbonated slags except EAFRS also has finer particle size than Portland Cement, making the stacking denser and causing the carbonated BOFS, RFS mortars have higher P_0 value. However, the P_0 values of carbonated EAFOS mortars are 2.6% to 14.6% smaller than the fresh EAFOS mortars despite the carbonated EAFOS has smaller particle size and more calcium to nucleate. This abnormal phenomenon is due to the expansion of alkali-aggregate reaction. Owing to the slag milled into finer particle size will have larger surface area, which makes the reaction get rapider, the alkali-silicate gel will fill in the structure and enhance the initial strength.

The k values of mortars with partial replacement in this study are usually lower than the OPC mortar. This was because these steelmaking slags do not contain sufficient active silicate to participate the reaction, such that the hydration product may not be strong enough to provide the strength development. Fortunately, carbonation seems to be a good way to improve the k constant. The mortars with carbonated EAFRS and EAFOS blended inside is 16% to 115% higher than those with fresh slags. The reason

doi:10.6342/NTU201902030

causing the carbonated EAFRS mortars have higher k values is calcium carbonate will react with C_3A and calcium hydroxide, which can be regarded as a kind of pozzolanic reaction that can produce C-A-$\bar{C}$-H type of hydration product to fill up cavity in the structure. Otherwise, the mechanism that cause carbonated EAFOS mortars have higher k values is inhibition of the alkali-aggregate reaction, which cause expansion and cracks in the specimens and weaken the long-age strength significantly. However, the k value of carbonated BOFS and RFS slags' mortars don't perform well in this study. This implies that the C-A-$\bar{C}$-H structure can only make the mortar denser but not stronger. Because the C-A-$\bar{C}$-H structure is similar to the ettringite, which grows like a hexagonal needle. This bonding strength between each needle-shape crystal is so weak that this type of structure has obvious shortcoming.

doi:10.6342/NTU201902030

Table 4-12 Kinetics of Compressive Strength Development of Blended Cement with Different Substitution Ratios.

Item		Replacement Ratio	P_0	k	R^2
OPC	-	-	12.5711±2.3816	7.6021±1.0281	0.982
BOFS	Fresh	5%	8.1703±3.6262	9.1723±1.5654	0.972
		10%	8.9205±2.0948	7.4237±0.9044	0.985
		15%	3.8324±2.2408	8.6413±0.9674	0.988
	Carbonated	5%	19.6208±2.6891	6.1062±1.1609	0.965
		10%	17.4093±2.1950	5.6882±0.9476	0.973
		15%	18.9914±1.4741	4.5675±0.6364	0.981
RFS	Fresh	5%	23.1505±3.3658	3.3792±1.4530	0.844
		10%	18.0620±0.6525	4.4716±0.2817	0.996
		15%	12.1184±3.5236	6.2799±1.5211	0.945
	Carbonated	5%	24.2304±0.0085	4.6119±0.0037	1.000
		10%	18.7685±3.1752	5.9426±1.3708	0.950
		15%	17.0255±2.6285	4.9906±1.1347	0.951
EAFRS	Fresh	5%	15.9041±2.4266	3.0561±1.0476	0.895
		10%	13.2901±2.9979	4.2545±1.2942	0.915
		15%	7.9061±0.7652	4.9683±0.3303	0.996
	Carbonated	5%	10.5589±1.3603	8.1113±0.5873	0.995
		10%	12.5491±3.9448	6.6575±1.7030	0.939
		15%	8.9873±2.8309	6.5454±1.2221	0.966
EAFOS	Fresh	5%	17.8419±1.2357	2.8501±0.5335	0.966
		10%	17.5876±0.3404	1.5427±0.1469	0.991
		15%	9.6762±1.8549	3.3358±0.8008	0.946
	Carbonated	5%	15.3762±0.9434	4.7785±0.4073	0.993
		10%	15.0148±3.6453	3.3177±1.5737	0.816
		15%	9.4237±4.0058	3.8780±1.7293	0.834

doi:10.6342/NTU201902030

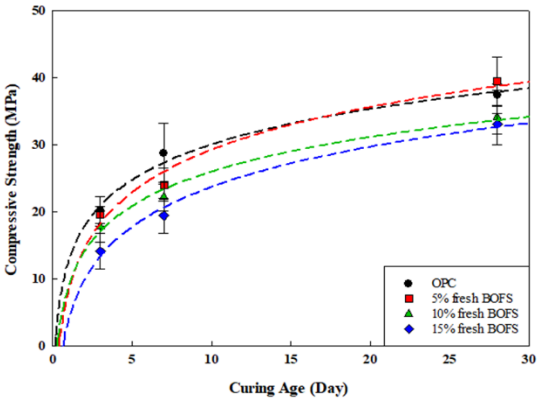

(a)

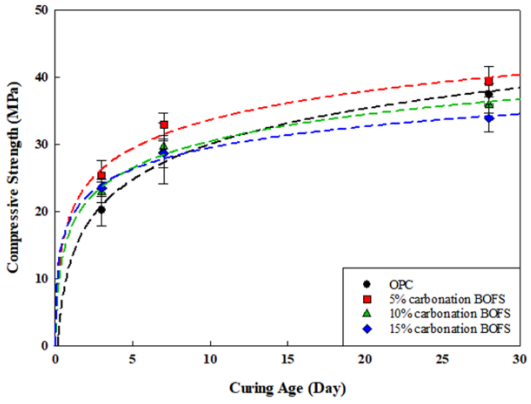

(b)

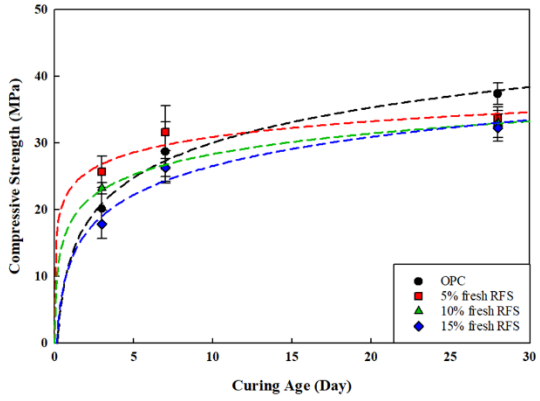

(c)

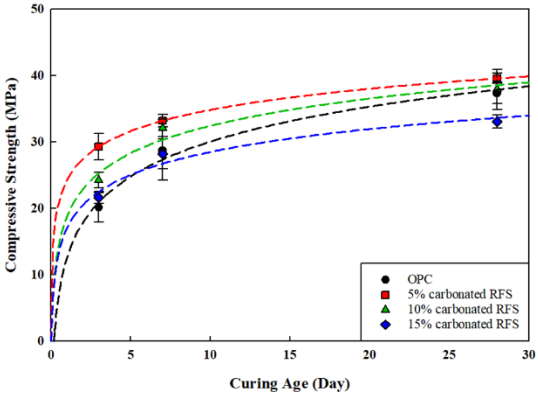

(d)

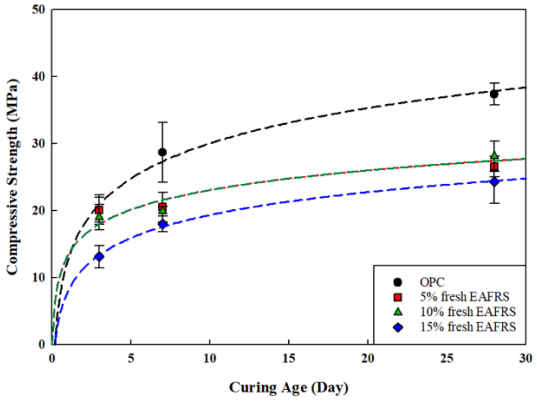

(e)

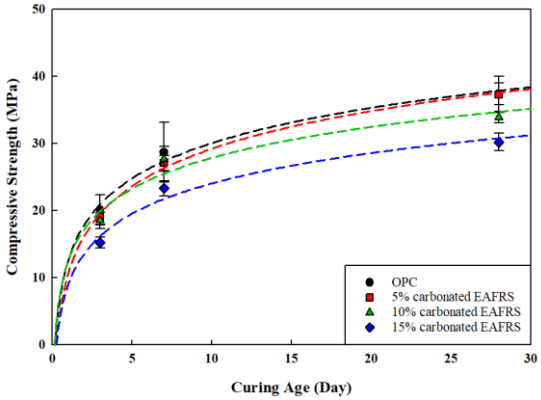

(f)

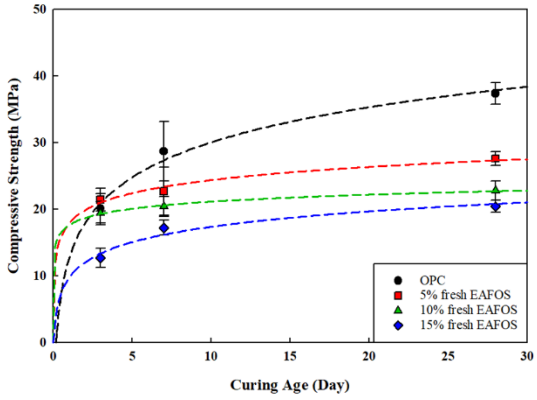

(g)

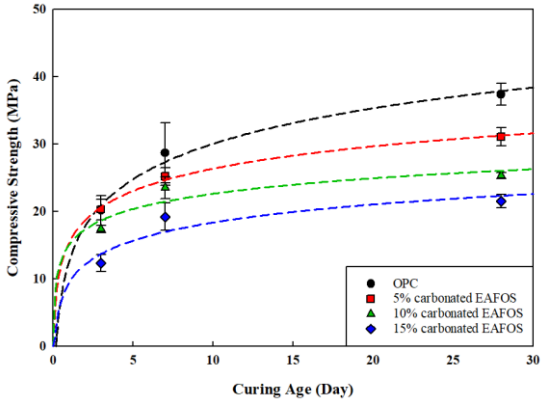

(h)

doi:10.6342/NTU201902030

Figure 4-21 Development of Compressive Strength of Blended Cement with Different Substitution Ratio of Steelmaking Slags.

Consider that the strength development of cement mortar is correlated to mineral composition of the clinker within a considerably large extent (Taylor, 1997). Thus, the relation between the composition of mortar and compressive strength development could be putted into discuss. In this study, the strength development of the blended reactant was correlated with the compositions of cement mortars, e.g., C_3A, C_4AF, silica, and other supplemental materials, by the multiple non-linear regression, as shown in table 4-13. Where the contents of silicates, C_3A, and C_4AF varied in the ranges between 65.9%-77.5%, 4.8%-5.6%, and 8.9%-10.5%, respectively. The correlation results are well fitted to the experimental data, with an R^2 value of 0.88. It implies that the contributions of mineral compositions to strength development are silica > C3A > C4AF. Comparing with other mineral compositions, the calcium silicates makes great contributions to strength development, which meets the observations results in the literature (Abd elaty, 2014). The calcite product is found to exhibit a positive effect on the strength development of cement mortar, with an exponent of 1.17.

Figure 4-22 shows the correlation of measured and calculated compressive strength of cement mortars with all kinds of steelmaking slags. The results point out that the developed model could properly describe the development of the compressive strength and all of the prediction compressive value is within 10% deviation. The developed model can properly describe the strength development with different ingredients, with an R^2 value of 0.979.

doi:10.6342/NTU201902030

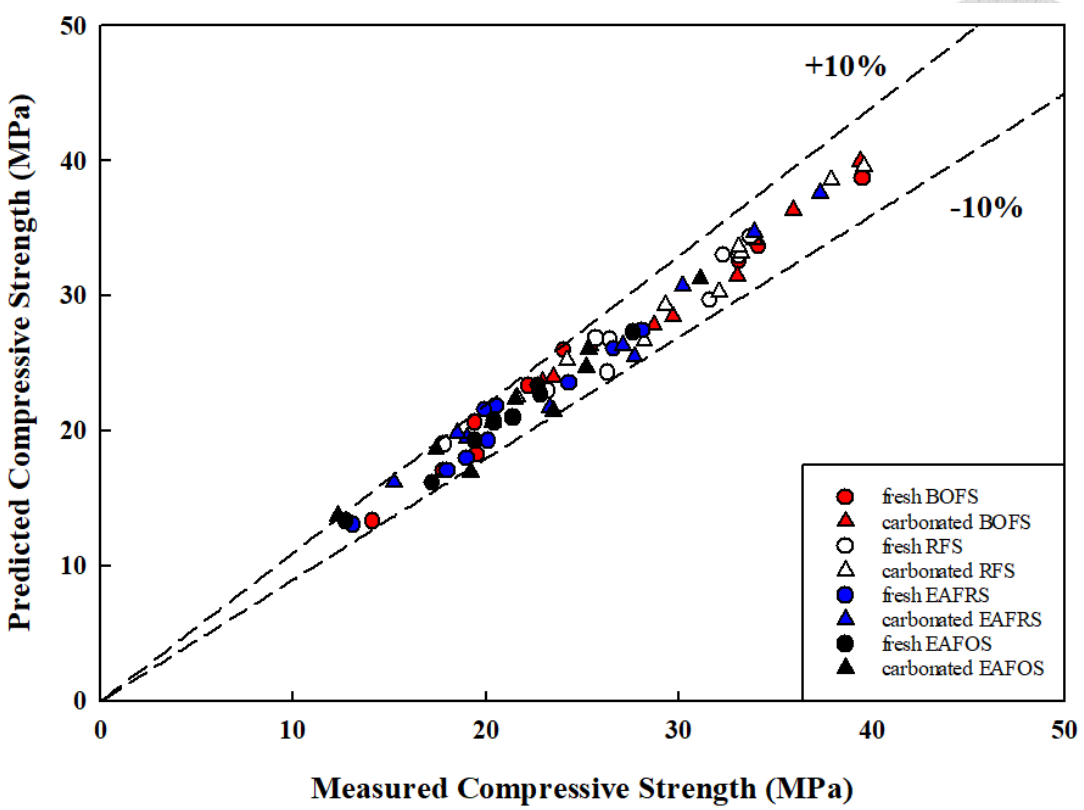

Figure 4-22 Comparison of Predicted Compressive Strength with Measured Compressive Strength.

doi:10.6342/NTU201902030

Chapter 5 Conclusions and Recommendations

5-1 Conclusions

In the first part of this study, the carbonation conversion yield varies with condition, such as particle size (32 to 160μm), liquid to slurry ratio (10 to 50 mL/g) and rotating speed (700 to 1300 rpm). According to the carbonation conversion yield calculated from the TGA results, the best operating condition in engineering was particle size: 32 μm; liquid to solid ratio: 20 mL-tap water/g-slag; rotating speed: 1100rpm, which can fixed 19.29±0.05 g-CO_2/g-EAFRS. Besides, the XRD and SEM images also certified that the carbonation process of steelmaking slags successfully converted free lime, calcium hydroxide and calcium silicates into calcium carbonate.

In the second part, with 5 to 15% of cement replaced by steelmaking slags, the fluidity of cement decreased slightly with viscosity increased together. This phenomenon might prevent the cement segregated from aggregates. In the setting test, the carbonation process could wash out the organic compounds in the EAFOS, prevent the retarding phenomenon and make the cement specimens set normally. Besides, the carbonation process could also eliminate harmful substances such as free lime, calcium hydroxide and alkali ions, which prevented the specimens expanding from the hydration process and the alkali-aggregate reaction. Furthermore, calcium carbonated generated form the carbonation process could react with tricalcium aluminate in clinker, which produced C-A-$\bar{C}$-H gel, filled up the porosity between hydration products and enhance the durability of cement specimens.

doi:10.6342/NTU201902030

In the third part, strength prediction model was established to illustrate the strength development process. According to the P_0 and k value in the model, cement specimens with partial replacement of carbonated steelmaking slags were certified to have denser filling and higher strength development trend.

5-2 Recommendations

It is suggested that these future works should be focused on:

a. The variation of cement specimens which are exposed in high sulfate environment can be further investigated.
b. Cost estimation and economic benefits of carbonation and cement replacement should be established.
c. Due to the poor strength development and low durability, different utilization approaches of EAFOS should be evaluated and adopted.

doi:10.6342/NTU201902030

Reference

1. Barnes, P. and J. Bensted (2002). Structure and Performance of Cements, Second Edition , Taylor & Francis.
2. Belhadj, E.; Diliberto, C.; Lecomte, A. (2012). Characterization and activation of Basic Oxygen Furnace slag. Cement and Concrete Composites, 34(1), 34-40.
3. Belhadj, E.; Diliberto, C.; Lecomte, A. (2014). Properties of hydraulic paste of basic oxygen furnace slag. Cement and Concrete Composites, 45, 15-21.
4. Bentz, D. P.; Ardani, A.; Barrett, T.; Jones, S. Z.; Lootens, D.; Peltz, M. A.; Weiss, W. J. (2015). Multi-scale investigation of the performance of limestone in concrete. Construction and Building Materials, 75, 1-10.
5. Bentz, D. P.; Sato, T.; De la Varga, I.; Weiss, W. J. (2012). Fine limestone additions to regulate setting in high volume fly ash mixtures. Cement and Concrete Composites, 34(1), 11-17.
6. Bobicki, E. R.; Liu, Q.; Xu, Z.; and Zeng, H. (2012). Carbon capture and storage using alkaline industrial wastes. Progress in Energy and Combustion Science, 38(2), 302-320.
7. Brand, A. S.; Roesler, J. R. (2015). Steel furnace slag aggregate expansion and hardened concrete properties. Cement and Concrete Composites, 60, 1-9.
8. Chang, E. E.; Chen, C. H.; Chen, Y. H.; Pan, S. Y.; Chiang, P. C. (2011). Performance evaluation for carbonation of steel making slags in a slurry reactor. Journal of Hazardous Materials , 186, 558 564.

doi:10.6342/NTU201902030

9. Cheng-HsiuYu; Ming-Tsz Chen; Hao Chen; Chung-SungTan (2016). Effects of process configurations for combination of rotating packed bed and packed bed on CO2 capture. Applied Energy, 175, 269-276.
10. Chen, Z.; Xie, J.; Xiao, Y.; Chen, J.; Wu, S. (2014). Characteristics of bonding behavior between basic oxygen furnace slag and asphalt binder. Construction and Building Materials, 64, 60-66.
11. Chindaprasirt, P.; Kanchanda, P.; Sathonsaowaphak, A.; Cao, H. (2007). Sulfate resistance of blended cements containing fly ash and rice husk ash. Construction and Building Materials, 21(6), 1356-1361.
12. De Weerdt, K.; Haha, M. B.; Le Saout, G.; Kjellsen, K. O.; Justnes, H.; Lothenbach, B. (2011). Hydration mechanisms of ternary Portland cements containing limestone powder and fly ash. Cement and Concrete Research, 41(3), 279-291.
13. Dri, M.; A. Sanna; M. M. Maroto Valer (2014). Mineral carbonation from metal wastes: Effect of solid to liquid ratio on the efficiency and characterization of carbonated products. Applied Energy, 113, 515-523.
14. Eloneva, S.; Said, A.; Fogelholm, C. J.; Zevenhoven, R. (2012) Preliminary assessment of a method utilizing carbon dioxide and steelmaking slags to produce precipitated calcium carbonate. Applied Energy, 90, 329-334.
15. Fernandez Bertos, M.; S. J. Simons; C. D. Hills; P. J. Carey (2004). A review of accelerated carbonation technology in the treatment of cement-based materials and sequestration of CO_2. J Hazard Mater, 112(3), 193-205.

doi:10.6342/NTU201902030

16. Gambhir, M. L. (2013). Concrete Technology: Theory and Practice: Tata McGraw-Hill Education.
17. Goto, S.; Suenaga, K.; Kado, T.; Fukuhara, M. (1995). Calcium silicate carbonation products. Journal of the American Ceramic Society, 78(11), 2867-2872.
18. Huijgen, W. J. J.; Comans , J. W. R. N. J. (2005) Mineral CO 2 sequestration by steel slag carbonation.
19. Jo, H.; S. H. Park; Y. N. Jang, S. C. Chae; P. K. Lee; H. Y. Jo (2014). Metal extraction and indirect mineral carbonation of waste cement material using ammonium salt solutions. Chemical Engineering Journal, 254, 313-323.
20. Juenger, M. C.; Siddique, R. (2015). Recent advances in understanding the role of supplementary cementitious materials in concrete. Cement and Concrete Research.
21. Keum-Il Song; Jin-Kyu Song; Bang Yeon Lee; Keun-Hyeok Yang (2014). Carbonation Characteristics of Alkali-Activated Blast-Furnace Slag Mortar, Advances in Materials Science and Engineering.
22. Kourounis, S.; Tsivilis, S.; Tsakiridis, P.; Papadimitriou, G.; Tsibouki, Z. (2007). Properties and hydration of blended cements with steelmaking slag. Cement and Concrete Research, 37(6), 815-822.
23. Laura Dembovska; Diana Bajare; Ina Pundiene; Laura Vitola (2017). Effect of Pozzolanic Additives on the Strength Development of High Performance Concrete. Procedia Engineering, 172, 202-210.
24. Lawrence, C. (1990). Sulphate attack on concrete. Magazine of Concrete Research, 42(153), 249-264.

doi:10.6342/NTU201902030

25. Lothenbach, B.; Le Saout, G.; Gallucci, E.; Scrivener, K. (2008). Influence of limestone on the hydration of Portland cements. Cement and Concrete Research, 38(6), 848-860.
26. Lothenbach, B.; Scrivener, K.; Hooton, R. (2011). Supplementary cementitious materials. Cement and Concrete Research, 41(12), 1244-1256.
27. Massazza, F.; Daimon, M. (1992). Chemistry of hydration of cements and cementitious systems. Paper presented at the Proceedings of 9th International Congress on the Chemistry of Cement.
28. Matschei, T.; Lothenbach, B.; Glasser, F. P. (2007). The role of calcium carbonate in cement hydration. Cement and Concrete Research, 37(4), 551-558.
29. Mechling, J.-M.; Lecomte, A.; Diliberto, C. (2009). Relation between cement composition and compressive strength of pure pastes. Cement and Concrete Composites, 31(4), 255-262.
30. Mehta, P. K.; Monteiro, P. J. (2006). Concrete: microstructure, properties, and materials (Vol. 3): McGraw-Hill New York.
31. Mindess, S.; Young, J. F.; Darwin, D. (2003). Concrete.
32. Monshi, A.; Asgarani, M. K. (1999). Producing Portland cement from iron and steel slags and limestone. Cement and Concrete Research, 29(9), 1373-1377.
33. Muftah H. El-Naas; Maisa El Gamal; Suhaib Hameedi; Abdel-Mohsen O. Mohamed (2015). CO_2 sequestration using accelerated gas-solid carbonation of pre-treated EAF steel-making bag house dust. Journal of Environmental Management, 156, 218-224.

doi:10.6342/NTU201902030

34. Murphy, J.; Meadowcroft, T.; Barr, P. (1997). Enhancement of the cementitious properties of steelmaking slag. Canadian Metallurgical Quarterly, 36(5), 315-331.
35. Nawaz Ahmad; Anders Wörman; Xavier Sanchez-Vila; Jerker Jarsjö; Andrea Bottacin-Busolin, Helge Hellevang (2016). Injection of CO2-saturated brine in geological reservoir: A way to enhanced storage safety. International Journal of Greenhouse Gas Control, 54, 129-144.
36. N.L. Ukwattage; P.G. Ranjith; X. Li (2017). Measurement, 97, 15-22.
37. Pan, S. Y. (2012). CO_2 Capture by Accelerated Carbonation of Alkali ne Wastes: A Review on Its Principles and Applications. Aerosol and Air Quality Research.
38. Pan, S. Y.; R. Adhikari; H. Chen; P. Li; P. C. Chiang (2016). Integrated and innovative steel slag utilization for iron reclamation, green material production and CO_2 fixation via accelerated carbonation. Journal of Cleaner Production, 137, 617-631.
39. Pan, S. Y., A. M. Lorente Lafuente and P. C. Chiang (2016). Engineering, environmental and economic performance evaluation of high-gravity carbonation process for carbon capture and utilization. Applied Energy, 170, 269-277.
40. Park, A. H. A. and L. S. Fan (2004). Mineral sequestration: Physically activated dissolution of serpentine and pH swing process. Chemical Engineering Science, 59 (22-23), 5241-5247.
41. Péra, J.; Husson, S.; Guilhot, B. (1999). Influence of finely ground limestone on cement hydration. Cement and Concrete Composites, 21(2), 99-105.

doi:10.6342/NTU201902030

42. Rosa M. Cue´llar-Franca; Adisa Azapagic (2015). Carbon capture, storage and utilization technologies: A critical analysis and comparison of their life cycle environmental impacts. Journal of CO_2 Utilization, 9, 82–102.
43. Rostami, V.; Shao, Y.; Boyd, A. J.; He, Z. (2012). Microstructure of cement paste subject to early carbonation curing. Cement and Concrete Research, 42(1), 186-193.
44. Shaik Hussain; Dipendu Bhunia; S.B. Singh (2017). Comparative study of accelerated carbonation of plain cement and fly-ash concrete. Journal of Building Engineering, 10. 26-31.
45. Shi, C., Qian, J. (2000). High performance cementing materials from industrial slags—a review. Resources, Conservation and Recycling, 29(3), 195-207.
46. Shu-Yuan Pan; Yi-Hung Chen; Chun-Da Chen; Ai-Lin Shen; Michael Lin; Pen-Chi Chiang (2015). High-Gravity Carbonation Process for Enhancing CO_2 Fixation and Utilization Exemplified by the Steelmaking Industry. Environmental Science & Technology, 49, 12380−12387
47. Si-Lu Pei; Shu-Yuan Pan; Xiang Gao; Yun-Ke Fang; Pen-Chi Chiang (2018) Efficacy of carbonated petroleum coke fly ash as supplementary cementitious materials in cement mortars. Journal of Cleaner Production, 180, 689-697.
48. Taylor, H. F. (1997). Cement chemistry: Thomas Telford.
49. Thomas, M. (2013). Supplementary cementing materials in concrete: CRC Press.
50. Tongsheng Zhang; Qijun Yu; Jiangxiong Wei; Pingping Zhang; Peixin Chen (2011). A gap-graded particle size distribution for blended cements: Analytical approach and experimental validation. Powder Technology, 214, 259-268.

doi:10.6342/NTU201902030

51. Tongsheng Zhang; Peng Gao; Ruifeng Luo; Jiangxiong Wei; Qijun Yu (2014). Construction and Building Materials, 54, 339-347.
52. Tongsheng Zhang; Xiangyang Liu; Jiangxiong Wei; Qijun Yu (2014). Cement & Concrete Composites, 52, 18-26.
53. Xiao-Hua Zheng; Guang-Wen Chu; De-Jia Kong; Yong Luo; Jing-Peng Zhang; Hai-Kui Zou; Li-Li Zhang; Jian-Feng Chen (2016). Mass transfer intensification in a rotating packed bed with surface-modified nickel foam packing. Chemical Engineering Journal, 285, 236-242.
54. Yang, K.-H.; Jung, Y.-B.; Cho, M.-S.; Tae, S.-H. (2014). Effect of supplementary cementitious materials on reduction of CO_2 emissions from concrete. Journal of Cleaner Production.
55. Yuting Tan; Worrada Nookuea; Hailong Li; Eva Thorin; Jinyue Yan (2016). Property impacts on Carbon Capture and Storage (CCS) processes: A review. Energy Conversion and Management, 118, 204–222.
56. Zhongya Zhang; Xiaoguang Jin; Wei Luo (2019). Long-term behaviors of concrete under low-concentration sulfate attack subjected to natural variation of environmental climate conditions. Cement and Concrete Research, 116, 217-230.

doi:10.6342/NTU201902030

doi:10.6342/NTU201902030

Appendix

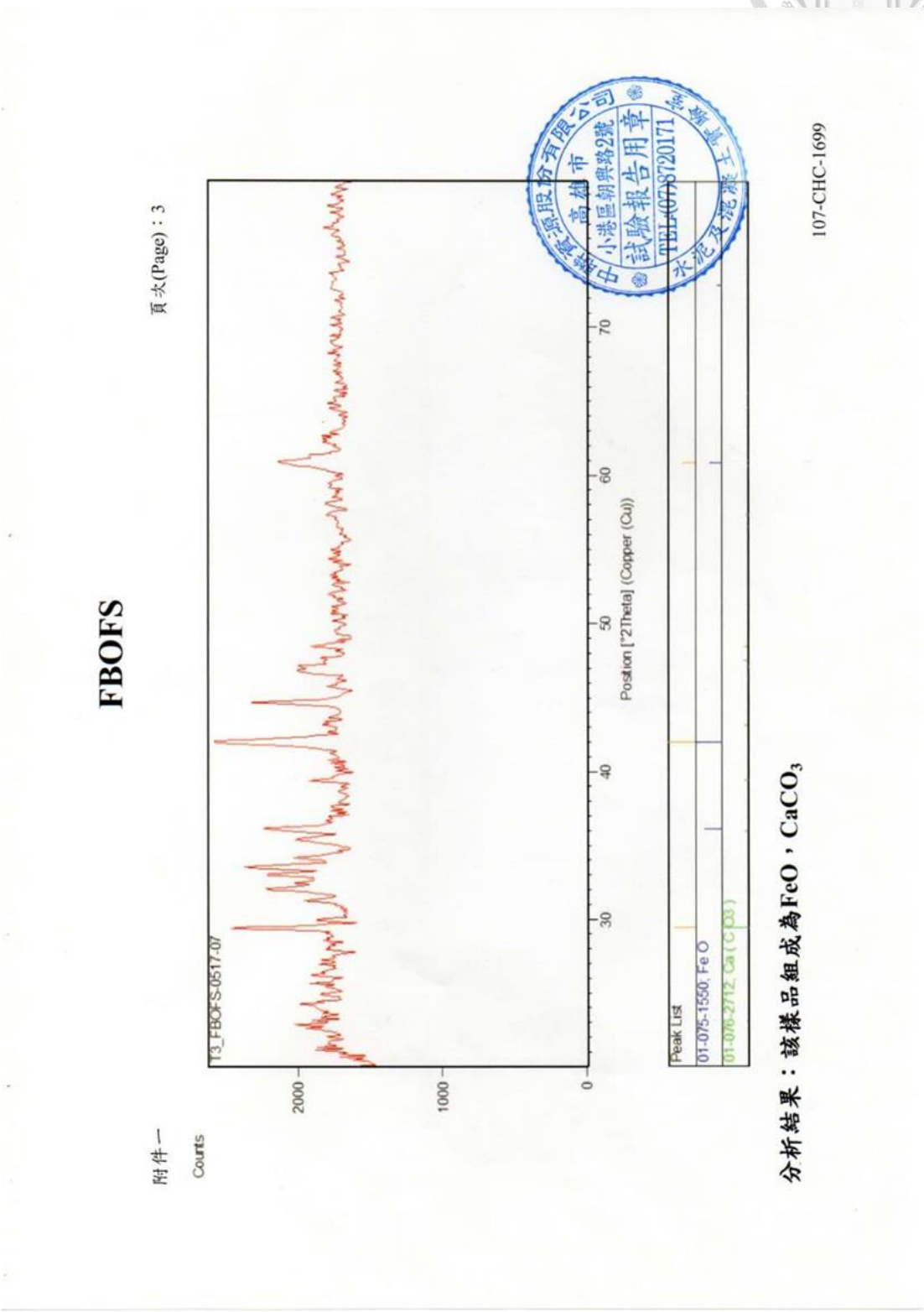

doi:10.6342/NTU201902030

CBOFS

附件一

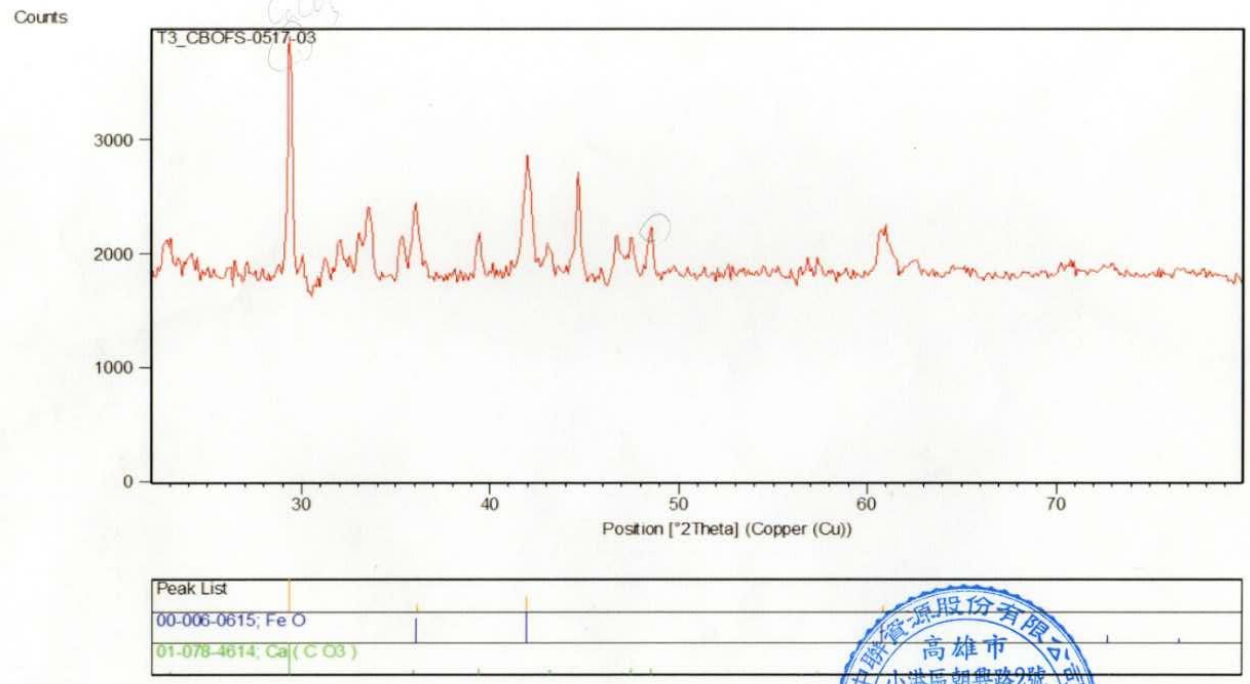

分析結果：該樣品組成為$CaCO_3$，FeO

中聯資源股份有限公司 高雄市小港區朝興路2號 試驗報告用章 TEL:(07)8720171 水泥及混凝土實驗室

107-CHC-1695

doi:10.6342/NTU201902030

FRFS

附件一

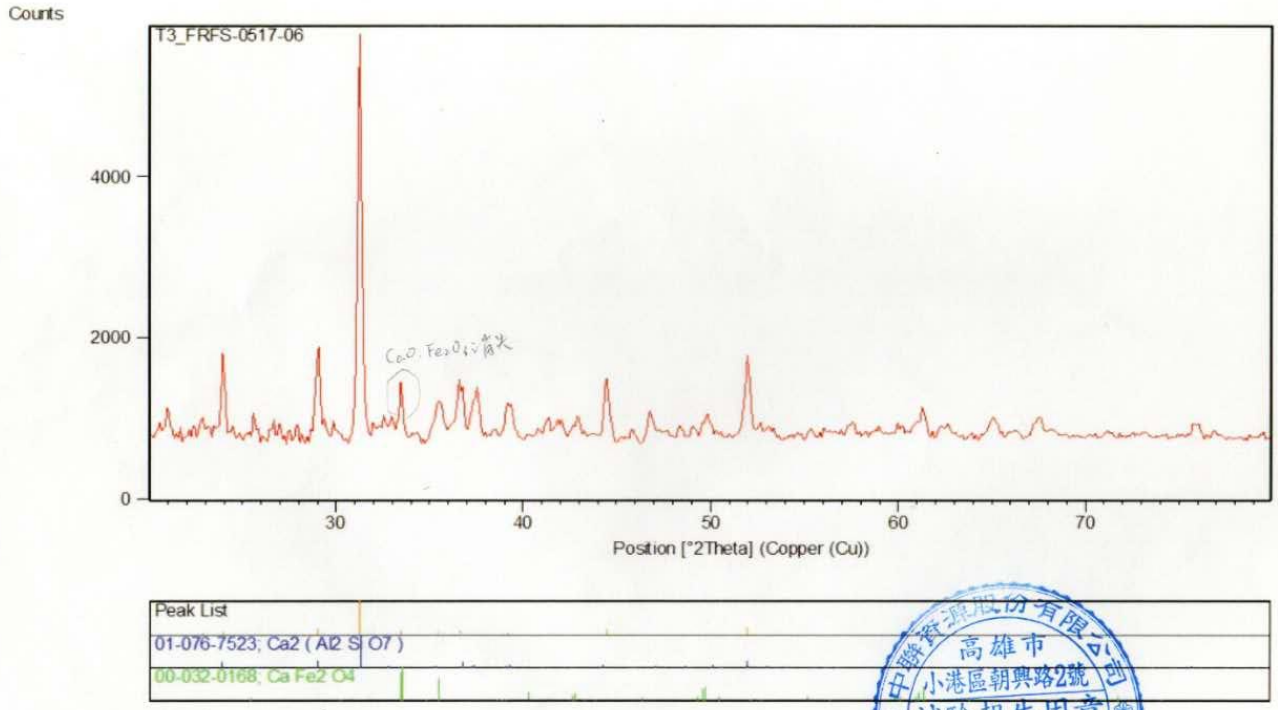

分析結果：該樣品組成為$2CaO \cdot SiO_2 \cdot Al_2O_3$，$CaO \cdot Fe_2O_3$

中聯資源股份有限公司 高雄市小港區朝興路2號 試驗報告用章 TEL:(07)8720171 水泥及混凝土實驗室

107-CHC-1698

doi:10.6342/NTU201902030

CRFS

附件一

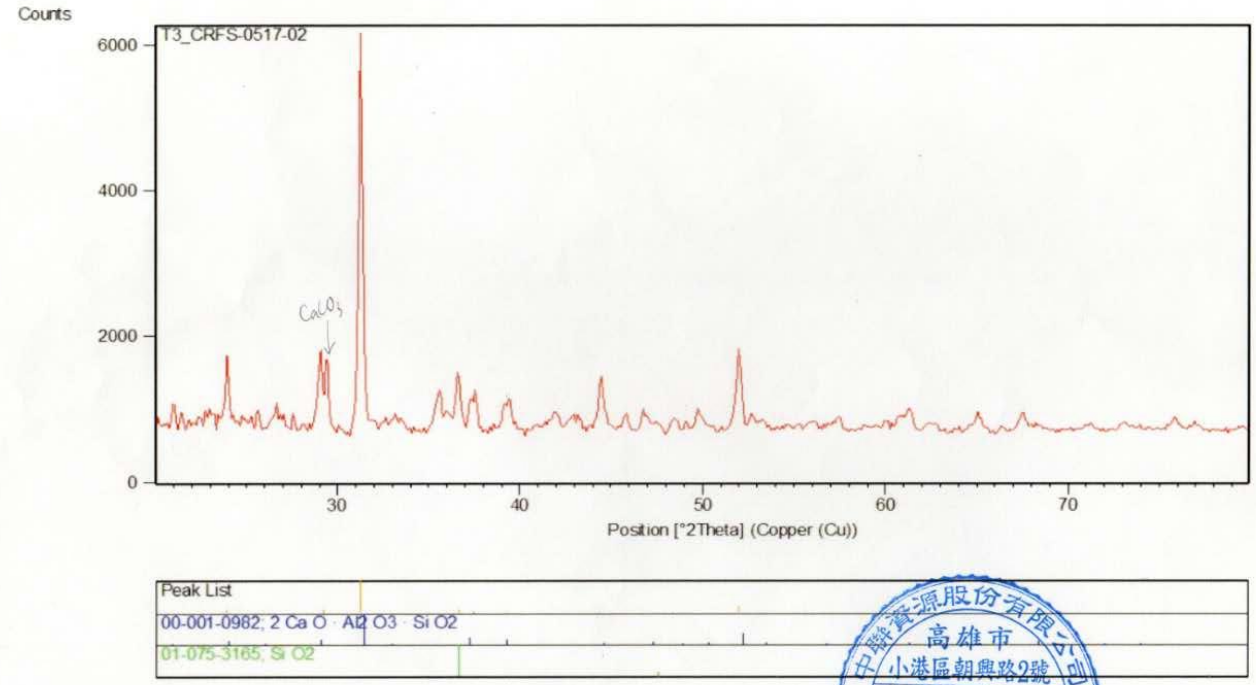

分析結果：該樣品組成為 $2CaO \cdot Al_2O_3 \cdot SiO_2$，$SiO_2$

中聯資源股份有限公司 高雄市 小港區朝興路2號 試驗報告用章 TEL:(07)8720171 水泥及混凝土實驗

107-CHC-1694

doi:10.6342/NTU201902030

FEAFRS

附件一

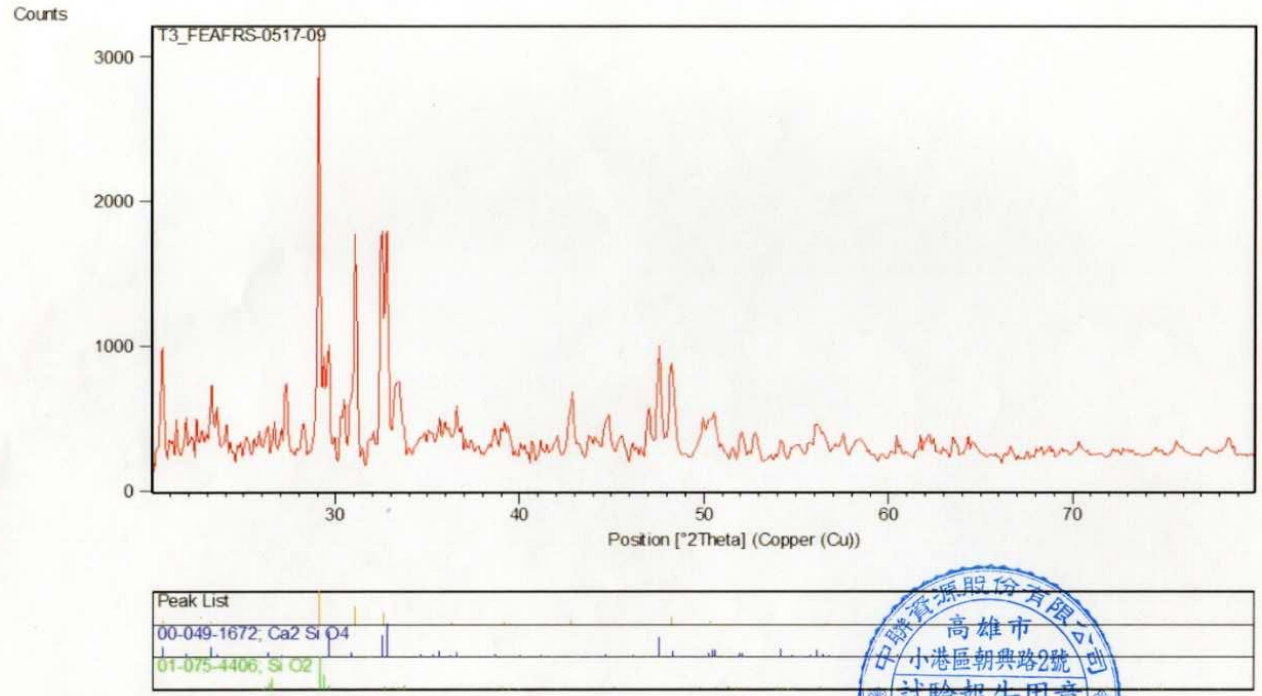

分析結果：該樣品組成為$2CaO \cdot SiO_2$，SiO_2

中聯資源股份有限公司 高雄市 小港區朝興路2號 試驗報告用章 TEL:(07)8720171 水泥及混凝土實驗室

107-CHC-1701

doi:10.6342/NTU201902030

CEAFRS

附件一

頁次(Page)：3

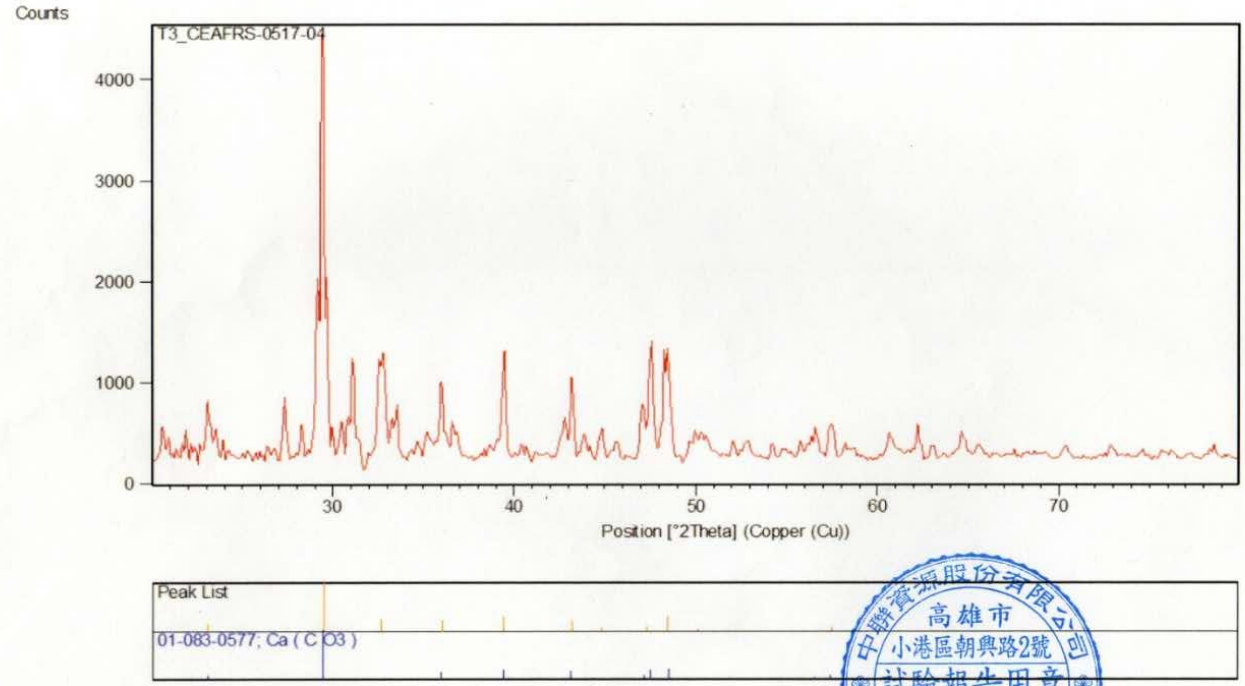

分析結果：該樣品組成為$CaCO_3$

中聯資源股份有限公司 高雄市 小港區朝興路2號 試驗報告用章 TEL:(07)8720171 水泥及混凝土實驗室

107-CHC-1696

doi:10.6342/NTU201902030

FEAFOS

附件一

頁次(Page)：3

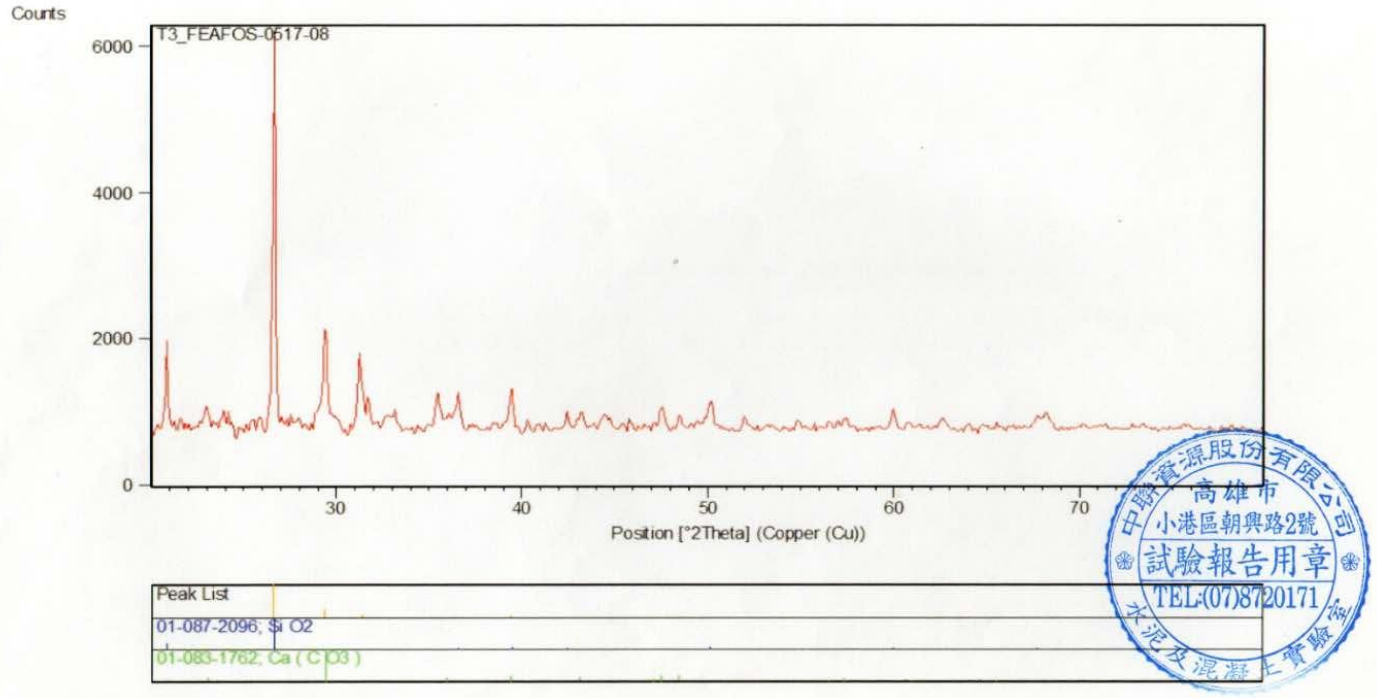

分析結果：該樣品組成為SiO_2、$CaCO_3$

107-CHC-1700

doi:10.6342/NTU201902030

CEAFOS

附件一

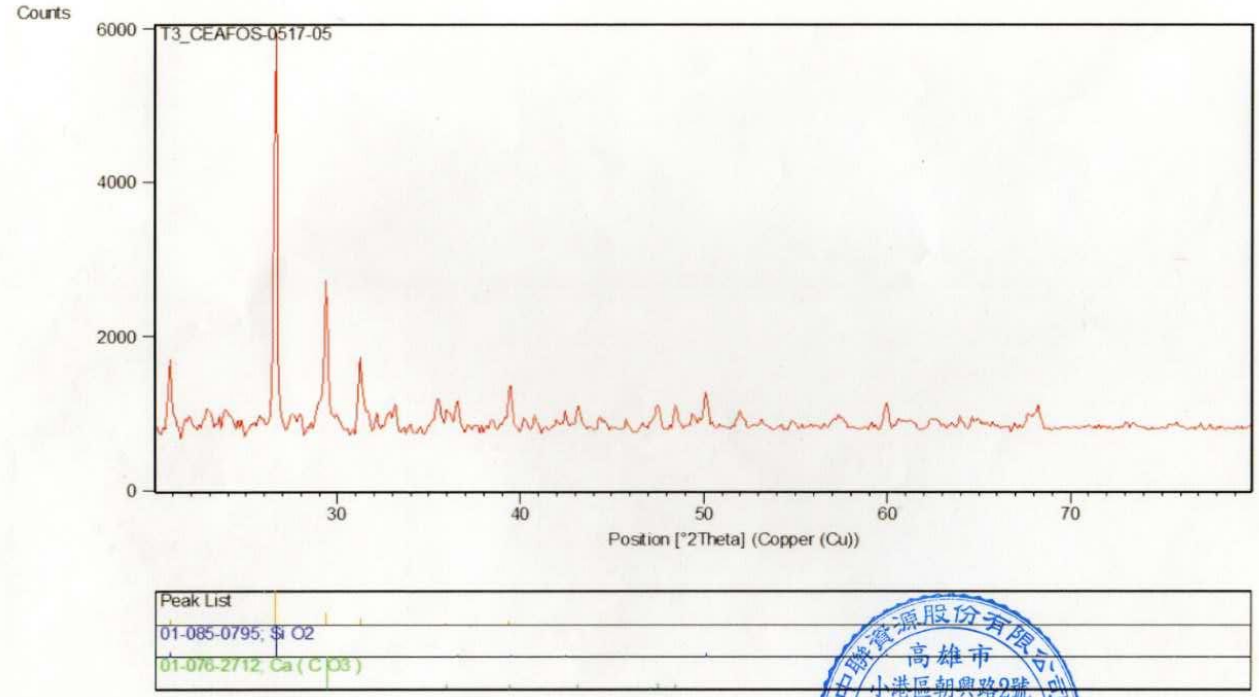

分析結果：該樣品組成為SiO_2，$CaCO_3$

中聯資源股份有限公司 高雄市 小港區朝興路2號 試驗報告用章 TEL:(07)8720171 水泥及混凝土實驗室

107-CHC-1697

doi:10.6342/NTU201902030